

OXYGEN AND SULFUR ISOTOPE CONSTRAINTS ON THE ORIGIN OF GOLD
DEPOSITS AT THE HAILE GOLD MINE, LANCASTER COUNTY, SC

by

HEATHER MARIE VEASEY

(Under the Direction of DOUGLAS E. CROWE)

ABSTRACT

Gold at the Haile Gold Mine, in the Carolina Slate Belt (CSB), is located within silicified metasediments of the Richtex Formation near the contact with the older, metavolcanic Persimmon Fork Formation. Deposits at Haile have been characterized either as epithermal forming due to hydrothermal activity associated with volcanism, or as orogenic forming from fluids derived during regional metamorphism.

Because pyrite and quartz are associated with gold mineralization at Haile, $\delta^{18}\text{O}$ values of 138 quartz samples and $\delta^{34}\text{S}$ values of 17 pyrite samples were measured in order to better constrain the origin of the gold deposits. $\delta^{18}\text{O}$ values for quartz ranged from 5.9 to 9.1 per mil and $\delta^{34}\text{S}$ values for pyrite ranged from -1.6 to +3.4 per mil. Assuming reasonable temperatures for orogenic and epithermal deposits (200-400°C), this data indicates that the gold deposits formed in an epithermal system.

INDEX WORDS: Gold, Stable Isotope, Carolina Slate Belt, $\delta^{18}\text{O}$, $\delta^{34}\text{S}$

OXYGEN AND SULFUR ISOTOPE CONSTRAINTS ON THE ORIGIN OF GOLD
DEPOSITS AT THE HAILE GOLD MINE, LANCASTER COUNTY, SC

by

HEATHER MARIE VEASEY

B.S., University of Alabama, 2009

A Thesis Submitted to the Graduate Faculty of The University of Georgia in Partial

Fulfillment of the Requirements for the Degree

MASTER OF SCIENCE

ATHENS, GEORGIA

2013

© 2013

Heather Marie Veasey

All Rights Reserved

OXYGEN AND SULFUR ISOTOPE CONSTRAINTS ON THE ORIGIN OF GOLD
DEPOSITS AT THE HAILE GOLD MINE, LANCASTER COUNTY, SC

by

HEATHER MARIE VEASEY

Major Professor: Douglas E. Crowe

Committee: Michael F. Roden
Paul A. Schroeder

Electronic Version Approved:

Maureen Grasso
Dean of the Graduate School
The University of Georgia
May 2013

ACKNOWLEDGEMENTS

I'll start by thanking everyone at the Haile Gold Mine, both for providing funding for this research, and also for giving me the opportunity to spend two summers there learning what I could about the somewhat unique geology. I particularly want to thank James Berry for his encouragement and willingness to share his knowledge of the area. Thanks to Reid as well for looking up information when I was not there to do it and to Pete for being willing to listen to new ideas.

The Geological Society of America and the Society of Economic Geologists provided funding for this project. I'd like to thank both organizations for their financial support.

I also want to thank my advisor Doug Crowe for his support, patience, and advise. His encouragement and willingness to explain difficult concepts have been extremely helpful during my time at the University of Georgia. Thanks also to Mike Roden and Paul Schroeder for serving on my committee. I also want to thank Julia Cox for all of her help in the stable isotope lab and Ben Powers for his work measuring sulfur isotope data. Further thanks to the all the faculty, staff, and students in the UGA Department of Geology who have made my time as a student both enjoyable and educational.

TABLE OF CONTENTS

	Page
ACKNOWLEDGEMENTS	iv
LIST OF FIGURES	vii
CHAPTER	
1 INTRODUCTION	1
2 GEOLOGY	5
Regional Geology	5
Local Geology.....	11
3 GENETIC MODELS	16
Orogenic Deposits.....	16
Epithermal Deposits.....	20
4 METHODS	25
Sampling	25
Isotopic Analysis.....	26
5 RESULTS	28
Petrography.....	28
Sulfur Isotopes	35
Oxygen Isotopes.....	35
6 DISCUSSION	40
7 CONCLUSSIONS	46

REFERENCES 47

APPENDICES

A Table of $\delta^{18}\text{O}$ values, $\delta^{34}\text{S}$ values, and sample descriptions 54

B XRD data for selected quartz samples 62

LIST OF FIGURES

	Page
Figure 1: Map of the Carolina Slate Belt with mine locations	10
Figure 2: Geologic map of the Haile Gold Mine	13
Figure 3: Locations of ore zones from which samples were taken.....	14
Figure 4: Orogenic and epithermal ore forming tectonic environments.....	17
Figure 5: Examples of pervasive silicification.....	29
Figure 6: Example of milky white quartz veins.....	30
Figure 7: Example of a banded quartz-potassium feldspar-pyrite vein	31
Figure 8: Examples of quartz-pyrite veins.....	32
Figure 9: Example of a bull quartz vein.....	33
Figure 10: Example of late-stage millimeter-scale clear quartz veins	34
Figure 11: Examples of pyrite sample types.....	36
Figure 12: Histogram of $\delta^{34}\text{S}$ values for pyrite samples.....	37
Figure 13: Histogram of $\delta^{18}\text{O}$ values for quartz samples.....	38
Figure 14: Range of $\delta^{18}\text{O}_{\text{fluid}}$ values (this study) for 200° C, 300° C, and 400° C compared to known values for possible fluid sources.....	41
Figure 15: Comparison of $\delta^{34}\text{S}$ pyrite values for samples from Haile and Ridgeway	43

CHAPTER 1

INTRODUCTION

The Haile Gold Mine is located near the town of Kershaw in Lancaster County, South Carolina and is one of several gold mines located within the Carolina Slate Belt (CSB). Gold mining within the CSB has occurred intermittently since 1800, including several episodes of mining taking place at the Haile mine. Gold was first discovered at Haile in 1827 in Haile Gold Mine Creek and not long after that open-pit and underground mining began. Maddry and Kilbey (1995) indicate that the most productive periods of mining occurred between 1888-1908 and 1936-1942. Piedmont Mining Company resumed mining during the period between 1985-1991. Speer and Maddry (1993) estimate that over 360,000 ounces of gold were mined at Haile during the period from 1827-1991.

Recent gold prices and advances in mining technology have lead to a resurgence of gold exploration in the CSB. In 2007, Romarco Minerals, Inc. acquired the Haile Gold Mine property, and since then exploration has been done to further define the mineralization at Haile. Current exploration and attempts to resume mining at Haile have provided access to samples from several new ore zones and from greater depth, which are less affected by supergene alteration. Currently the Haile Gold Mine is thought to include several ore zones composed of moderate to deeply northwest dipping mineralized bodies found within a northeast-southwest trending zone that is approximately 3500 ft. wide and 2.1 miles long.

Due to the complex geologic history of the CSB, many of the gold deposits have enigmatic origins. The possible origins that have been proposed can be broadly separated into two groups. The first group invokes an orogenic model in which fluids derived by devolatilization from existing rocks during a regional metamorphic event carried the gold and concentrated it into economic deposits within zones of structural weakness. The second group includes those that suggest a syngenetic to epigenetic hydrothermal model ranging from seafloor massive sulfide deposits to shallow marine or subaerial epithermal deposits. Many studies have focused on the origin of gold mineralization in these Slate Belt deposits (Worthington and Kiff, 1970; Feiss, 1982a; McKee and Butler, 1986; Klein and Criss, 1988; Eager, 1997; Clark et al., 1999; Seal et al., 2001; Ayuso et al., 2005; Klein et al., 2007).

Spence et al. (1980) considered alteration and the distribution of major and minor elements, which led to the determination that a hot spring exhalative model could best explain mineralization. Worthington et al. (1980) also supported this model, as did Hardy (1987; 1989) who based her interpretation on the presence of hydrothermal potassium feldspar associated with the deposit. However, structural studies at Haile that focused on the relationships between structures and ore zones pointed toward a metamorphic origin for the gold mineralization (Tomkinson, 1988; Hayward, 1992). Feiss (1988) suggested that the structural and stratigraphic setting of deposits at Haile were consistent with a syngenetic model. Other later studies supported an epithermal model, though there were indications that partial remobilization of gold during regional metamorphism had occurred (Feiss, 1982a; Worthington, 1992; Speer and Maddry, 1993). Foley et al (2001) studied pyrite at Haile and also determined that pyrite and gold were pre-metamorphic

and that post-mineralization metamorphic events only served to remobilize and further concentrate the gold.

Stable isotope studies are often used to distinguish the source of fluids involved in the formation of ore deposits due to differences in the ratios of stable isotopes of the elements C, H, O, and S (Ohmoto, 1972; O'Neil and Silberman, 1974; Taylor, 1974; Ohmoto and Rye, 1979; Ohmoto, 1986; Klein and Criss, 1988; Feiss and Wenner, 1989; Rye, 1993). Klein and Criss (1988) and Feiss and Wenner (1989) measured the oxygen isotope values of whole rocks at Haile and other CSB gold deposits and concluded that they supported the epithermal model of ore formation.

This study focuses on the oxygen isotope values of quartz to help constrain the source of fluids involved in silicification. In epithermal hot spring systems, fluids tend to be mainly meteoric with low to negative $\delta^{18}\text{O}$ values (the total range of meteoric $\delta^{18}\text{O}$ values is broad but can be limited to approximately -5 to 0 per mil for this study based on the paleolocation of the CSB at the time of ore formation), but a magmatic component (~+5 to +10 per mil) may be present, especially at depth (O'Neil and Silberman, 1974; Taylor, 1974). A seawater component could also be present if the system formed subaqueously. In the metamorphic model that has been suggested for Haile, fluid $\delta^{18}\text{O}$ values would be between +5 and +25 per mil with water being derived from devolatilization reactions (Taylor, 1974). This model of ore formation is similar to Phanerozoic lode gold deposits, which typically have $\delta^{18}\text{O}$ values that range from +6 to +13 per mil (Bierlein and Crowe, 2000; Goldfarb et al., 2005). Due to the variation in values for the two different models, the $\delta^{18}\text{O}$ values of quartz can aid in the

identification of the source fluid and therefore the deposit type if an assumption about formation temperature is made.

Because the two major models proposed at Haile involve fluids of different oxygen isotopic composition and because silicification is strongly associated with gold mineralization at Haile, a sampling of the different generations of silicification was conducted from core samples and the $\delta^{18}\text{O}$ values were measured. The quartz samples included quartz from pervasive silicified zones, stockwork breccias, and different generations of veins. Gold at Haile is associated with pyrite, so $\delta^{34}\text{S}$ values were also determined for a set of pyrite samples. The purpose of this study is to determine the composition of the fluid responsible for pyrite and quartz formation and use that data to constrain the origin of the Haile deposit.

CHAPTER 2

GEOLOGY

Regional Geology

The CSB is a northeast-southwest trending belt of greenschist facies metamorphosed sedimentary and volcanic rocks. It is bounded by the amphibolite grade Charlotte Belt to the northwest with the boundary between the two belts being variably interpreted as a shear zone, a suture, or a metamorphic gradient (Feiss, 1982a). The CSB is bounded by the amphibolite grade Kiokee Belt to the southeast. The contact between the CSB and the Kiokee Belt is interpreted to be primarily a metamorphic gradient between analogous stratigraphic units rather than a major fault zone, though the contact may represent a brittle fault or deformed intrusive contact in some places (Snoke et al., 1980).

Rast et al. (1976) and Foley et al. (2001) have suggested that CSB rocks, as part of the Carolina superterrane, can be correlated with Avalonian rocks (625-550 Ma) (Hatcher, 2010). Hibbard et al. (2009) suggest that this association is problematic due to differences in ages of volcanism. Noel et al. (1988) also conclude that the assemblages do not correlate based on paleomagnetic data from North Carolina. Hatcher (2010) notes that although the Avalon and Carolina assemblages have similarities and formed near Gondwana, there are enough differences in their histories to discard the possibility of correlation. Secor et al. (1983) note faunal differences between the two assemblages that further support this opinion.

Several different explanations based on various types of evidence have been put forth to describe the origin of the CSB. Whitney et al. (1978) suggest that the Lincoln-McCormick area of the CSB is characterized by submarine to subaerial tholeiitic volcanism indicative of a primitive island arc in which oceanic crust was likely being subducted under oceanic crust. Feiss (1982b) suggests that the late Proterozoic to Cambrian volcanic rocks of the CSB actually represent a bimodal, calc-alkaline suite generated in a subduction zone, with the volcanic arc being located on the west side of the closing Iapetus ocean. The geochemical data from Feiss (1982b) across the CSB does not support the primitive arc setting described by Whitney et al. (1978). Schmidt and Klein (1985) agree that the CSB formed in a volcanic arc environment during the late Precambrian to early Paleozoic suggesting that the rocks formed in an island arc environment along a continental margin. Bell et al. (1980) describe the CSB as an upper Precambrian to Ordovician volcanic island arc setting as well, but also suggest that alternatively it could represent a rift basin. Paleomagnetic and oxygen isotope data suggests that the CSB accreted to Laurentia by the late Ordovician (Vick et al., 1987; Feiss, 1995). Hatcher (2010) argues that the paleomagnetic data is not conclusive due to a large degree of uncertainty and that docking of the Carolina superterrane with Laurentia occurred in the middle Paleozoic.

Studies also describe the environment of the slate belt at the time of formation of gold deposits. Feiss et al. (1993) state that whole rock $\delta^{18}\text{O}$ values from the Uwharrie Formation and Albemarle Group suggest that mineralization occurred during extension in a rifted arc. These oxygen isotope studies indicate that the volcano-sedimentary transition also marked the transition from an arc-related subaerial phase to a rift-dominated system

in which the arc collapsed below sea level (Feiss, 1995). $^{206}\text{Pb}/^{204}\text{Pb}$ and $^{207}\text{Pb}/^{204}\text{Pb}$ ratios of sulfides at Haile and other deposits may indicate that deposits formed near continental blocks linked to a back-arc tectonic setting (Ayuso et al., 2005).

It was originally thought that correlations could be made between units of the CSB located in North Carolina and in South Carolina and that these units formed at the same time. Stratigraphic correlations between the North Carolina Uwharrie Formation and Albemarle Group and the South Carolina Persimmon Fork Formation and Richtex Formation are complicated by faulting and age differences (Bell et al., 1980; Samson et al., 1990). Current age data indicates that the North Carolina portion of the CSB is older than the South Carolina portion and that the units cannot be directly correlated though they formed in similar environments. Bell et al. (1980) propose that the sedimentary sequence in the Lincolnton-McCormick area may correlate with the Richtex Formation. According to Whitney et al. (1978) the volcanic rocks of the Lincolnton-McCormick area are of similar lithology to the rocks of the Uwharrie formation.

In the central region of the CSB in South Carolina, the contact between the metavolcanic Persimmon Fork Formation and the metasedimentary Richtex Formation is likely gradational (Snook et al., 1980; Speer and Maddry, 1993). Though the units may not correlate, this transition is similar to the conformable contact between the Albemarle Group and the Uwharrie Formation (Hibbard et al., 2009).

Radiometric dating of zircons from the metavolcanic rocks of the CSB yield ages of 586 ± 10 Ma for the Uwharrie Formation (North Carolina) and 553 ± 2 Ma for the Persimmon Fork Formation at Haile (Wright and Seiders, 1980; Ayuso et al., 2005). The zircon U-Pb age from the volcanic rocks of the Cid formation (which is in the upper part

of the Albemarle group) is 547 +/- 2 Ma (Hibbard et al., 2009). Ayuso (1999) indicates that host rocks at Ridgeway, Haile, and Brewer are all ~560 Ma. In contrast, U-Pb and Th-Pb dating yield ages of 466 +/- 40 (2 σ) and 462 +/- 53 Ma respectively for volcanoclastic rocks and massive pyrite from rocks in the Haile-Brewer block, with a Pb-Pb age of 455 Ma (LeHuray, 1987). Ayuso et al. (2005) indicate that the methods used by LeHuray (1987) are less precise and the 553 +/- 2 Ma age is more consistent with other age data such as fossil data from the area. Sedimentary rocks in the South Carolina portion of the CSB are of early to middle Cambrian age, based on the presence of *Paradoxides*, *Peronopsis*, and *Tomagnostus* trilobites in the sediments near Batesburg, South Carolina (Secor et al., 1983; Samson et al., 1990). Fossil data also helps constrain the age of the CSB in south-central North Carolina to late Precambrian (Gibson et al., 1984; Gibson, 1989).

Peak metamorphism of the CSB was determined to have occurred at approximately 455 Ma from $^{40}\text{Ar}/^{39}\text{Ar}$ dating of rocks from the Abermarle Group in North Carolina, indicating deformation during the early Phanerozoic, which correlates with the Taconic Orogeny (Noel et al., 1988). A 318 Ma Alleghenian overprint was identified for Ridgeway, Haile, and Brewer by U-Pb dating of zircon by Ayuso (1999). Ar-Ar and Pb-Pb variations in sulfides at these deposits also indicate remobilization of sulfides during the Taconic and Alleghenian orogenies (Ayuso, 1999).

The age of the mineralization is best constrained by Re-Os dating of molybdenite which yielded ages of 553.8 +/- 9 and 586.6 +/- 3.6 Ma at Haile and 551.9 +/- 2.6 and 557.9 +/- 3.3 Ma at Ridgeway (Stein et al., 1997). Four measurements of three new molybdenite samples from Haile yielded slightly younger ages of 548.7 +/- 4.2, 549.0 +/-

3.1, 548.4 +/- 2.4, and 541.2 +/- 2.3 Ma (Mobley et al., 2012). These molybdenite ages are still consistent with the ages of host rocks and are significantly older than the ages of known regional metamorphic events.

Haile along with Ridgeway, Brewer, and Barite Hill are important gold deposits in the CSB that likely have similar origin (Figure 1). Gold deposits at Ridgeway are located at the transition between an older volcanic unit and a younger sedimentary unit which correspond to the Persimmon Fork Formation and Richtex Formation respectively (Gillon et al., 1995). A north and south pit have been studied, and in both gold tends to be associated with pyrite and silicification (Gillon et al., 1995). Gold is also often of higher grade in zones with strongly developed cleavage which may indicate remobilization (Gillon et al., 1995). Muscovite (referred to as sericite throughout this study) and multiple quartz veining events are also associated with gold in the south pit (Gillon et al., 1995).

Gold at Brewer is located in the matrix of brecciated zones of the volcanic rocks of the Persimmon Fork Formation (Zwaschka and Scheetz, 1995). The location of the gold in the volcanic Persimmon Fork Formation rather than the sedimentary Richtex Formation differs from deposits at Haile and Ridgeway. Alteration is concentric with advanced argillic alteration grading outward to sericitic and then propylitic alteration (Zwaschka and Scheetz, 1995). Some minerals present that are not important at Haile or Ridgeway are topaz, rutile, covellite, and andalusite, and enargite while pyrite and quartz are also present, indicating higher temperatures and pH values for ore forming fluids than those at Haile and Ridgeway (Zwaschka and Scheetz, 1995). Based on the alteration

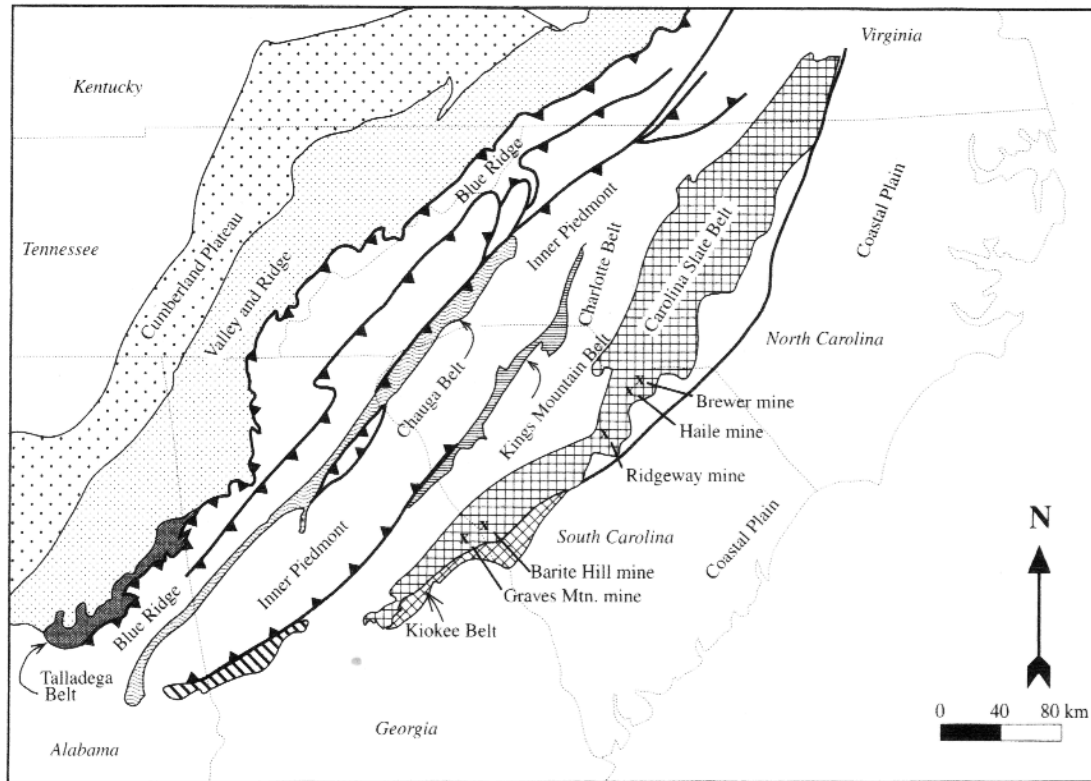


Figure 1: Map of the Carolina Slate Belt with mine locations (from Bierlein and Crowe 2000).

pattern and mineralogy of the deposit Brewer is likely a porphyry or high-sulfidation epithermal deposit.

Deposits at Barite Hill are also located in the Persimmon Fork Formation (Clark et al., 1999). Gold tends to be associated with quartz, pyrite, and barite (Clark et al., 1999). Barite Hill is interpreted to represent the transition from a subaqueous massive sulfide system that led to the formation of barite, massive pyrite, and silica to an epithermal type deposit (Clark et al., 1999). Sulfur isotope data from barite and pyrite along with lead isotope data supports a seafloor setting for ore formation (Seal et al., 2001).

Local Geology

The Persimmon Fork Formation is composed mainly of felsic volcanic rocks including crystal-lapilli tuffs with some interlayered sedimentary units derived from volcanics. The metavolcanic rocks of the Persimmon Fork Formation were originally rhyolitic or rhyodacitic (Bell, 1985; Bell, 1986). The main minerals within this unit include quartz, albite, sericite, and chlorite, with minor biotite and carbonate, indicative of greenschist-grade metamorphism. The Richtex Formation overlies the Persimmon Fork Formation and is composed mainly of bedded mudstones and silty mudstones with sandstone and conglomerate lenses. Phyllites and schists predominate due to the regional metamorphism. The minerals making up the unit are mainly quartz with sericite along with minor chlorite, biotite and carbonates. Much younger Cretaceous coastal plain sediments often cover the other units at Haile.

Several intrusive bodies are present in or near the mine area. Lamprophyre and diabase dikes that post date metamorphism crosscut the Persimmon Fork Formation and

Richtex Formation. The bodies referred to as lamprophyre dikes are composed mainly of alkali feldspar, quartz, and apatite and trend in different orientations (Maddry and Kilbey, 1995). Mesozoic diabase dikes trend northwest-southeast, and are related to a period of regional tension, and are common across the southern Appalachians. In addition, the Pageland and Liberty Hill plutons are emplaced near the mine. These plutons are of Pennsylvanian age and are not responsible for gold formation (Bell, 1982). Figure 2 shows the orientation of the major units present at Haile.

The rocks at Haile tend to be foliated, with foliation more strongly developed in the metasediments than the metavolcanics. Foliation is axial planar to folding, strikes to the northeast, and generally dips moderately to the northwest. The mine is located near the axis of a regional-scale anticline (Bell, 1986). Tight to isoclinal folding is also common in the area, and several sets of faults are also present.

Alteration to saprolite is common near the surface at Haile. Hydrothermal alteration is present at depth with silicification and sericitization being common. Silicification is often pervasive but quartz veining is also common with veins varying from pure quartz to quartz-sulfide or quartz-carbonate veins. Potassium feldspar can also be present in areas that have undergone significant degrees of hydrothermal alteration. Though hydrothermal alteration likely related to the ore forming event is present, it is important to note that the degree of this alteration is unclear because the rocks have undergone greenschist facies metamorphism which also leads to the formation of quartz, sericite, calcite, and chlorite.

The relative locations of sampled ore zones at Haile are shown in Figure 3. Gold mineralization is located mostly in the Richtex Formation, though some older

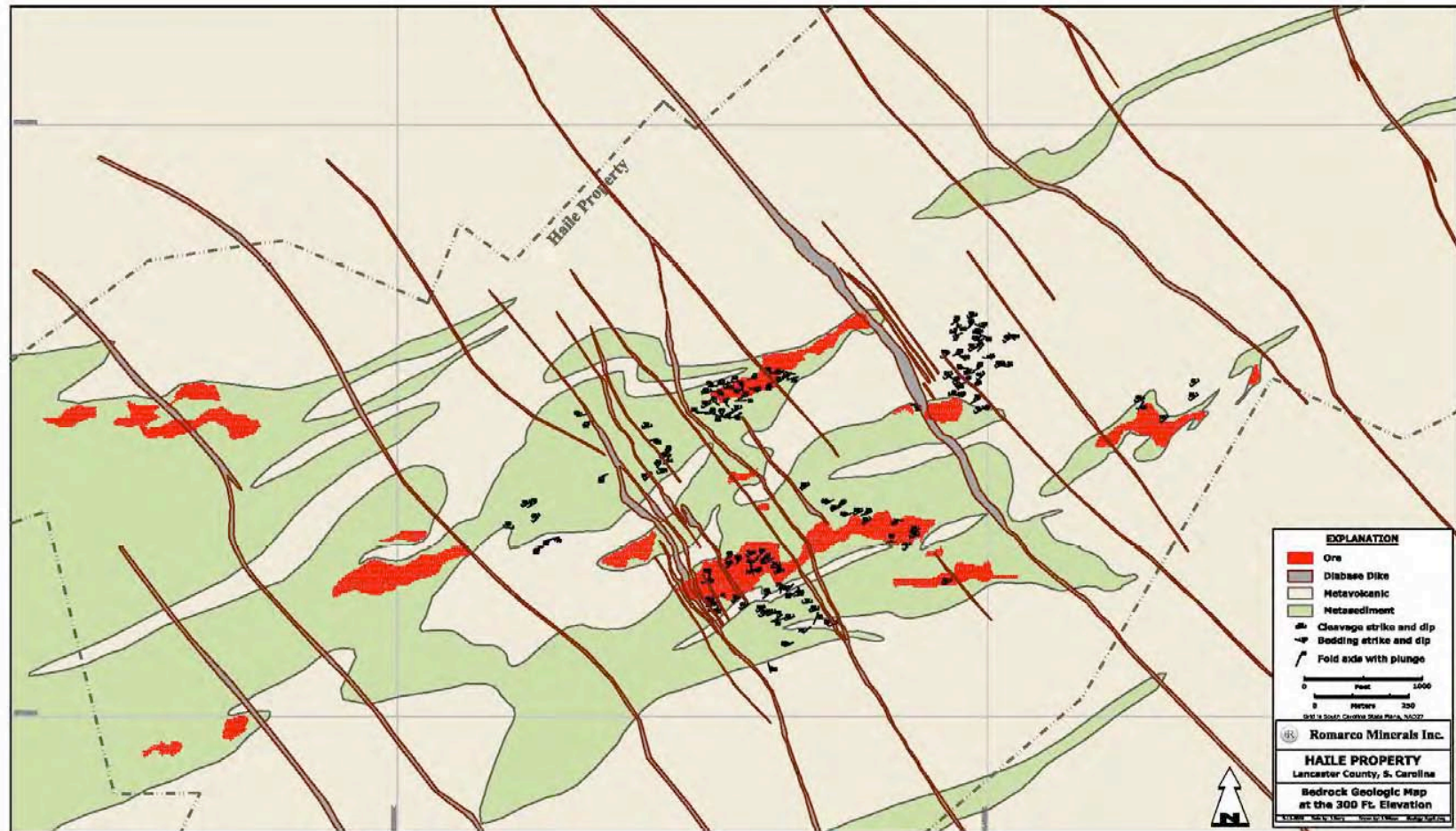


Figure 2: Geologic map of the Haile Gold Mine. Based on data from 2009 (from Snider et al., 2012). Tan = Metavolcanics. Green = Metasediments. Red = Ore. Grey-Brown = Diabase dikes.

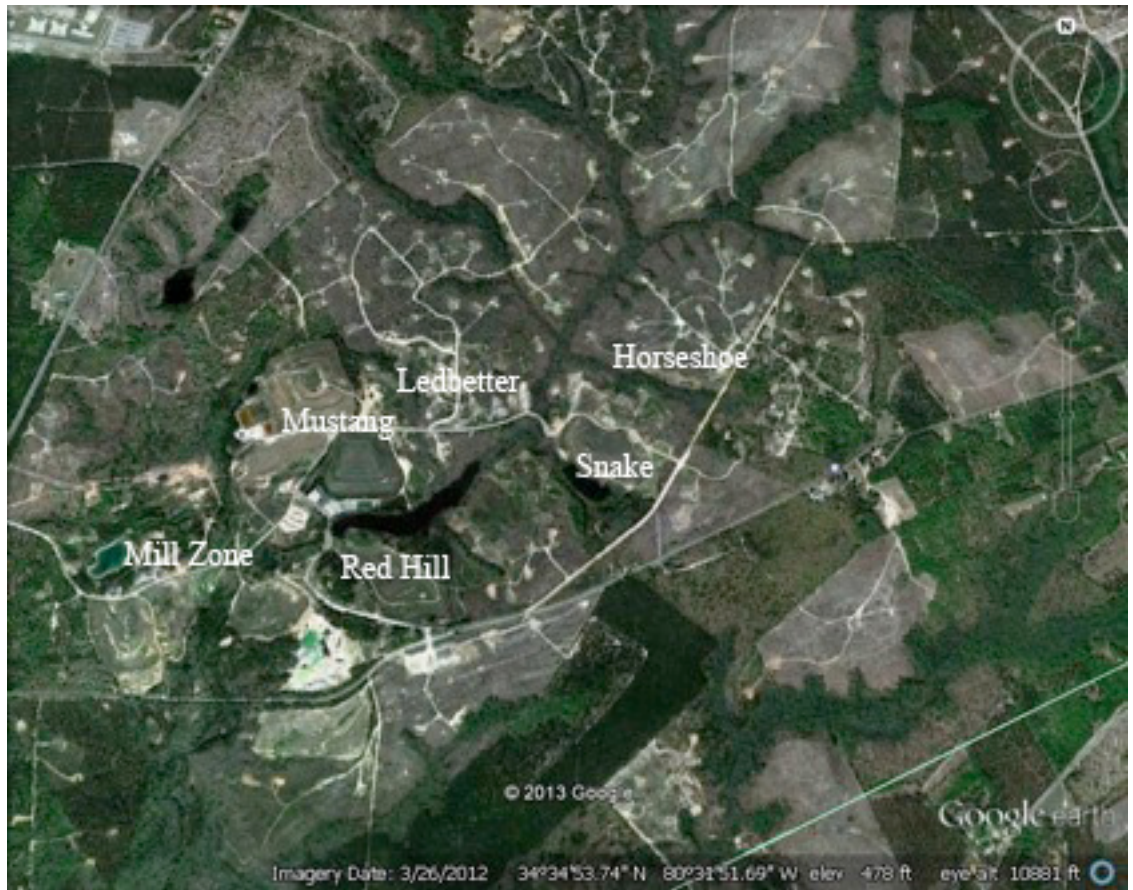


Figure 3: Locations of ore zones from which samples were taken (*modified from Google Earth. March 26, 2012. April 25, 2013*).

publications indicate that it is located in the volcanoclastic portions of the Persimmon Fork Formation instead (Maddry and Kilbey, 1995). The ore is usually found in silicified and pyritic zones of the Richtex Formation. Pyrite in these zones tends to be fine grained and disseminated throughout the rock, but may also be located in veins or massive to semi-massive irregular-shaped bodies as described by Maddry and Kilbey (1995). Molybdenite is also associated with gold. Most gold-bearing ore zones also tend to be located at the volcano-sedimentary transition. These ore bodies tend to trend in the same northeast-southwest manner as the CSB, often dipping moderately to deeply to the northwest.

CHAPTER 3

GENETIC MODELS

Although gold deposition at the Haile Gold Mine has been described as both orogenic and epithermal in nature, the two models of gold formation have several significant differences. Comparison of these characteristics to Haile will help to better constrain the origin of Haile, although the rocks at Haile have undergone greenschist grade post-mineral regional metamorphism, obscuring some of the comparative characteristics such as mineralogy and morphology. The two models are described below, and examples of each are given in order to provide a better characterization of the typical characteristics of and variability within these deposit types. Figure 4 shows the tectonic environments in which both orogenic and epithermal deposits tend to form.

Orogenic Deposits

Orogenic deposits form during regional metamorphic events, often during the late stages of orogeny postdating the bulk of the regional metamorphism. The style of mineralization is often characterized by quartz vein systems, but varies depending on the pressure and temperature conditions such that these deposits may be present as stockworks and breccias, crack-seal veins, or disseminated ore bodies (Groves et al., 1998; Goldfarb et al., 2005). Orogenic deposits are most often found in greenschist facies rocks, although examples have been found in both higher and lower grade zones. Usually any spatial correlation between these deposits and intrusive units is due to the presence of zones of structural weakness rather than any association between their formation, but

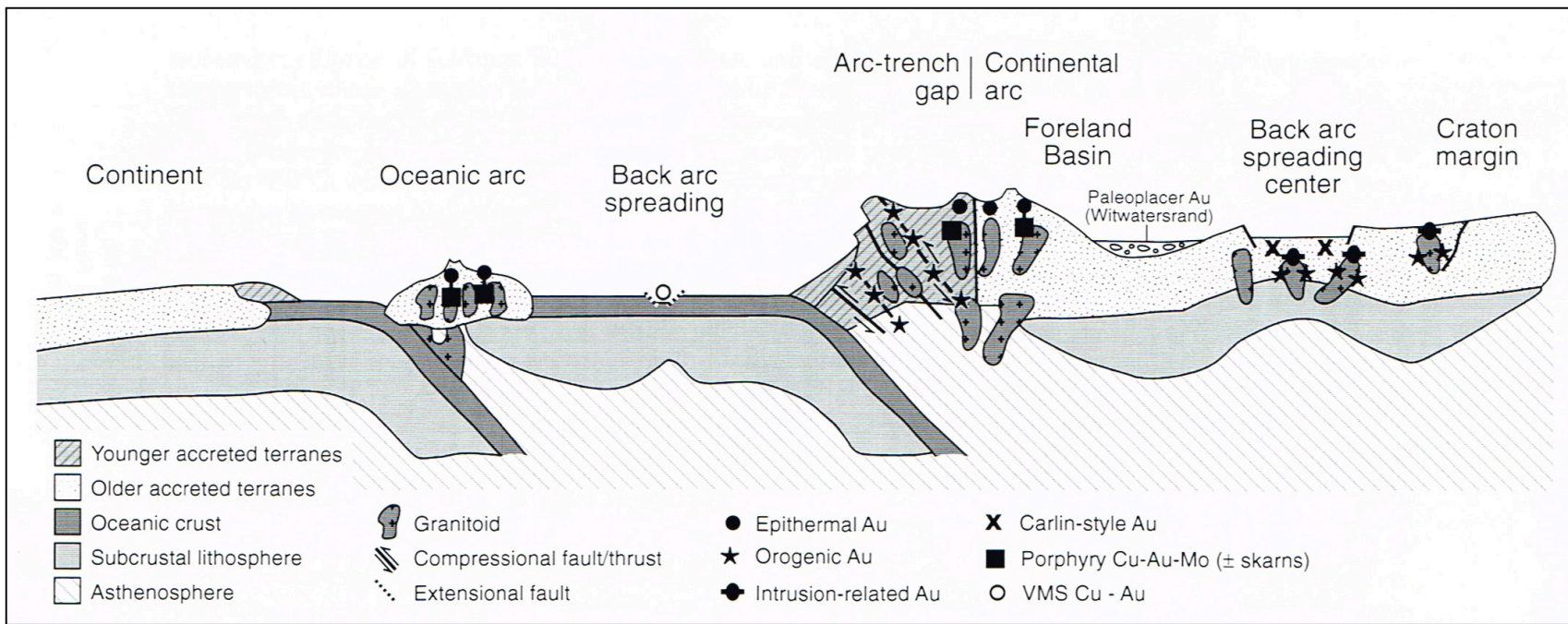


Figure 4: Orogenic and epithermal ore forming tectonic environments (from Goldfarb et al., 2005).

most orogenic deposits form near intrusions of approximately the same age, and a subtype of these deposits is referred to as “intrusion-related” (Goldfarb et al., 2005).

Orogenic deposits are associated with large first-order fault zones, but most major orogenic deposits are hosted in lower order faults associated with these major structures. Along with lower order faults, areas of uplift or folding can provide zones of weakness in which ore deposition occurs. In Precambrian greenstone environments the large zones of regional weakness occur between lithologic units parallel to volcanic stratigraphy, but in Phanerozoic environments they tend to occur in sedimentary rocks formed along continental margins or in volcanic arcs that have undergone greenschist facies metamorphism during collisional events (Bierlein and Crowe, 2000; Goldfarb et al., 2005) The Archean orogenic gold deposits formed during periods of greenstone belt evolution while Phanerozoic deposits formed during growth of Gondwana and Laurentia or during circum-Pacific tectonism in greenschist facies rocks (Goldfarb et al., 2005).

Mineralogically, arsenopyrite (in metasedimentary rock hosted deposits) and pyrite (in mafic or granitoid hosted deposits) are the common sulfide minerals in this type of deposit, but pyrrhotite can be important if the ore formed at temperatures greater than approximately 400° C (Groves et al., 1998; Goldfarb et al., 2005). Stibnite is also common in many metasedimentary-hosted deposits. Though zones of alteration associated with orogenic deposits are often unclear, common alteration minerals include quartz, carbonate, muscovite, chlorite, potassium feldspar, biotite, tourmaline, and albite. Orogenic gold deposits commonly have anomalous amounts of W, Te, and/or Bi (Goldfarb et al., 2005).

Ore forming fluids for orogenic deposits tend to be CO₂ and ¹⁸O-rich and have near neutral pH (Groves et al., 1998; Goldfarb et al., 2005). Temperatures of ore formation tend to fall between the range of 250-400°C but are not restricted to this range, and ore formation occurs at pressures of 1 to 3 kbars (Groves et al., 1998; Bierlein and Crowe, 2000; Goldfarb et al., 2005). δ¹⁸O values for ore forming fluids tend to range from 6 to 13 per mil indicating the lack of a significant meteoric component (Groves et al., 1998; Bierlein and Crowe, 2000; Goldfarb et al., 2005). δ³⁴S values of sulfide minerals often range from 0 to 10 per mil but much higher and lower values have also been measured (Goldfarb et al., 2005).

Orogenic gold deposits in the Lachlan fold belt in Victoria, Australia are associated with low salinity, CO₂ bearing fluids (Jia et al., 2001; Fu et al., 2012). In the Bendigo Zone, gold is mainly found in domes and reverse-fault zones (Jia et al., 2001). Gold was deposited at temperatures of 350° +/- 25°C, and veins tend to be composed of quartz, carbonate, mica, and sulfide minerals (Jia et al., 2001). Pyrite samples in gold bearing veins from the Central and North Deborah mine have an average sulfur isotope value of 2.0 per mil and quartz samples from gold bearing veins have oxygen isotope values of 15.9 to 17.2 per mil (Jia et al., 2001). Ore fluids have δ¹⁸O values ranging from 8 to 11 per mil (Jia et al., 2001). The source of the sulfide in the mineralizing fluid was likely desulfidation of existing sulfide minerals (Jia et al., 2001). Metamorphic devolatilization deep in the crust led to the formation of the ore forming fluid, but there is evidence of interaction between this fluid and shallower sediments during fluid ascent (Jia et al., 2001; Fu et al., 2012).

The Donlin Creek gold deposit in southwestern Alaska is another example of an orogenic type deposit. Mineralization is hosted in a rhyolitic to rhyodacitic dike complex and is associated with quartz-carbonate veinlets with arsenopyrite, pyrite, and younger stibnite (Goldfarb et al., 2004). Sericite is also present as an alteration phase. Ore formation occurred at temperatures of 275-300° C (Goldfarb et al., 2004). Oxygen isotope values of quartz associated with gold range from 11 to 25 per mil, with the calculated fluid $\delta^{18}\text{O}$ values ranging from 7 to 12 per mil (Goldfarb et al., 2004). Sulfide minerals associated with gold have a range of $\delta^{34}\text{S}$ values between -16 and -10 per mil. These isotopic values indicate a crustal source for the ore forming fluid with the source for sulfur being sedimentary pyrite and organic matter (Goldfarb et al., 2004).

Epithermal Deposits

Epithermal deposits tend to form near the surface at depths less than 1.5 km and at temperatures less than 300° C (Simmons et al., 2005). They form under these low pressure and temperature conditions via mixing of fluids from depth with near surface waters or boiling caused by pressure changes (White and Hedenquist, 1990). They tend to form in subaerial, hydrothermal systems and are related to volcanism, often forming near the end of volcanic events in an area. They tend to form in areas with multiple generations of faults or fractures such as calderas that provide structural control on fluid flow and thus control the site of ore deposition (Heald et al., 1987). These deposits often form as vein fillings and stockworks or breccias, but they can also be disseminated throughout the host rock. They are typically found in volcanic rocks, but in some cases associated sediments have been mineralized, and for adularia-sericite type deposits the composition of the host rock is more or less unimportant for ore formation (Heald et al.,

1987; Simmons et al., 2005). Epithermal deposits may or may not be clearly associated with intrusions or other intrusion-related deposits such as porphyries, although in most cases the connection between the two is clear.

Elements often associated with gold in epithermal deposits are Ag, Cu, Zn, Pb, As, Sb, Bi, Se, Te, Tl, Mo, W, Sn, and Hg (Simmons et al., 2005). Epithermal deposits can be characterized as low sulfidation (adularia-sericite) or high sulfidation (acid-sulfate) type, and different minerals are associated with the two subtypes. High sulfidation deposits are characterized by enargite, pyrite, and covellite, and the gangue minerals quartz, alunite, pyrophyllite, dickite, and kaolinite, which indicate acidic solutions (Heald et al., 1987; Simmons et al., 2005). Acidic fluids responsible for the advanced argillic alteration at these deposits form by the addition of SO₂, H₂S, HCl, and HF derived from magmas to hydrothermal fluids (Vennemann et al., 1993). Zones of vuggy silica are common in the central regions of these deposits and advanced argillic alteration is characteristic of these types of deposits, commonly spatially associated with silicification (Heald et al., 1987). Typically moving outward from these deposits are zones of argillic and propylitic alteration.

Low sulfidation-type deposits are associated with some combination of the gangue minerals quartz, calcite, adularia, illite and sericite and form at near neutral pH (Heald et al., 1987; Simmons et al., 2005). Alteration tends to be characterized by a zone of silicification surrounded by a zone of sericitic alteration. Chlorite and potassium feldspar may also be alteration minerals present in these deposits (Heald et al., 1987). The texture of gangue minerals in low sulfidation deposits often shows crustiform banded

quartz interbedded with other minerals such as sulfides and adularia (Simmons et al., 2005).

Stable isotope data indicates that fluids responsible for ore formation in epithermal deposits are composed mainly of meteoric and magmatic water with the amounts of each varying in high and low sulfidation deposits. Low sulfidation deposits typically have a greater amount of meteoric influence while high sulfidation deposits typically show a greater amount of magmatic influence (Heald et al., 1987; Hedenquist and Lowenstern, 1994; Simmons et al., 2005). Sulfur isotope values measured for sulfide minerals in high sulfidation epithermal deposits are usually close to 0 per mil and indicate a predominantly magmatic source (Heald et al., 1987; Simmons et al., 2005).

One example of an epithermal deposit is the Pueblo Viejo acid sulfate deposit in the Dominican Republic. The deposit is hosted by greenschist facies metavolcanic and intrusive rocks overlain by volcanoclastic and metasedimentary units which have been cut across by a maar-diatreme complex of the same age as the hydrothermal activity responsible for ore formation (Vennemann et al., 1993). According to Kesler et al. (1981) the hydrothermal system was active during sedimentation and alteration occurred before regional metamorphism as indicated by foliation in the pyrophyllite. Much of the ore is disseminated but late stage gold bearing veins were also present (Vennemann et al., 1993). Two stages of advanced argillic alteration occurred, the first being characterized by zones of alunite or kaolinite with pyrite, quartz, and rutile with gold being associated with the disseminated pyrite (Vennemann et al., 1993). The second stage overprinted the first with pyrophyllite, diaspore, and massive silicification, with sulfides including pyrite, enargite, and sphalerite often present in veins (Vennemann et al., 1993). $\delta^{18}\text{O}$ values for

quartz have a mean value of 13.5 per mil for stage one and 14.3 per mil for stage two, indicating a largely magmatic source of fluid along with mixing of meteoric fluid (<25%) or seawater (Vennemann et al., 1993). $\delta^{34}\text{S}$ values of sulfides and sulfates range from -10.1 to +21.6 per mil and suggest that a seawater source and magmatic fluid or sulfur derived from sulfides in the volcanic rocks of the formation played a role in formation of these minerals (Kesler et al., 1981; Vennemann et al., 1993).

The Kushikino mining area in southern Kyushu, Japan is an example of a low sulfidation deposit. The deposit is characterized by epithermal veins of quartz, calcite, adularia, sericite, and sulfide minerals (Matsuhisa et al., 1985). $\delta^{18}\text{O}$ values of vein quartz range from 5.5 to 10.7 per mil, while the range of calculated $\delta^{18}\text{O}$ values for the hydrothermal fluid is similar to groundwater in the area indicating meteoric fluid as the main component of the ore forming fluid (Matsuhisa et al., 1985). Three stages of vein formation occurred, with gold being associated with the first stage of translucent quartz and the main stage with milky quartz and calcite (Matsuhisa et al., 1985). The veins formed at temperatures of approximately 140-220°C due to rapid cooling (Matsuhisa et al., 1985).

The Ladolam deposit at Lihir Island in Papua, New Guinea is an example of the transition from porphyry to low sulfidation epithermal style gold mineralization due to a collapse of the stratovolcano which hosts the deposit (Müller et al., 2002). Most of the gold was deposited during the transition between the two styles of ore formation and is hosted in the phreatomagmatic stockwork breccia containing biotite, magnetite, and chalcopyrite, but a late stage of low sulfidation style veining was also associated with gold (Müller et al., 2002). $\delta^{34}\text{S}$ values range from -8.8 to -3.4 per mil for pyrites from

hydrothermal breccias and -6.0 to -0.1 per mil for pyrite from quartz-chalcedony-adularia-pyrite veins suggesting a magmatic sulfur source (Müller et al., 2002) The late stage epithermal veins formed at temperatures of 160-200°C based on fluid inclusion studies and oxygen isotope values (Müller et al., 2002). $\delta^{18}\text{O}$ values of quartz and chalcedony from the veins range from +14.5 to +18.1 (Müller et al., 2002). Nearby submarine mineralization at Conical seamount may be related to the same magmatic events, and resembles epithermal deposits rather than sea-floor massive sulfide deposits indicating that these deposits may not be limited to subaerial environments (Petersen et al., 2002).

CHAPTER 4

METHODS

Sampling

Quartz and pyrite samples were selected from 23 diamond drill holes across the Haile property in two rounds of sampling. These samples were taken from several different ore zones (Horseshoe, Ledbetter, Mustang, Mill Zone, Snake, and Red Hill) in order to account for variation across the property. Standard and reflected light microscopy of thin sections from the first round of sampling from the Horseshoe zone led to a second round of more extensive sampling. Petrography of the thin sections and hand samples led to the selection of 138 quartz samples and 17 pyrite samples for isotopic analysis.

Quartz samples were chosen from different styles and generations of veins. These veins were mainly quartz, with minor amounts of carbonate, sericite, and chlorite, with sulfide minerals such as pyrite and pyrrhotite occasionally being present. Quartz samples from pervasively silicified zones were also selected. Pyrite samples were selected based on style, relative absence of other sulfide minerals, and in some cases association with silicified zones that had been selected as quartz samples.

Quartz and pyrite were sampled using a dental drill. Quartz purity was determined by visual observation and a preliminary petrographic study of thin sections representative of rock types and alteration common at Haile. Compositions of samples for which purity could not be determined visually were evaluated using a Bruker D8

Advance X-ray diffractometer using Co K α radiation ($\lambda=1.7902 \text{ \AA}$). Samples were measured from 2° to $70^\circ 2\Theta$ at a speed of $10^\circ/\text{min}$. Minor sericite was ignored due to similar fractionation of oxygen between the fluid and quartz or muscovite. Samples containing carbonate were treated with HCl and rinsed with deionized water. Samples containing abundant sulfide underwent two overnight treatments with aqua regia and were then rinsed with deionized water four times until the rinsing solution had a neutral pH, in order to remove sulfides. Samples that underwent treatment with aqua regia were checked for purity using the Bruker D8 Advance X-ray diffractometer (Appendix B).

Isotopic Analysis

SO₂ was extracted from pyrite samples using a modified method from Ueda and Krouse (1986) in which samples were finely crushed and reacted with V₂O₅. $\delta^{34}\text{S}$ values of SO₂ were measured using a Finnigan MAT 252 gas source mass spectrometer. All $\delta^{34}\text{S}$ values are reported relative to the Canyon Diablo Troilite Standard. Precision of all analyses is ± 0.2 per mil (2σ) based on replicate analysis of NBS-123 and University of Georgia Lab standards.

Oxygen was extracted from quartz using a modified version of the laser fluorination method described by Spicuzza et al. (1998), and was converted to CO₂ using a heated graphite in Pt rod. $\delta^{18}\text{O}$ values of samples analyzed were measured using a Finnigan MAT Delta E gas source mass spectrometer or a Finnigan MAT 252 gas source mass spectrometer. All $\delta^{18}\text{O}$ values are reported relative to VSMOW.

$\delta^{18}\text{O}$ values were corrected based on 34 runs of standard NBS-28 for samples analyzed on the Finnigan MAT Delta E gas source mass spectrometer and 54 runs of standard NBS-28 for samples analyzed on the Finnigan MAT 252 gas source mass

spectrometer. Corrections were made by taking the average values of the standard over all runs and correcting that average to the accepted value of +9.6 per mil. Precision of all analyses is +/- 0.7 per mil (2σ) based on replicate analysis of NBS-28.

CHAPTER 5

RESULTS

Petrography

Different styles of silicification and pyrite formation were identified via hand sample examination and thin section petrography. Quartz samples can be broken into six main types: pervasive silicification with and without disseminated pyrite (Figure 5), clear to milky white quartz veins typically < 2 cm across (Figure 6), banded quartz-potassium feldspar-sulfide veins of varying thickness (Figure 7), massive quartz-sulfide veins ~0.5-4 cm wide (Figure 8), late stage bull quartz (Figure 9), and late-stage millimeter-scale quartz veins (Figure 10).

Pervasively silicified samples are characterized by mosaic quartz with minor foliated sericite and minor chlorite and carbonate. Fine- to very fine- grained pyrite may be disseminated in these zones. Quartz in veins that have a clear to milky white appearance in hand sample often crosscut the pervasive silicification. These veins are composed almost exclusively of quartz with minor sericite and carbonate. This style of quartz acts as the matrix in breccias with pervasively silicified clasts. Quartz bands in veins of banded quartz, sulfide, and potassium feldspar have also been sampled. These banded veins are common in high-grade areas and are likely crack/seal veins. Two types of quartz-sulfide veins were sampled with the first characterized by quartz inter grown with coarse-grained pyrite and/or pyrrhotite, with carbonate and sericite also commonly present. The second type is made up of quartz with very fine-grained pyrite and minor



Figure 5: Examples of pervasive silicification. Top) Pervasively silicified sample with minor sericite. Sample RCT0061-863. Bottom) Pervasively silicified sample with clear quartz flooding. Sample DDH389-702.



Figure 6: Example of milky white quartz veins. Sample DDH347-407.



Figure 7: Example of a banded quartz-potassium feldspar-pyrite vein. Sample DDH396-1331.

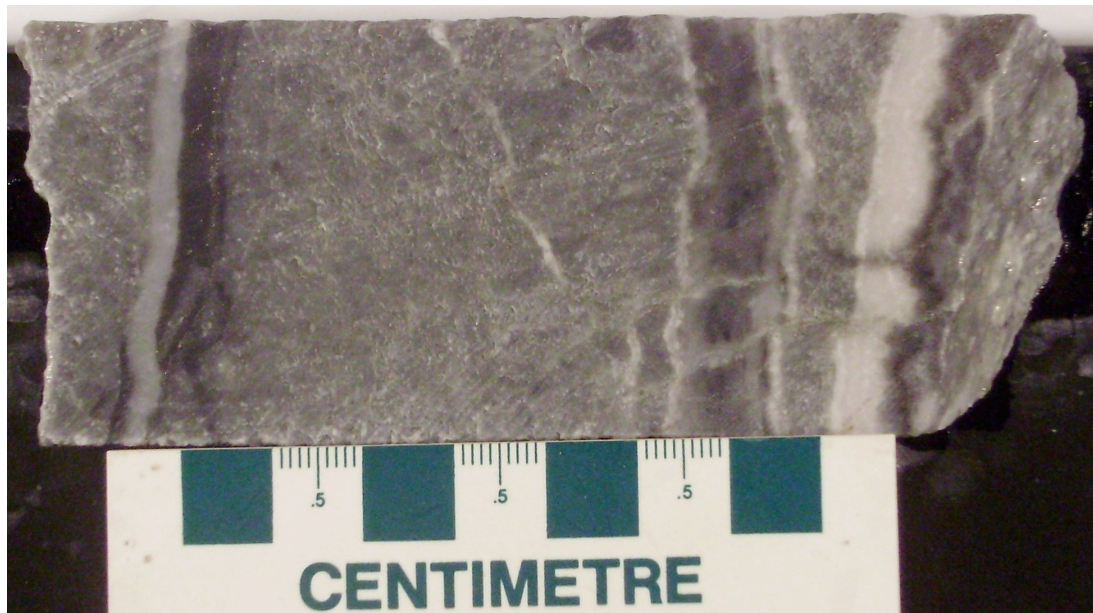


Figure 8: Examples of quartz-pyrite veins. Top) Quartz-pyrite vein with fine-grained pyrite. Sample DDH396-1068. Bottom) Quartz-pyrite veins with very fine-grained disseminated pyrite. Sample RCT0087-1174.



Figure 9: Example of a bull quartz vein. Sample DDH389-1200.



Figure 10: Example of late-stage millimeter-scale clear quartz veins. Sample RCT0056-1142.

sericite and resembles the pervasively silicified zones with very fine-grained pyrite. Large coarse-grained bull quartz veins are composed almost exclusively of quartz with occasional coarse-grained calcite and very minor sericite or chlorite. These veins are late stage and crosscut other silicification events. Very thin (millimeter scale) quartz veins/selvages absent of other minerals are also late stage and cut across other styles of veins.

Pyrite samples were taken either from pervasively silicified zones with disseminated pyrite or quartz-sulfide veins (Figure 11). Grain size varies from very fine- to fine- grained. Large porphyroblastic pyrite cubes are also present, but they are not associated with gold formation at either Haile or the nearby Ridgeway mine, and therefore were not sampled.

Sulfur Isotopes

Sulfur isotope values are reported relative to the Canyon Diablo Troilite standard. Corrected $\delta^{34}\text{S}$ values for 17 pyrite samples range from -1.6 to +3.4 per mil with a mean value of 2.0 per mil (Figure 12). Values for all samples with sample descriptions are in Appendix A.

Oxygen Isotopes

Oxygen isotope values are reported relative to VSMOW. Corrected $\delta^{18}\text{O}$ values for 138 quartz samples range from +5.9 to +9.1 per mil (Figure 13). Values for all samples with sample descriptions are in Appendix A. Using these $\delta^{18}\text{O}$ values for quartz and a mineralization temperature of 300°C along with the Clayton et al. (1972) oxygen isotope fractionation factor for quartz-water, a range of calculated $\delta^{18}\text{O}$ values for the fluid was calculated to be -1.0 to +2.2 per mil. This temperature was chosen because it is



Figure 11: Examples of pyrite sample types. Top) Massive pyrite around a banded quartz-pyrite vein. Sample RCT0033-1147. Bottom) Disseminated pyrite. Sample DDH347-219.

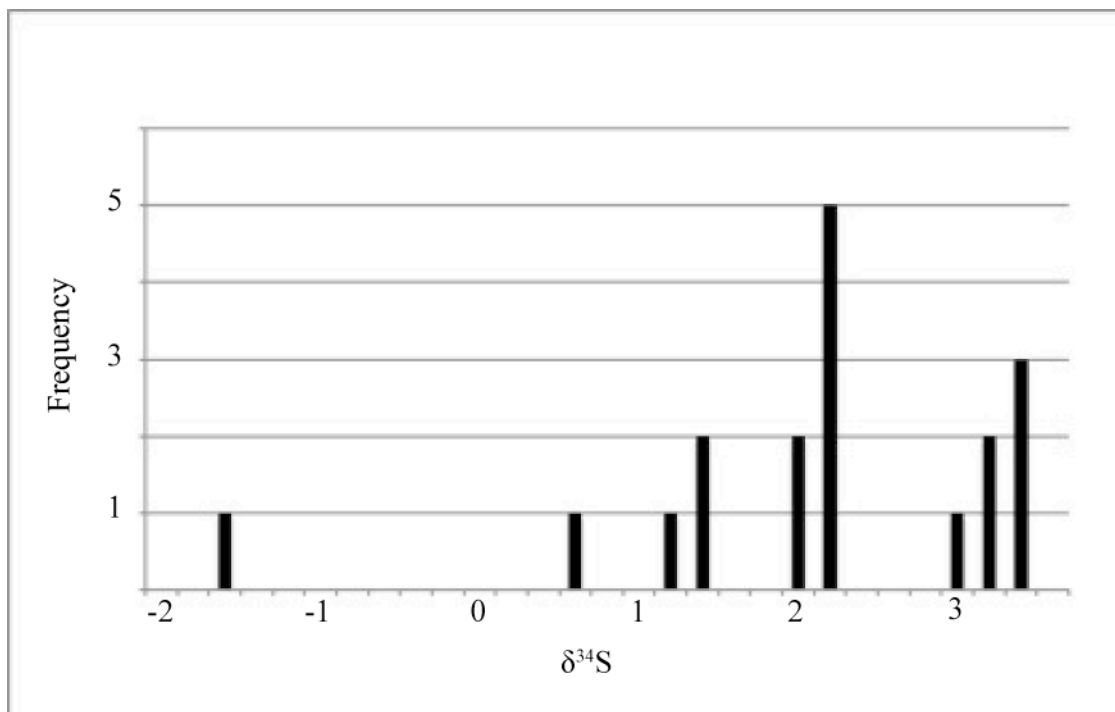


Figure 12: Histogram of $\delta^{34}\text{S}$ values for pyrite samples.

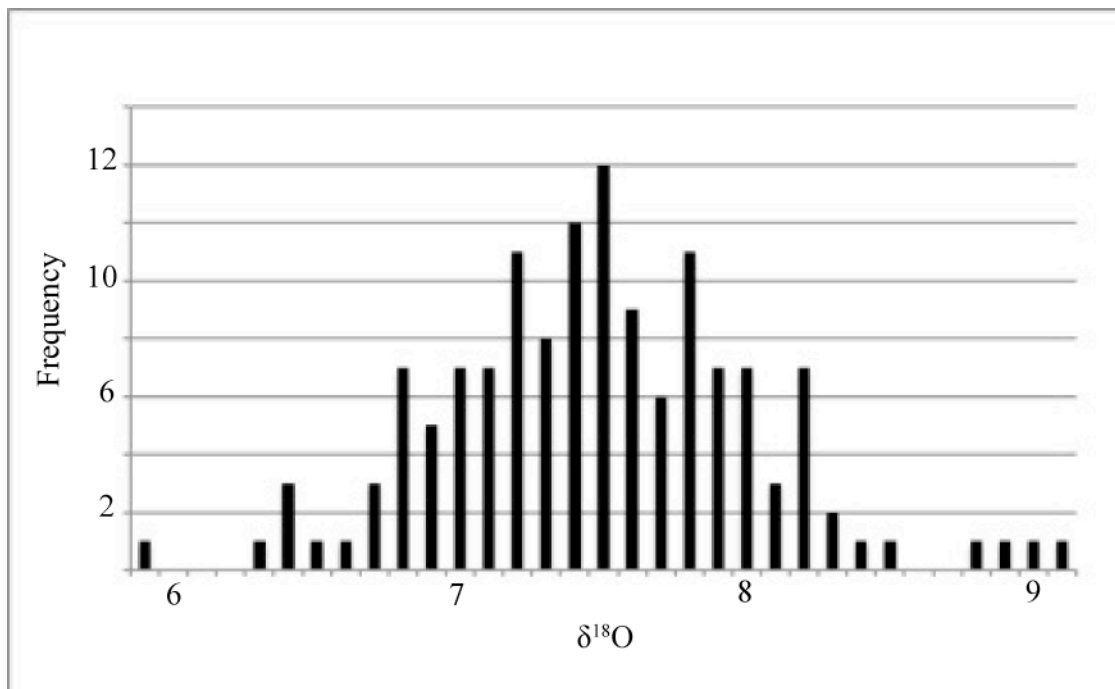


Figure 13: Histogram of $\delta^{18}\text{O}$ values for quartz samples.

a reasonable temperature for both orogenic and epithermal ore forming fluids. However, the $\delta^{18}\text{O}$ values of the fluid were also determined for the temperatures 200°C and 400°C and those ranges were -5.8 to -2.6 per mil and +1.8 to +5.0 per mil respectively.

CHAPTER 6

DISCUSSION

The oxygen isotope values for the quartz samples (+5.9 to +9.1 per mil) are comparable to the values measured in smaller scale studies using whole rock samples from Haile. Klein and Criss (1988) measured a range of values from +6.5 to +11.6 per mil while Feiss and Wenner (1989) measured values from +3.8 to +10.2. It's likely that the larger range in $\delta^{18}\text{O}$ values in these studies was due to the inclusion of other minerals in the samples used.

Figure 14 shows the range of $\delta^{18}\text{O}$ values for the quartz-forming fluid at Haile for three temperatures (200°C, 300°C, and 400°C) relative to the known $\delta^{18}\text{O}$ values for possible fluid sources. The silicifying fluid was likely derived from meteoric water and magmatic fluid with a possible seawater component. No overlap is shown with the expected range of values for the ore forming fluids in orogenic type deposits or even the wider range of values expected of metamorphically derived fluids. The range of $\delta^{18}\text{O}$ values for the quartz forming fluid shifts to become more ^{18}O -enriched with increasing temperature, but in order to see an overlap with the range expected in orogenic systems it would be necessary to increase the temperature beyond what is reasonable at Haile based on the lower greenschist metamorphic grade of the rocks.

Although oxygen isotope values for samples from several different quartz forming events were measured, no major differentiation of the events could be made based on these values. A lack of change in the isotopic signature of the quartz forming fluids over

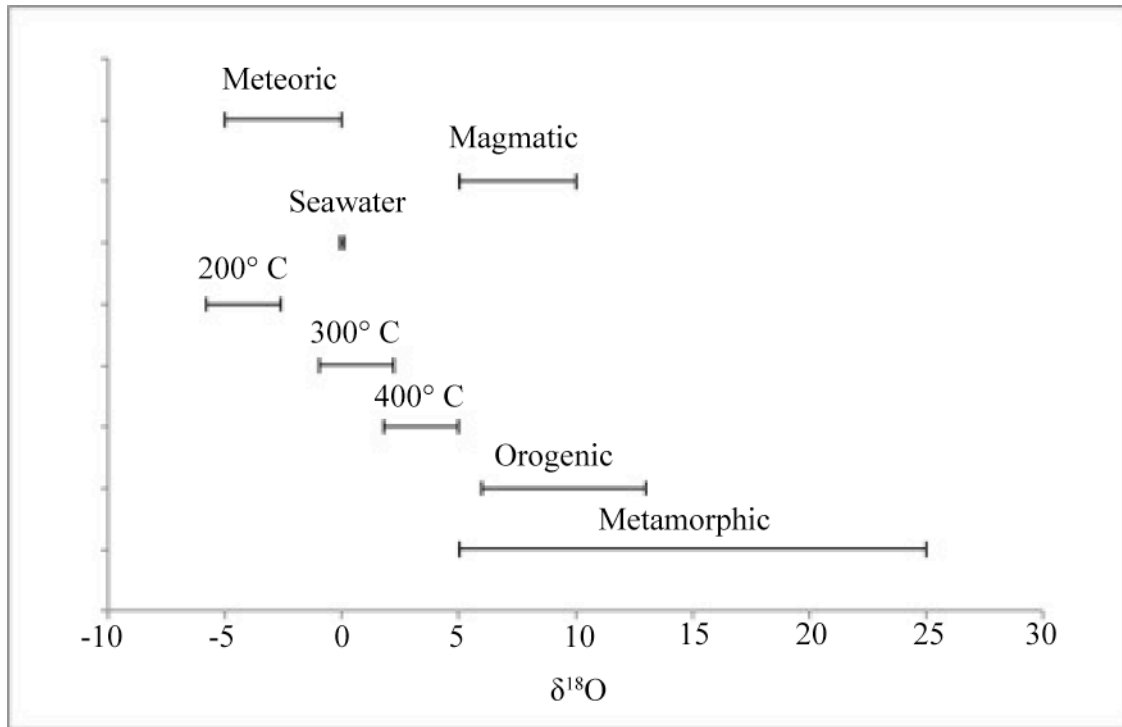


Figure 14: Range of $\delta^{18}\text{O}_{\text{fluid}}$ values (this study) for 200° C, 300° C, and 400° C compared to known values for possible fluid sources. The orogenic range is from Bierlein and Crowe (2000) and Goldfarb et al. (2005), and the metamorphic and magmatic ranges are from Taylor (1974). The meteoric range is estimated based on the paleolocation of the CSB during ore formation.

time indicates that similar processes were at work throughout the formation of the deposit. There is no indication that the environment in which ore formation occurred varied greatly over time, so meteoric and magmatic water with a possible seawater component were likely responsible for all silicification events.

Figure 15 shows $\delta^{34}\text{S}$ values (-1.6 to +3.4 per mil) for pyrite samples from Haile relative to the values measured by Eager (1997) for 183 pyrite samples from the Ridgeway deposit that ranged from -18.5 to +5.5 per mil. Eager (1997) distinguished between a hypogene pyrite population with a range of $\delta^{34}\text{S}$ values from -1.4 to +5.5 per mil and an average value of 2.7 per mil and a second population with a range from -18.5 to -1.4 per mil. The second population correlates with the coarse-grained porphyroblastic pyrite that is often present at Haile but that is not associated with gold and therefore wasn't sampled in this study. The pyrite-forming fluids for both the hypogene population at Ridgeway and the samples from Haile had a magmatic source based on the $\delta^{34}\text{S}$ values near 0 per mil, but some samples are enriched in ^{34}S indicating that a heavier source of sulfur was also involved. Late Proterozoic/early Cambrian seawater sulfate was approximately 30 per mil (Claypool et al., 1980) and small amounts of this sulfate would have led to slightly ^{34}S -enriched $\text{H}_2\text{S}_{\text{fluid}}$ values that ultimately produced $\delta^{34}\text{S}_{\text{pyrite}}$ values such as those seen at Haile in this study.

Several lines of evidence indicate that the gold mineralization at Haile Gold Mine is the result of a low sulfidation epithermal deposit that underwent post mineralization greenschist facies metamorphism. The oxygen isotopic evidence indicates that the source of fluids was a mixture of magmatic and meteoric fluid. The oxygen isotopic values are

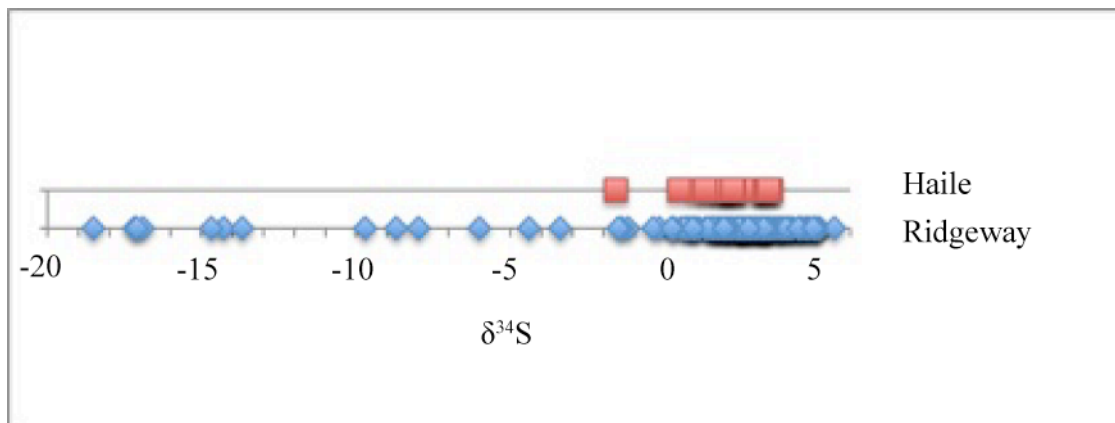


Figure 15: Comparison of $\delta^{34}\text{S}$ pyrite values for samples from Haile and Ridgeway. Ridgeway data is from Eager (1997).

not consistent with an orogenic type deposit. The sulfur data indicate that a seawater component was also involved and a shift in the environment of formation for CSB rocks from subaerial to subaqueous would allow for this scenario. It is common for epithermal deposits to have both magmatic and meteoric components, but seawater components are less common. However, the modern-day epithermal system seen at Conical Seamount near Lihir indicates that these deposits can form in a subaqueous setting rather than just the traditionally understood subaerial deposits.

The mineralogy at Haile composed of quartz, carbonate, chlorite, potassium feldspar, and sericite with the sulfides pyrite and pyrrhotite, is typical in low sulfidation type epithermal deposits. Arsenopyrite is also only present in minor amounts at Haile though it is a common sulfide mineral in orogenic type deposits and often the most abundant sulfide mineral in sedimentary-hosted orogenic deposits. Stibnite is also absent at Haile though common in many orogenic deposits.

The timing (~550 Ma) of molybdenite formation at Ridgeway and Haile is the same as the timing of arc-associated volcanism in the rocks of the CSB. While volcanism can be associated with orogenic type deposits, there is no known regional metamorphic event of the same age as the molybdenite formation at Ridgeway and Haile. Rather, peak metamorphism of Slate Belt rocks occurred during the Taconic Orogeny which was ~460-455 Ma in the southern Appalachians (Moecher et al., 2004). The association of gold with the volcano-sedimentary transition also supports the interpretation of gold forming shortly after volcanism in the arc rocks. As volcanism waned and sedimentation began, hot spring systems associated with the waning volcanism could have produced

epithermal mineralization in the overlying sediments. Brecciation, which is common at Haile, indicates that the sediments were present prior to mineralization.

Based on oxygen and pyrite stable isotope values measured from quartz and pyrite, mineralogy, and Re/Os age data along with interpretations of the history of the CSB it is possible to describe the formation of the deposits at Haile. Subaerial arc volcanism lead to the formation of the Persimmon Fork Formation rocks. As volcanism waned and the environment shifted to a rift related environment causing the arc to collapse below sea level (Feiss, 1995), sedimentation occurred, leading to deposition of the Richtex Formation. As the sediments of the Richtex Formation accumulated, the mixed magmatic/meteoric fluid plus minor amounts of seawater, driven by heat from the volcanic rocks, circulated through the sediments and formed the gold deposits at Haile and other CSB mines such as Ridgeway. Much later, during the Taconic Orogeny the arc collided with Laurentia and greenschist facies metamorphism occurred within the rocks of the Persimmon Fork and Richtex Formations. This collision produced substantial brittle deformation and likely remobilized gold and sulfides and produced the structural fabrics described by Tomkinson (1988) and Hayward (1992).

CHAPTER 7

CONCLUSIONS

1. $\delta^{18}\text{O}$ values for 138 quartz samples range from +5.9 to +9.1 per mil, and the range of calculated fluid oxygen isotope values based on reasonable temperatures for ore formation indicate Haile mineralization formed from a hydrothermal fluid that was a mixture of meteoric and magmatic fluids with a possible seawater component.
2. $\delta^{34}\text{S}$ values for 18 pyrite samples range from -1.6 to +3.4 per mil, indicating a magmatic fluid component influenced by a minor seawater component.
3. Evidence from stable isotope values, mineralogy, and Re/Os dating of molybdenite indicate that the deposits at the Haile Gold Mine formed due to a low sulfidation epithermal system active near the time of arc volcanism (~550 Ma).
4. Greenschist facies metamorphism occurred during the Taconic Orogeny (~460-455 Ma) when the CSB arc rocks collided with Laurentia overprinting and deforming the original deposit and causing some remobilization of gold and other components.

REFERENCES

- Ayuso, R. A., 1999, Gold deposits of the Carolina slate belt; zircon geochronology and isotopic characteristics: Abstracts with Programs – Geological Society of America, v. 31, p. A-3.
- Ayuso, R. A., Wooden, J. L., Foley, N. K., Seal, R. R. II, and Sinha, A. K., 2005, U-Pb zircon ages and Pb isotope geochemistry in gold deposits of the Carolina Slate Belt of South Carolina: *Economic Geology*, v. 100, no. 2, p. 225-252.
- Bell, H., 1982, Strata-bound sulfide deposits, wall-rock alteration, and associated tin-bearing minerals in the Carolina Slate Belt, South Carolina and Georgia: *Economic Geology*, v. 77, no. 2, p. 294-311.
- Bell, H., 1985, Some geologic aspects of the Haile Gold Mine, Lancaster County, South Carolina *in* Misra, K. C., ed., *Volcanogenic sulfide and precious metal mineralization in the southern Appalachians*: University of Tennessee, *Studies in Geology*, no. 16, p. 124-145.
- Bell, H., 1986, Geology of the Haile Gold Mine, Lancaster County, South Carolina *in* Neathery, T. L., ed., *Centennial Field Guide – Southeastern section of the Geological Society of America*, Geological Society of America Centennial Field Guide, v. 6, p. 247-250.
- Bell, H., III, Carpenter, R. H., and Feiss, P. G., 1980, Volcanogenic ore deposits of the Carolina Slate Belt, *in* Frey, R. W. ed., *Excursions in Southeastern Geology*, Field trip guidebook, GSA Annual Meeting, Atlanta, Georgia, v. 1, p. 149-178.
- Bierlein, F. P., and Crowe, D. E., 2000, Phanerozoic orogenic lode gold deposits *in* Hagemann, S. G. and Brown, P. E. ed., *Gold in 2000: Reviews in Economic Geology*, v. 13, p. 103-139.
- Clark, S. H. B., Gray, K. J., and Back, J. M., 1999, Geology of the Barite Hill Gold-Silver Deposit in the Southern Carolina Slate Belt: *Economic Geology*, v. 94, p. 1329-1346.
- Claypool, G.E., Holser, W.T., Kaplan, I.R., Sakai, H., Zak, I., 1980, The age curves of sulfur and oxygen isotopes in marine sulfate and their mutual interpretation: *Chemical Geology*, v. 28, p. 199-260.

- Eager, W. E., 1997, Geology and stable isotope geochemistry of the Ridgeway north pit Au-Ag deposit, Ridgeway, SC: Evidence for a syngenetic origin: Unpub. M.S. Thesis, University of Georgia 154p.
- Feiss, P. G., 1982a, Ore deposits of the northern parts of the Carolina Slate Belt, North Carolina: Geological Society of America Special Paper, no. 191, p. 153-164.
- Feiss, P. G., 1982b, Geochemistry and tectonic setting of the volcanics of the Carolina Slate Belt: *Economic Geology*, v. 77, p. 273-293.
- Feiss, P. G., 1988, Structural settings of the Haile mine, Lancaster Co., SC: Abstracts with Programs – Geological Society of America, v. 20, no. 4, p. 264.
- Feiss, P. G., 1995, The Carolina Terrane gold district; rift-related volcanogenic gold deposits of the southern Appalachian Piedmont: Abstracts with Programs – Geological Society of America, v. 27, p. 116.
- Feiss, P. G., Vance, R. K., and Wesolowski, D. J., 1993, Volcanic rock-hosted gold and base-metal mineralization associated with Neoproterozoic–Early Paleozoic back-arc extension in the Carolina terrane, southern Appalachian Piedmont: *Geology*, v. 21, p. 439-442.
- Feiss, P. G. and Wenner, D. B., 1989, Genesis of the Haile gold mine, Kershaw, SC: geological and stable isotopic constraints: Abstracts with Programs – Geological Society of America, v. 21, p. 15.
- Foley, N., Ayuso, R. A., Seal, R., II, 2001, Remnant colloform pyrite at the Haile Gold deposit, South Carolina: A textural key to genesis: *Economic Geology*, v. 96, p. 891-902.
- Fu, B., Kendrick, M. A., Fairmaid, A. M., Phillips, D., Wilson, C. J. L., and Mernagh, T. P., 2012, New constraints on fluid sources in orogenic gold deposits, Victoria, Australia: *Contributions to Mineralogy and Petrology*, v. 163, p. 427-447.
- Gibson, G. G., 1989, Trace Fossils from Late Precambrian Carolina Slate Belt, South-Central North Carolina: *Journal of Paleontology*, v. 63, p. 1-10.
- Gibson, G. G., Teeter, S. A., and Fedonkin, M. A., 1984, Ediacaran fossils from the Carolina slate belt, Stanly County, North Carolina: *Geology*, v. 12, p. 387-390.
- Gillon, K. A., Spence, W. H., Duckett, R. P., and Benson, C. J., 1995, Geology of the Ridgeway gold deposits, Ridgeway, South Carolina *in* Thompson, T. B. ed. Selected Mineral Deposits of the Gulf Coast and Southeastern United States: SEG Guidebook Series v. 24, p. 53-87.

- Goldfarb, R. J., Ayuso, R., Miller, M. L., Ebert, S. W., Marsh, E. E., Petsel, S. A., Miller, L. D., Bradley, D., Johnson, C., and McClelland, W., 2004, The Late Cretaceous Donlin Creek gold deposit, southwestern Alaska: Controls on epizonal ore formation: *Economic Geology*, v. 99, p. 643-671.
- Goldfarb, R. J., Dubé, B., Groves, D. I., Hart, C. J. R., and Gosselin, P., 2005, Distribution, character, and genesis of gold deposits in metamorphic terranes: *Economic Geology 100th Anniversary Volume*, p. 407-450.
- Groves, D. I., Goldfarb, R. J., Gebre-Mariam, M., Hagemann, S. G., and Robert F., 1998, Orogenic gold deposits: A proposed classification in the context of their crustal distribution and relationship to other gold deposit types: *Ore Geology Reviews*, v. 13, p. 7-27.
- “Haile Gold Mine.” 34°34’33.74” N and 80°31’51.69” W. **Google Earth**. March 26, 2012. April 25, 2013.
- Hardy, L. S., 1987, Mineralogy and petrology of the Haile gold mine, Lancaster County, South Carolina: Unpub. M.S. thesis, University of Georgia 96p.
- Hardy, L. S., 1989, Hydrothermal potassium feldspar at the Haile Gold Mine, South Carolina: *Economic Geology*, v. 84, no. 8, p. 2307-2310.
- Hatcher, R. D., Jr., 2010, The Appalachian orogeny: A brief summary, *in* Tollo, R. P., Bartholomew, M. J., Hibbard, J. P., and Karabinos, P. M. ed., *From Rodinia to Pangea: The Lithotectonic Record of the Appalachian Region*, The Geological Society of America Memoir 206. p. 1-20.
- Hayward, N., 1992, Controls on Syntectonic Replacement mineralization in parasitic antiforms, Haile Gold Mine, Carolina Slate Belt: *Economic Geology*, v. 87, no. 1, p. 91-112.
- Heald, P., Foley, N. K., and Hayba, D. O., 1987, Comparative anatomy of volcanic-hosted epithermal deposits: Acid-sulfate and adularia-sericite types: *Economic Geology*, v. 82, p. 1-26.
- Hedenquist, J. W., and Lowenstern, J. B., 1994, The role of magmas in the formation of hydrothermal ore deposits: *Nature*, v. 370, p. 519-527.
- Hibbard, J. P., Pollock, J. C., Brennan, M., Samson, S. D., and Secor, D., 2009, Significance of New Ediacaran fossils and U-Pb zircon ages from the Albemarle Group, Carolina Terrane of North Carolina: *Journal of Geology*, v. 117, p. 487-498.

- Jia, Y., Li, X., and Kerrich, R., 2001, Stable Isotope (O, H, S, C, and N) systematics of quartz vein systems in the turbidite-hosted central and north Deborah gold deposits of the Bendigo Gold Field, Central Victoria, Australia: Constraints on the origin of ore-forming fluids: *Economic Geology*, v. 96, p. 705-721.
- Kesler, S. E., Russell, N., Seaward, M., Rivera, J., McCurdy, K., Cumming, G. L., and Sutter, J. F., 1981, Geology and geochemistry of sulfide mineralization underlying the Pueblo Viejo gold-silver oxide deposit, Dominican Republic: *Economic Geology*, v. 76, p. 1096-1117.
- Klein, T. L. and Criss, R. E., 1988, An oxygen isotope and geochemical study of meteoric – hydrothermal systems at Pilot Mountain and selected other localities, Carolina Slate Belt: *Economic Geology*, v. 83, no. 4, p. 801-821.
- Klein, T. L., Cunningham, C. G., Logan, M. A. V., and Seal, R. R., II, 2007, The Russell Gold Deposit, Carolina Slate Belt, North Carolina: *Economic Geology*, v. 102, p. 239-256.
- LeHuray, A. P., 1987, U-Pb and Th-Pb whole-rock isochrons from metavolcanic rocks of the Carolina slate belt: *Geological Society of America Bulletin*, v. 99, p. 354-361.
- Maddry, J. W. and Kilbey, T. R., 1995, Geology of the Haile Gold Mine *in* Crowe, D. E. ed. *Gold Deposits of the Carolina Slate Belt*, *in* Thompson, T. B. ed. *Selected Mineral Deposits of the Gulf Coast and Southeastern United States: SEG Guidebook Series v. 24*, p. 147-172.
- Matsuhisa, Y., Morishita, Y., and Sato, T., 1985, Oxygen and carbon isotope variation in gold-bearing hydrothermal veins in the Kushikino mining area, southern Kyushu, Japan: *Economic Geology*, v. 80, p. 283-293.
- McKee, L. H., and Butler, J. R., 1985, Hydrothermal alteration and mineralization at four gold mines in southern Union County, North Carolina Slate Belt *in* Misra, K. C., ed., *Volcanogenic sulfide and precious metal mineralization in the southern Appalachians: University of Tennessee Studies in Geology no. 16*, p. 113-123.
- Mobley, R., Creaser, R. A., and Yogodzinski, G., 2012, Re-Os dating of molybdenite formation at the Haile Gold Mine, Lancaster County, South Carolina: *Abstracts with Programs – Geological Society of America*, v. 44, no. 7, p. 199.
- Moecher, D. P., Samson, S. D., and Miller, C. F., 2004, Precise time and conditions of peak Taconian granulite facies metamorphism in the southern Appalachian orogeny, USA, with implications for zircon behavior during crustal melting events: *The Journal of Geology*, v. 112, p. 289-304.

- Müller, D., Kaminski, K., Uhlig, S., Graupner, T., Herzig, P. M., and Hunt, S., 2002, The transition from porphyry- to epithermal-style gold mineralization at Ladolam, Lihir Island, Papua New Guinea: a reconnaissance study: *Mineralium Deposita*, v. 37, p. 61-74.
- Noel, J. R., Spariosu, D. J., and Dallmeyer, R. D., 1988, Paleomagnetism and $^{40}\text{Ar}/^{39}\text{Ar}$ ages from the Carolina Slate Belt, Albemarle, North Carolina: Implications for terrane amalgamation with North America: *Geology*, v. 16, no. 1, p. 64-68.
- Ohmoto, H., 1972, Systematics of sulfur and carbon isotopes in hydrothermal ore deposits: *Economic Geology*, v. 67, p. 551-578.
- Ohmoto, H., 1986, Stable isotope geochemistry of ore deposits: *Reviews in Mineralogy*, v. 16, p. 491-559.
- Ohmoto, H., Rye, R. O., 1979, Isotopes of sulfur and carbon *in* Barnes, H. L., ed., *Geochemistry of Hydrothermal Ore Deposits*, 2nd ed., Wiley, New York, p. 509-567.
- O'Neil, J. R. and Silberman, M. L., 1974, Stable isotope relations in epithermal Au-Ag deposits: *Economic Geology*, v. 69, no. 6, p. 902-909.
- Petersen, S., Herzig, P. M., Hannington, M. D., Jonasson, I. R., and Arribas, A., Jr., 2002, Submarine gold mineralization near Lihir Island, New Ireland Fore-Arc, Papua New Guinea: *Economic Geology*, v. 97, p. 1795-1813.
- Rast, N., O'Brien, B. H., and Wardle, R. J., 1976, Relationships between Precambrian and lower Palaeozoic rocks of the 'Avalon Platform' in New Brunswick, the Northeast Appalachians and the British Isles: *Tectonophysics*, v. 30, p. 315-338.
- Rye, R. O., 1993, The evolution of magmatic fluids in the epithermal environment: The stable isotope perspective: *Economic Geology*, v. 88, p. 733-753.
- Samson, S., Palmer, A. R., Robison, R. A., and Secor, D. T., Jr., 1990, Biogeographical significance of Cambrian trilobites from the Carolina slate belt: *Geological Society of America Bulletin*, v. 102, no. 11, p. 1459-1470.
- Schmidt, R. G. and Klein, T. L., 1985, High-Alumina hydrothermal alteration systems and their role in mineral exploration, southeastern United States *in* Krafft, Kathleen, *USGS Research on Mineral Resources - 1985, Program and Abstracts*. U. S. Geological Survey Circular 949, p. 47-48.

- Seal, R. R., Ayuso, R. A., Foley, N. K., and Clark, S. H. B., 2001, Sulfur and lead isotope geochemistry of hypogene mineralization at the Barite Hill Gold Deposit, Carolina Slate Belt, southeastern United States: a window into and through regional metamorphism: *Mineralium Deposita*, v. 36, p. 137-148.
- Secor, D. T., Jr., Samson, S. L., Snoke, A. W., and Palmer, A. R., 1983, Confirmation of the Carolina Slate Belt as an exotic terrane: *Science*, v. 221, no. 4611, p. 649-651.
- Simmons, S. F., White, N. C., and John, D. A., 2005, Geological characteristics of epithermal precious and base metal deposits: *Economic Geology* 100th Anniversary Volume, p. 485-522.
- Snider, J., Marek, J., Drielick, T. L., Finch, A., and Gochnour, L.P., 2012, Haile Gold Mine Project Form 43-101 Technical Report: [http://www.romarco.com/files/110137_NI_43-101-Report_Haile Gold Mine Final_Condensed\[6\].pdf](http://www.romarco.com/files/110137_NI_43-101-Report_Haile_Gold_Mine_Final_Condensed[6].pdf)
- Snoke, A. W., Secor, D. T., Jr., Bramlett, K. W., and Prowell, D. C., 1980, Geology of the eastern Piedmont fault system in South Carolina and eastern Georgia *in* Frey, R. W., ed., *Excursion in Southeastern Geology*, v. 1, p. 59-100.
- Speer, W. E., and Maddry, J. W., 1993, Geology and recent discoveries at the Haile Gold Mine, Lancaster County, South Carolina: *South Carolina Geology*, v. 35, p. 9-26.
- Spence, W. H., Worthington, J. E., Jones, E. M., and Kiff, I. T., 1980, Origin of the gold mineralization at the Haile Mine, Lancaster County, South Carolina: *Mining Engineering*, v. 32, p. 70-73.
- Spicuzza, M. J., Valley, J. W., John, M. J., Girard, J. P., and Fouillac, A. M., 1998, The rapid heating, defocused beam technique: a CO₂-laser-based method for highly precise and accurate determination of $\delta^{18}\text{O}$ values of quartz: *Chemical Geology*, v. 144, p. 195-203.
- Stein, H. J., Markey, R. J., Morgan, J. W., Hannah, J. L., Zák, K., and Sundblad, K., 1997, Re-Os dating of shear-hosted Au deposits using molybdenite, *in* Papunen, H., ed.: *Mineral Deposits: research and exploration – where do they meet?*: Rotterdam, Balkema, p. 313-317.
- Taylor, H. P., Jr., 1974, The application of oxygen and hydrogen isotope studies to problems of hydrothermal alteration and ore deposition: *Economic Geology*, v. 69, no. 6, p. 843-883.
- Tomkinson, M. J., 1988, Gold mineralization in phyllonites at the Haile Mine, South Carolina: *Economic Geology*, v. 83, no. 7, p. 1392-1400.
- Ueda, A., and Krouse, H. R., 1986, Direct conversion of sulphide and sulphate minerals to SO₂ for isotope analyses: *Geochemical Journal*, v. 20, p. 209-212.

- Vennemann, T. W., Muntean, J. L., Kesler, S. E., O'Neil, J. R., Valley, J. W., and Russell, N., 1993, Stable isotope evidence for magmatic fluids in the Pueblo Viejo epithermal acid sulfate Au-Ag deposit, Dominican Republic: *Economic Geology*, v. 88, p. 55-71.
- Vick, H. K., Channell, E. T., and Opdyke, N. D., 1987, Ordovician docking of the Carolina Slate Belt: Paleomagnetic data: *Tectonics*, v. 6, no. 5, p. 573-583.
- White, N. C., and Hedenquist, J. W., 1990, Epithermal environments and styles of mineralization: variations and their causes, and guidelines for exploration: *Journal of Geochemical Exploration*, v. 36, p. 445-474.
- Whitney, J. A., Paris, T. A., Carpenter, R. H., and Hartley, M. E., III, 1978, Volcanic evolution of the southern slate belt of Georgia and South Carolina: A primitive oceanic island arc: *Journal of Geology*, v. 86, p. 173-192.
- Worthington, J. E., 1992, The Carolina Slate Belt and its gold deposits: reflections after a quarter century: *South Carolina Geology*, v. 35, p. 1-8.
- Worthington, J. E., and Kiff, I. T., 1970, A suggested volcanogenic origin for certain gold deposits in the Slate Belt of the North Carolina Piedmont: *Economic Geology*, v. 65, p. 529-537.
- Worthington, J. E., Kiff, I. T., Jones, E. M. and Chapman, P. E., 1980, Applications of the hot springs or fumarolic model in prospecting for lode gold deposits: *Mining Engineering*, v. 32, p. 73-79.
- Wright, J. E., and Seiders, V. M., 1980, Age of zircon from volcanic rocks of the central North Carolina Piedmont and tectonic implications for the Carolina volcanic slate belt: *GSA Bulletin*, v. 91, no. 5, p. 287-294.
- Zwaschka, M. and Scheetz, J. W., 1995, Detailed mine geology of the Brewer gold mine, Jefferson, South Carolina *in* Thompson, T. B. ed. *Selected Mineral Deposits of the Gulf Coast and Southeastern United States: SEG Guidebook Series v. 24*, p. 95-141.

APPENDIX A

Table of $\delta^{18}\text{O}$ values, $\delta^{34}\text{S}$ values, and sample descriptions

Sample #	$\delta^{18}\text{O}$	$\delta^{34}\text{S}$	Description
DDH347-219-1	7.5	-1.6	2-3cm wide vein/band of quartz with disseminated to massive pyrite
DDH347-221	7.5		~1 cm wide milky white quartz vein with minor sericite
DDH347-249-1	7.1		Quartz flooding with very fine grained pyrite in silicified metasediments with potassium feldspar
DDH347-268	6.8		2-4 cm wide milky white quartz vein/flooding crosscutting silicified sediments
DDH347-282	7.4		~1 mm wide thin clear quartz vein crosscutting silicified sediments
DDH347-292-1	7.7		Quartz-pyrite flooding/veins crosscutting silicified sediments
DDH347-292-2	7.2		Thin (<0.5cm) clear quartz vein crosscutting silicified sediments
DDH347-308		1.3	Quartz-pyrite veining/flooding across silicified sediments
DDH347-328-1	6.6		Thin (<0.5 cm) clear quartz vein crosscutting silicified sediments
DDH347-407-2	7.1		Thin (<0.5 cm) clear quartz vein crosscutting silicified sediments
DDH351-723-1	7.2		Quartz from pervasively silicified zone with minor sericite
DDH351-723-2	6.7		White quartz flooding in silicified sediments
DDH351-742-1	7.7	2.2	Zone of quartz and fine-grained disseminated pyrite
DDH351-755-1	7.3		0.5-1 cm wide white quartz vein/flooding with minor sericite crosscutting silicified sediments
DDH351-782	8.1		Thin (~0.5cm) clear to grey quartz vein crosscutting silicified sediments with potassium feldspar
DDH351-825-2	6.9		Clear to milky white quartz vein crosscutting silicified sediments
DDH351-867-1	8.2		~1 cm wide milky white quartz vein
DDH351-867-2	7.5		White quartz vein crosscutting silicified sediments
DDH368-454-1	7.7		White bull quartz
DDH368-777-1	8.1		White bull quartz
DDH368-931-1	7.9		Thin (<0.5 cm) clear quartz vein crosscutting silicified metasediments
DDH368-936-1	8.8		Quartz from pervasively silicified zone with minor sericite

Sample #	$\delta^{18}\text{O}$	$\delta^{34}\text{S}$	Description
DDH369-471-1	7.7		White bull quartz
DDH369-817-1	7.5		White bull quartz
DDH370-1497-1	7.9		Milky white quartz flooding with minor sericite
DDH370-1503-2	8.1		Quartz-pyrite zone in pervasively silicified sediments
DDH370-1510-3	7.6		Quartz from a pervasively silicified zone with minor sericite
DDH370-1537-1	8.1		Quartz from a pervasively silicified zone with minor sericite and very fine-grained pyrite
DDH370-1550-1	8.2		Quartz from a pervasively silicified zone with minor sericite and pyrite
DDH370-1550-2	8.0		Quartz-pyrite vein crosscutting silicified sediments
DDH370-1572-1	7.5		White bull quartz
DDH384-927-1	6.5		Band of massive pyrite and quartz flooding
DDH384-927-2	7.0		Pervasive quartz flooding with minor sericite and very fine-grained pyrite
DDH384-1135-1	6.3		Milky white quartz flooding
DDH384-1162-1	5.9		Milky white quartz flooding with minor sericite
DDH384-1162-2	6.9		Quartz from a pervasively silicified zone with minor sericite and pyrite
DDH384-1163-1	7.2		Quartz from a pervasively silicified zone with minor sericite
DDH384-1163-2		2.9	Pyrite in zone of pervasive silicification
DDH384-1180	7.9		~0.5 cm wide milky white quartz vein crosscutting silicified sediments
DDH384-1253-1	7.6		Thin (~0.5cm) quartz-pyrite vein crosscutting silicified sediments
DDH389-702	7.8		Clear quartz from a pervasively silicified zone
DDH389-929-1	7.3		0.5-1 cm wide white quartz vein crosscutting silicified sediments
DDH389-1008	7.2		Milky white quartz flooding with minor sericite
DDH389-1009	7.8		Quartz from a pervasively silicified zone with minor sericite
DDH389-1124		3.4	Massive pyrite around edges of quartz vein
DDH389-1149	6.4		~1 cm wide milky white quartz vein
DDH389-1165-1	7.1		~1cm wide clear quartz center of quartz-potassium feldspar banded vein
DDH389-1184-1	7.2		0.5-1 cm wide milky white quartz vein crosscutting silicified metasediments

Sample #	$\delta^{18}\text{O}$	$\delta^{34}\text{S}$	Description
DDH389-1200	6.8		White bull quartz
DDH396-833-1	7.2		~0.5 cm milky white its flooding/vein crosscutting silicified sediments with very fine-grained disseminated pyrite
DDH396-833-2	7.4		milky white quartz flooding through silicified sediments with very fine-grained disseminated pyrite
DDH396-907-1	7.3		Milky white quartz flooding
DDH396-937-1	7.9		0.5-1 cm wide milky white quartz vein crosscutting silicified sediments
DDH396-1034	6.3		White bull quartz
DDH396-1052-1	7.3		Milky white quartz flooding with minor sericite and very fine-grained pyrite
DDH396-1068-1	7.3	3.3	3-4 cm wide quartz and fine-grained pyrite vein/band across silicified sediments
DDH396-1101-2	7.0		~0.5 cm wide white quartz vein crosscutting silicified sediments
DDH396-1116-1	7.1		Flooding/vein of quartz and very fine-grained pyrite across pervasively silicified sediments
DDH396-1168-2	7.5		Clear quartz veins crosscutting silicified metasediments with potassium feldspar
DDH396-1263-1	7.4		Milky white quartz flooding with minor sericite from a zone of silicified sediments
DDH396-1331-1	6.3		Thin (~0.25 cm) clear quartz band of banded quartz-potassium feldspar vein
DDH396-1383-2	7.3		Thin (<0.5 cm) clear to white quartz veins crosscutting other quartz veins and silicified sediments
DDH396-1450-1	7.5		Milky white quartz flooding from pervasively silicified zone
DDH396-1450-2	7.6		~1 cm wide clear to milky white quartz vein with minor sericite and pyrite
DDH396-1464-1	7.4		Thin (<0.5 cm) quartz with very fine-grained pyrite bands of quartz-pyrite banded vein
RCT0002-675-1	7.6		White bull quartz
RCT0002-1181		3.2	~1 mm wide quartz-pyrite veins across pervasively silicified sediments
RCT0002-1781-1	7.8		0.25-0.5 cm wide quartz-sulfide veins crosscutting silicified sediments
RCT0003-1007-1	7.7		Quartz from quartz-carbonate vein
RCT0003-1401-1	8.7		Milky white quartz flooding with minor sericite
RCT0003-1420-1	8.2		Quartz-pyrite vein/flooding crosscutting pervasively silicified sediments

Sample #	$\delta^{18}\text{O}$	$\delta^{34}\text{S}$	Description
RCT0003-1423-1	8.1		Thin (<0.5 cm) clear quartz vein crosscutting silicified sediments
RCT0003-1423-2	8.3		Very thin (<1mm) clear quartz vein
RCT0003-1441-1	6.9		Milky white quartz flooding with minor sericite
RCT0003-1441-2	6.9		Milky white quartz flooding with minor sericite
RCT0003-1457-1	8.4		Thin (<0.5 cm) clear quartz vein crosscutting silicified sediments
RCT0004-1550b-1	6.9		1-2 mm wide clear quartz veins
RCT0004-1550b-2	7.9		Pervasively silicified breccia clast with disseminated pyrite
RCT0004-1561-1	7.8		Thin (~0.25 cm) quartz-sulfide vein crosscutting pervasively silicified sediments
RCT0004-1656-1	7.4		Clear to white quartz flooding
RCT0008-1131-1	9.1		White bull quartz
RCT0008-1313-1	8.9		1-2 mm wide clear quartz veins
RCT0008-1313-2	8.0	1.4	Zone of pervasive silicification with disseminated pyrite
RCT0008-1329-1	6.9		<1 mm wide clear thin quartz vein
RCT0008-1342-1	7.7		Milky white quartz vein with minor sericite crosscutting silicified sediments
RCT0008-1342-2	7.7		Pervasive quartz with disseminated pyrite
RCT0008-1343-1	7.5		Milky white quartz vein crosscutting silicified sediments
RCT0008-1379-1	6.7		Thin (<0.5 cm) clear quartz vein crosscutting silicified sediments
RCT0008-1380b-1	6.7		Quartz from zone of pervasive silicification
RCT0013-2131-1	8.1		0.5 cm wide vein/band of quartz and very fine-grained pyrite
RCT0014-944-1	7.2		Thin (<0.5 cm) milky white quartz vein crosscutting silicified sediments
RCT0014-1076-1	7.3		White bull quartz
RCT0025-1131-1	7.7		~1 mm wide thin clear quartz vein crosscutting silicified sediments with potassium feldspar
RCT0025-1199		1.1	Pyrite from zone of pervasive silicification with disseminated pyrite
RCT0025-1328-1	7.9		~1 cm wide quartz-sulfide vein crosscutting silicified sediments
RCT0033-1085	7.5		Clear quartz from pervasively silicified zone
RCT0033-1111-1	7.3	2.1	~0.5 cm wide quartz-pyrite veining/stockwork crosscutting pervasively silicified sediments

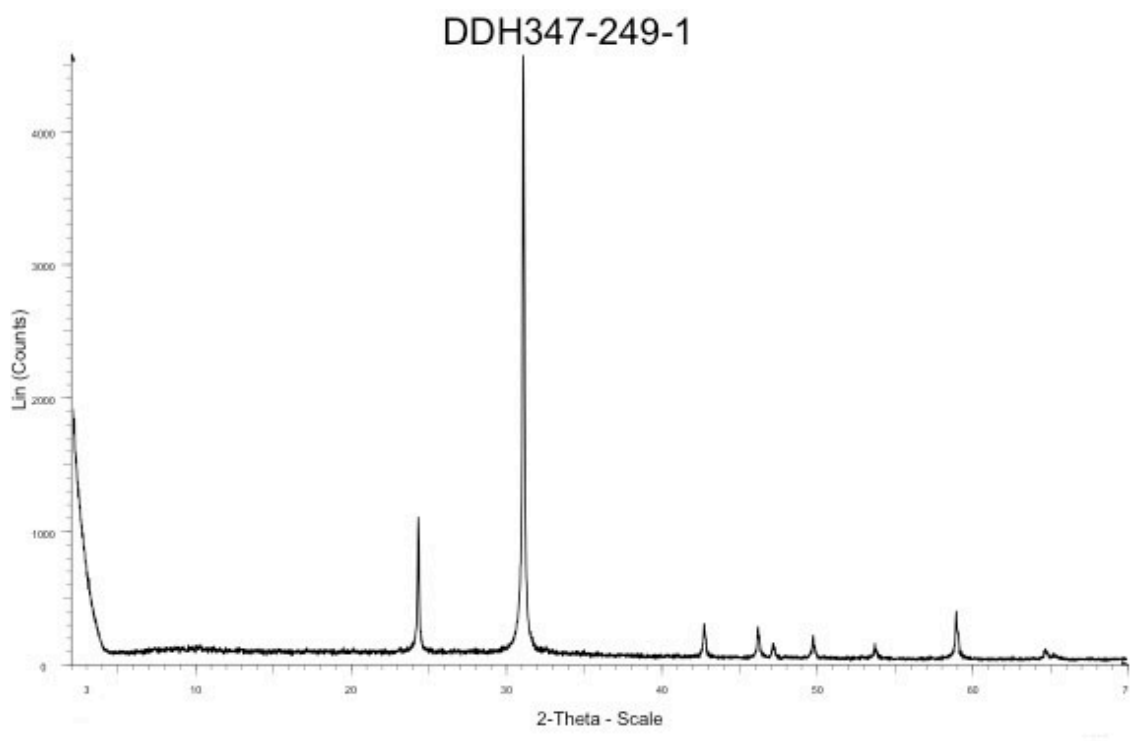
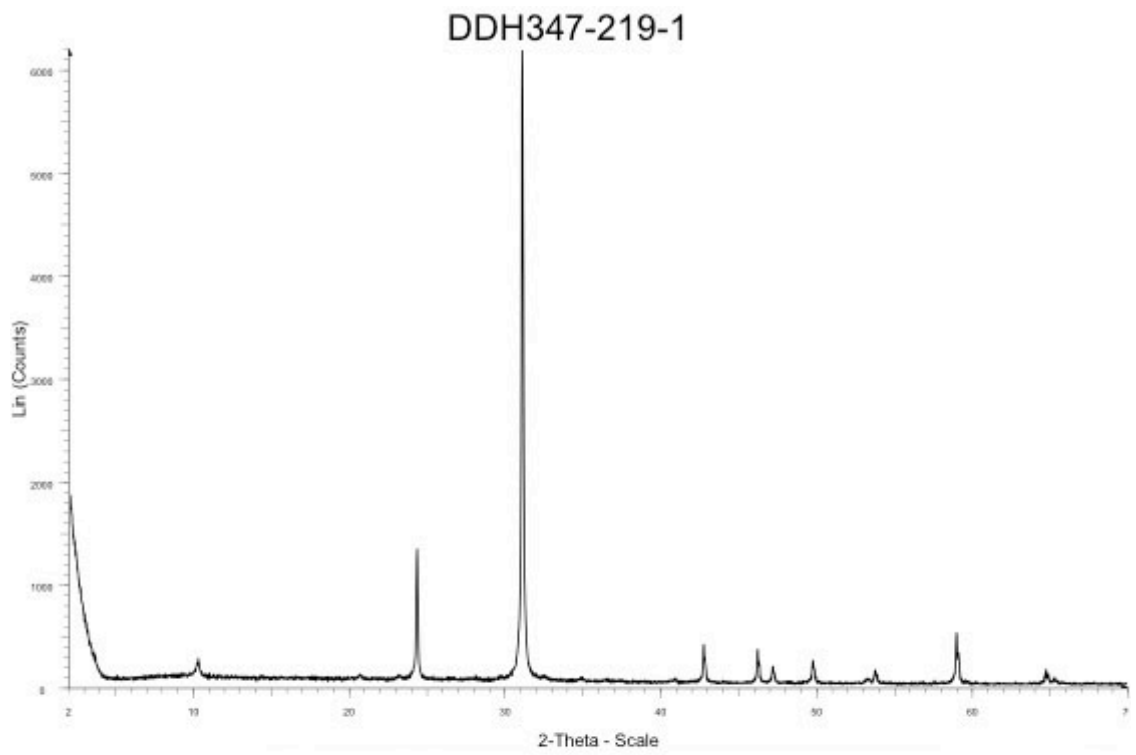
Sample #	$\delta^{18}\text{O}$	$\delta^{34}\text{S}$	Description
RCT0033-1147		1.9	Massive pyrite around edges of quartz-pyrite banded vein
RCT0034-1017-1	7.2		Clear quartz flooding with minor sericite
RCT0034-1017-2	7.0		Thin <0.5 cm wide clear quartz vein crosscutting silicified sediments
RCT0034-1053-1	8.0		~0.5 cm white quartz vein crosscutting silicified sediments with disseminated pyrite
RCT0034-1118-1	7.4		Milky white quartz flooding with minor sericite
RCT0034-1118-2	7.1		Quartz from a zone of pervasively silicified sediments with minor sericite and very fine-grained pyrite
RCT0035-615-2	7.6		~1 cm wide quartz-carbonate vein crosscutting silicified sediments
RCT0035-949	7.0		Clear to milky white quartz flooding
RCT0035-976	6.6		~1 cm wide white quartz vein crosscutting silicified sediments
RCT0051-2359-1	6.8		Milky white quartz from a zone of pervasively silicified sediments
RCT0051-2365	6.7		Clear quartz from quartz-carbonate vein (~0.5-1 cm wide)
RCT0051-2467	7.0		Quartz from quartz-carbonate vein
RCT0051-2474	7.1		~1 cm wide white quartz vein crosscutting silicified sediments
RCT0051-2489	7.0		~2 mm wide clear quartz vein crosscutting silicified sediments
RCT0056-595	7.9		Milky white quartz from a pervasively silicified zone
RCT0056-1142	8.0		~1 mm wide clear quartz vein crosscutting silicified sediments
RCT0056-1379		2.2	Massive pyrite flooding/vein with quartz
RCT0056-1390-1	8.3		0.5-1 cm wide bands of quartz and very fine-grained pyrite in a banded quartz-pyrite vein with minor chlorite
RCT0056-1430-1	7.7		~0.5 cm wide clear quartz vein crosscutting silicified sediments
RCT0056-1442-1	7.9		~2 cm wide quartz vein with disseminated very fine-grained pyrite
RCT0056-1453-1	7.9	0.5	Pervasively silicified zone of quartz and very fine-grained disseminated pyrite
RCT0061-857	7.3		White bull quartz
RCT0061-863	7.1		Quartz from pervasively silicified zone with minor sericite

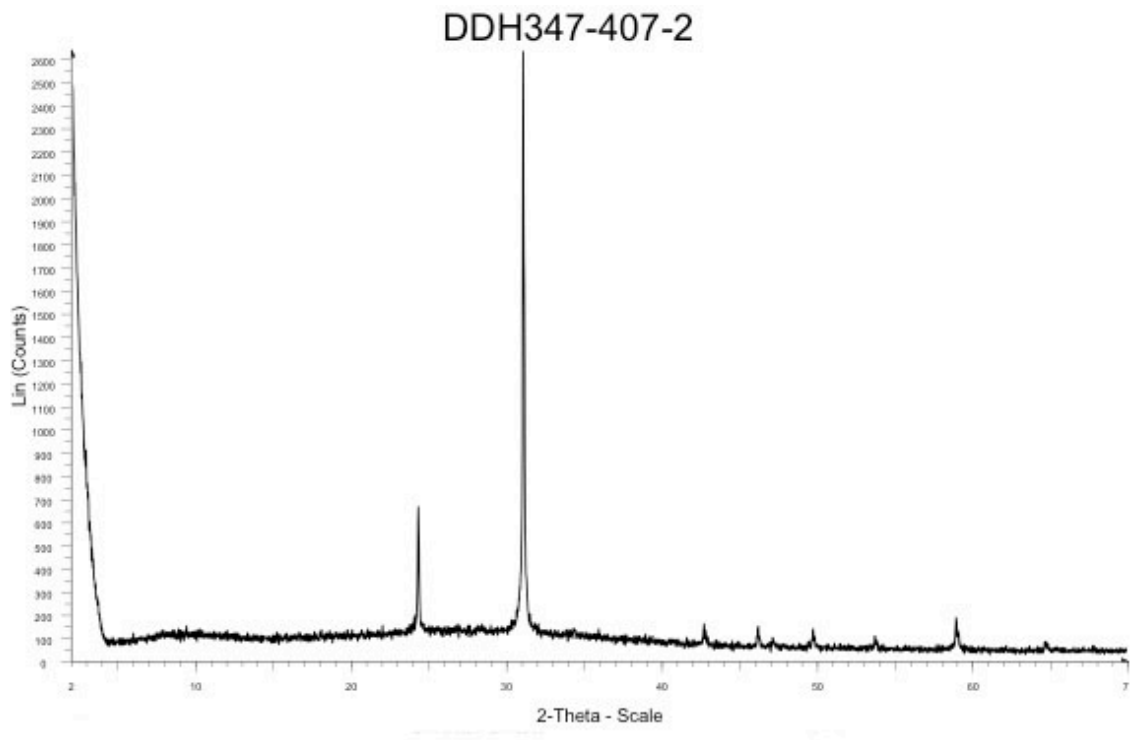
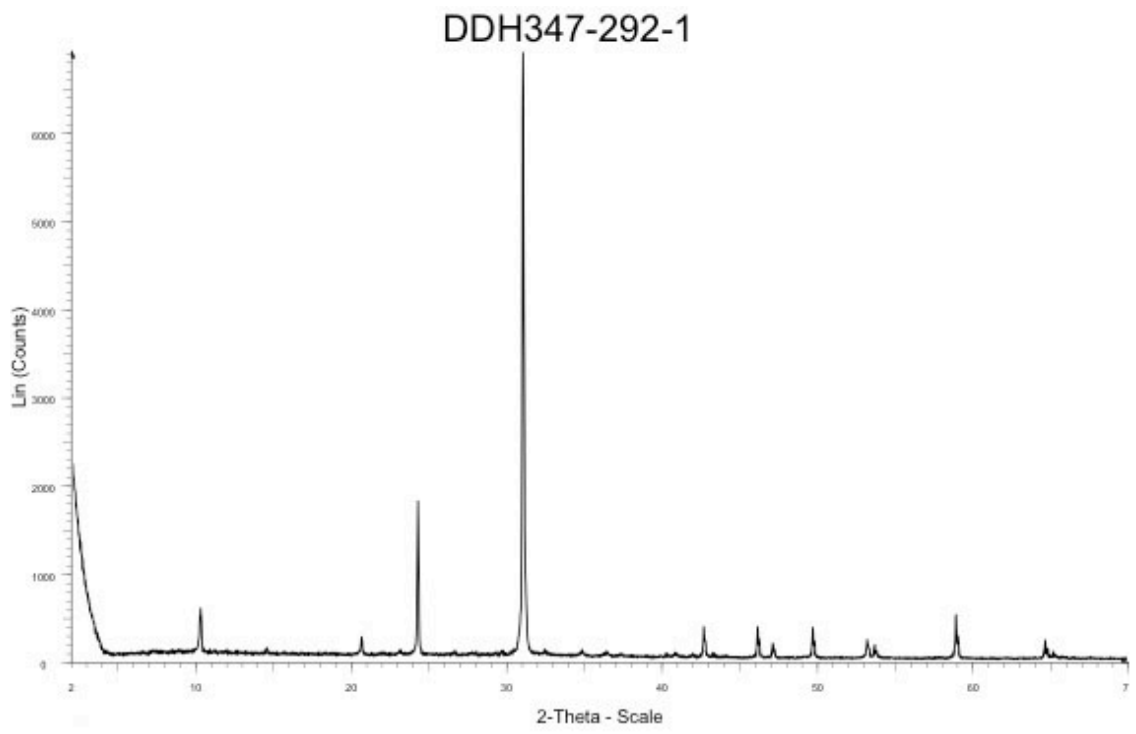
Sample #	$\delta^{18}\text{O}$	$\delta^{34}\text{S}$	Description
RCT0061-897	7.5		Milky white quartz flooding from a pervasively silicified zone
RCT0061-929	7.6		Clear thin (<0.5 cm) quartz veins crosscutting silicified sediments
RCT0061-950	7.2		~0.5 cm wide milky white quartz vein crosscutting silicified sediments
RCT0061-977-1	7.2		~0.5 cm wide milky white quartz vein crosscutting silicified sediments
RCT0061-977-2	7.4		Clear pervasive quartz flooding with minor sericite and potassium-feldspar
RCT0061-1014-1	7.5		~2 cm wide vein of quartz with very fine-grained disseminated pyrite crosscutting silicified sediments
RCT0069-805-1	7.5	3.3	2-3 cm wide vein of quartz and very fine-grained pyrite crosscutting silicified sediments
RCT0069-805-2	6.7		~0.5 cm wide white quartz vein crosscutting silicified sediments
RCT0069-848-2	6.7		~1 mm wide thin clear quartz vein crosscutting silicified sediments and other veins
RCT0069-848-3	7.5		~1-1.5 cm wide milky white quartz vein with minor sericite crosscutting silicified sediments
RCT0069-890	7.1		Milky white quartz flooding/veins with minor sericite crosscutting silicified sediments with potassium feldspar
RCT0069-973-1	7.3		Quartz-pyrite bands of banded quartz and quartz-pyrite vein
RCT0069-982-1	6.7		White quartz with minor sericite from a zone of pervasively silicified sediments
RCT0069-1077	7.5		Milky white quartz from a zone of pervasively silicified sediments with minor sericite and very fine-grained pyrite
RCT0069-1094		2.2	2-4 cm wide quartz and fine grained pyrite veins/bands across silicified sediments
RCT0087-895-1	7.4		~1 cm wide milky white quartz vein with minor sericite
RCT0087-895-2	7.9		<1 mm wide clear thin quartz vein
RCT0087-945-1	7.3		~0.5 cm wide white quartz band in banded quartz-pyrite vein
RCT0087-945-2	7.1		Clear quartz flooding with minor sericite and potassium feldspar

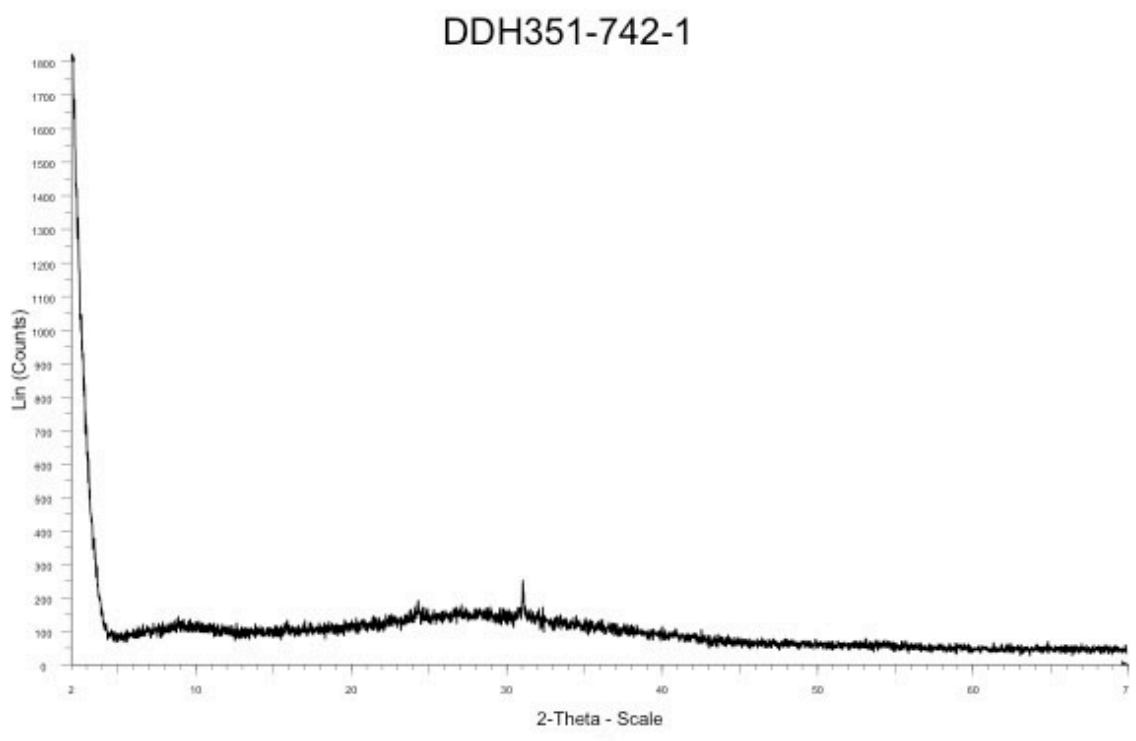
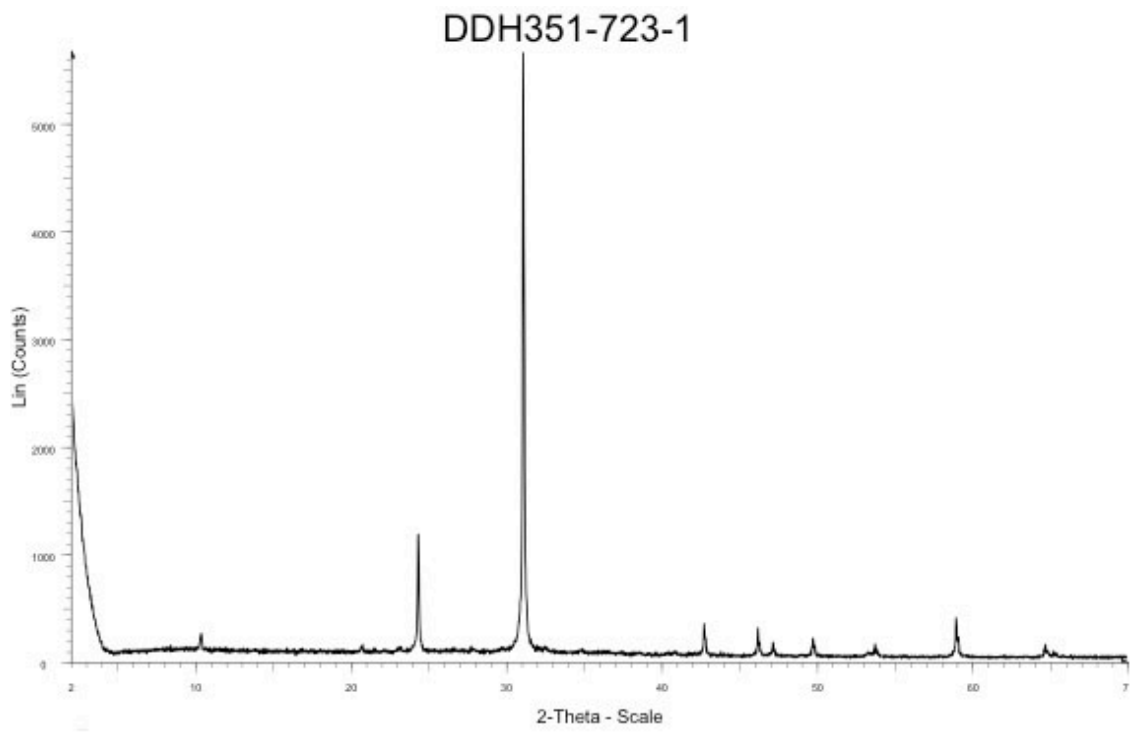
Sample #	$\delta^{18}\text{O}$	$\delta^{34}\text{S}$	Description
RCT0087-1061		2.2	Pyrite from a pervasively silicified zone with disseminated pyrite
RCT0087-1077	7.4		~1 mm wide thin clear quartz vein crosscutting silicified sediments with potassium feldspar
RCT0087-1114-1	7.0		~0.25 cm wide clear quartz portion of quartz-potassium feldspar vein
RCT0087-1125-1	6.8		Clear quartz band of ~1 cm wide quartz-potassium feldspar vein
RCT0087-1132-1	7.4		White quartz flooding/vein with minor sericite
RCT0087-1132-2	7.3		light grey ~1 cm wide quartz vein with minor sericite
RCT0087-1157-1	7.7	3.2	~1cm wide quartz-pyrite band of banded quartz-pyrite-potassium feldspar vein
RCT0087-1174-1	7.8		~1 cm wide quartz and very fine-grained pyrite vein

APPENDIX B

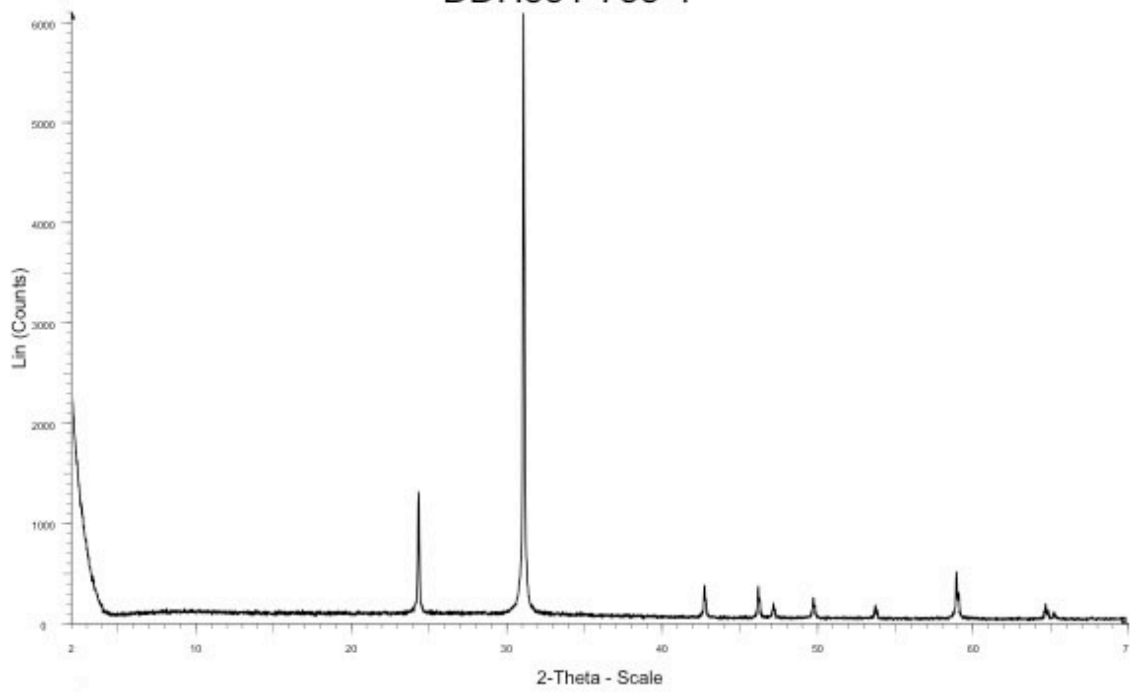
XRD data for selected quartz samples



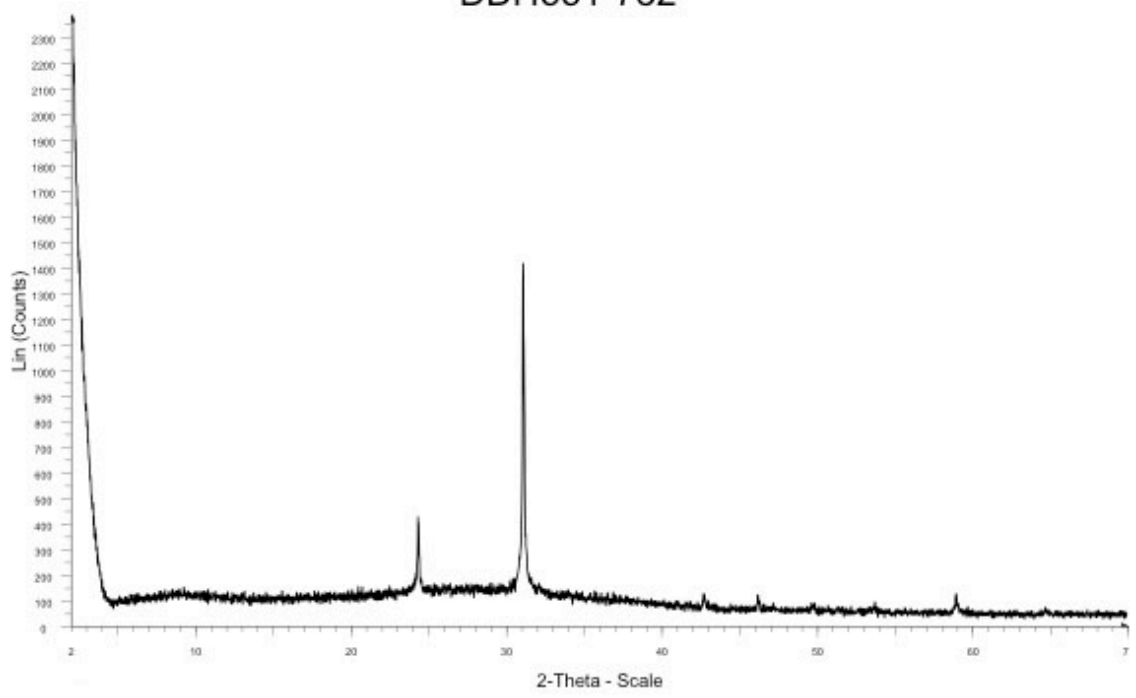




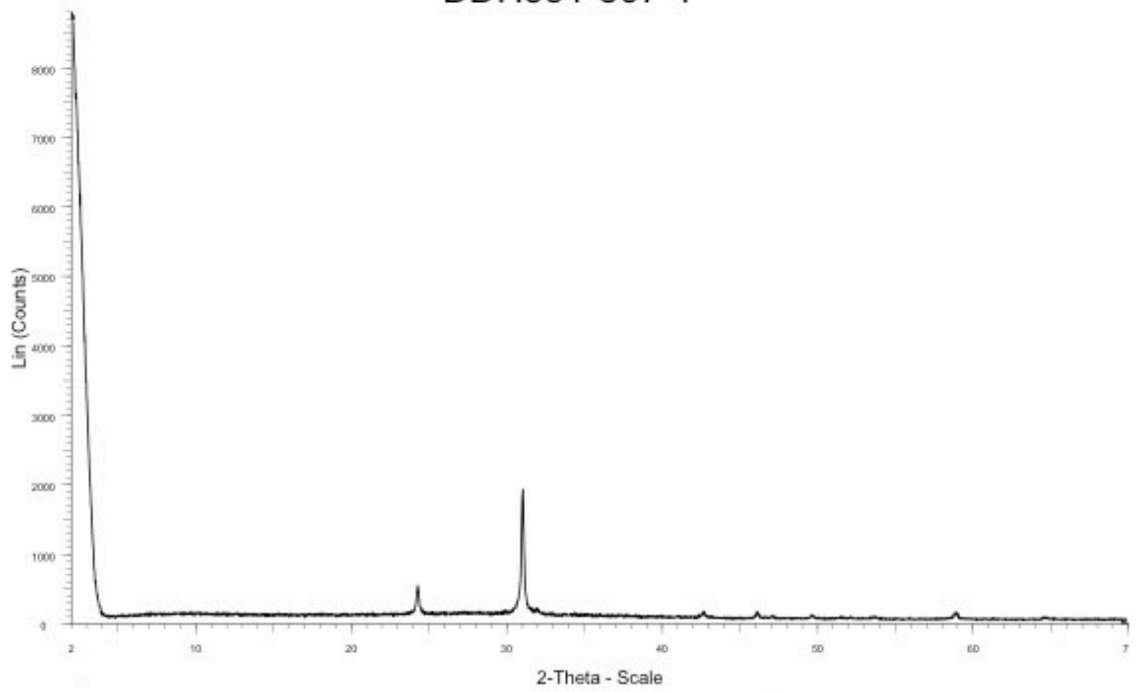
DDH351-755-1



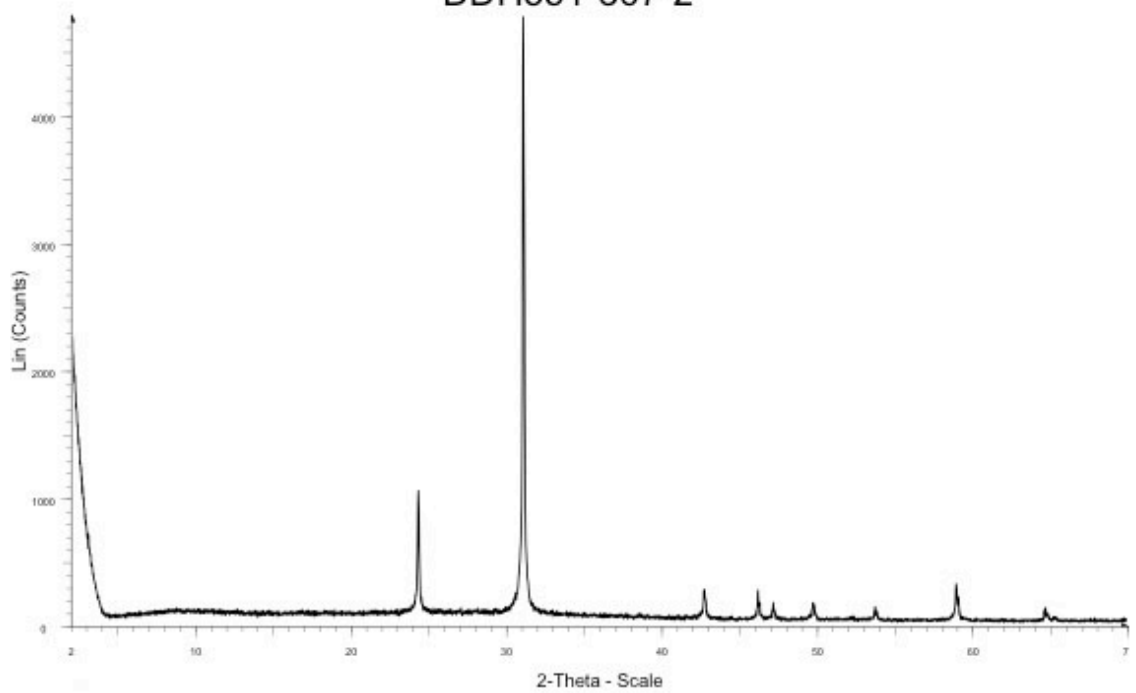
DDH351-782

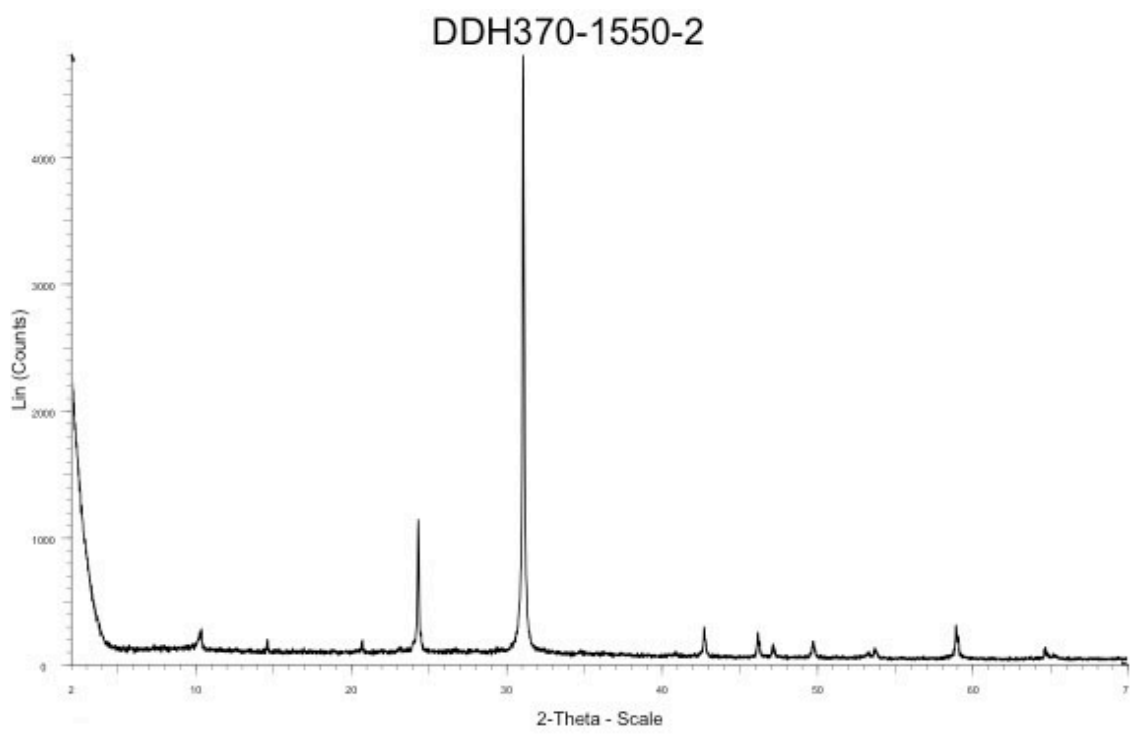
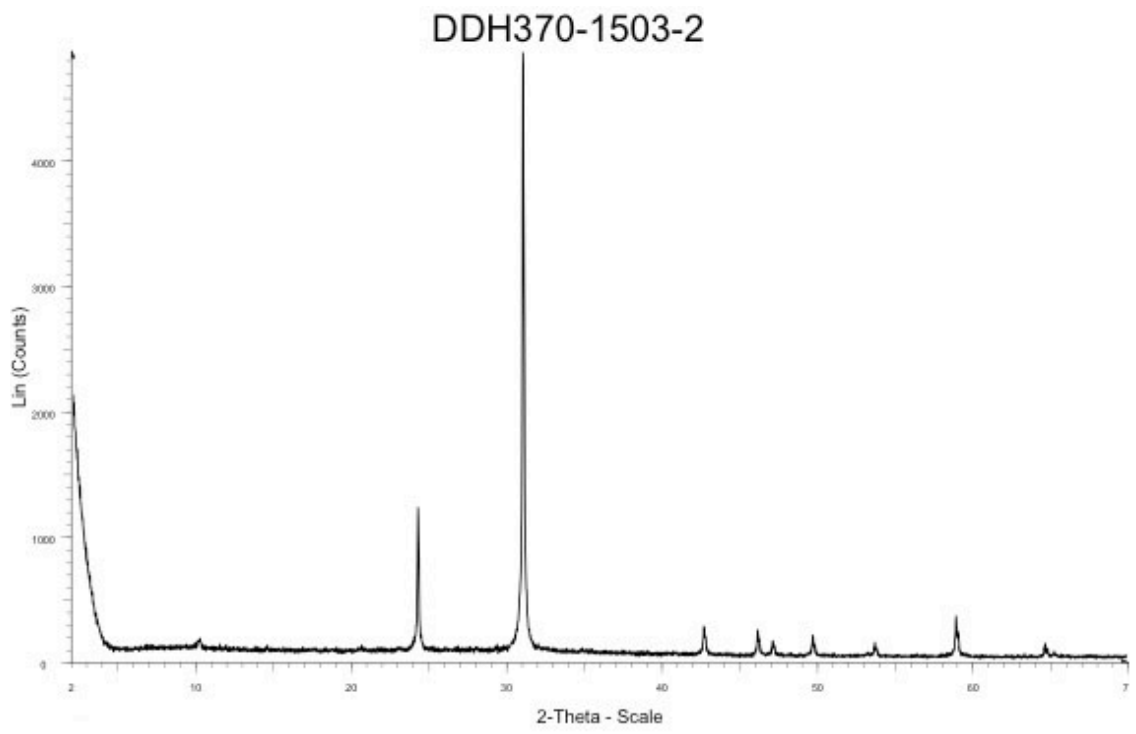


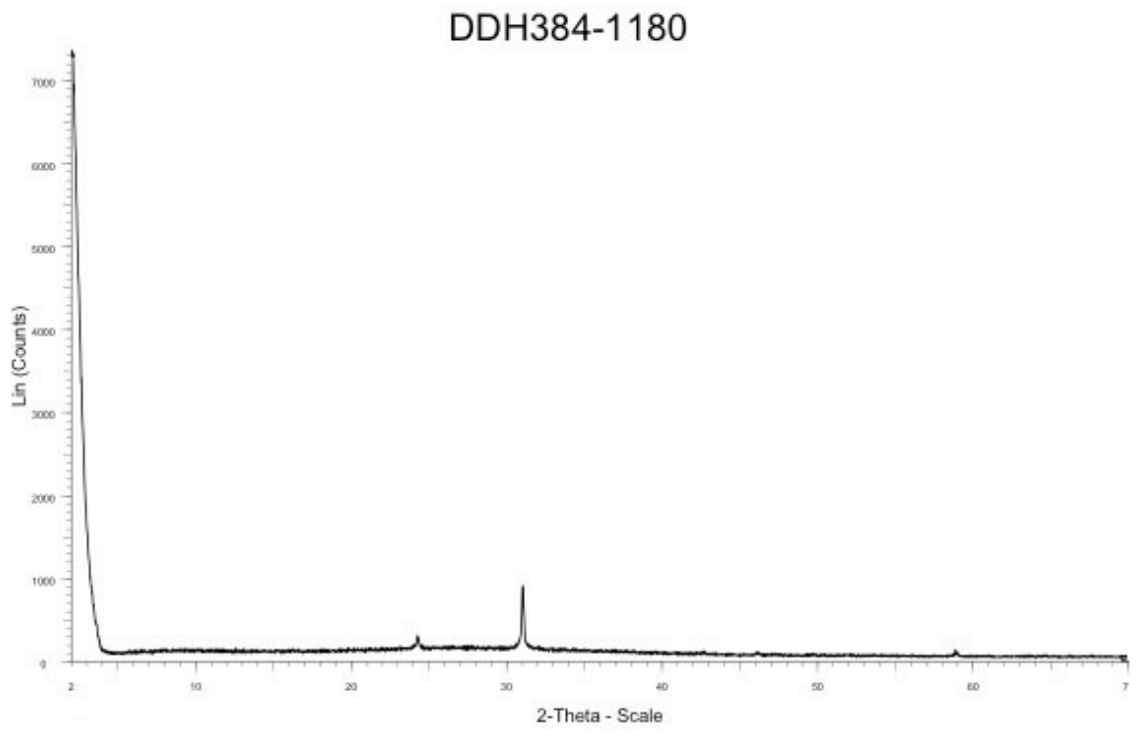
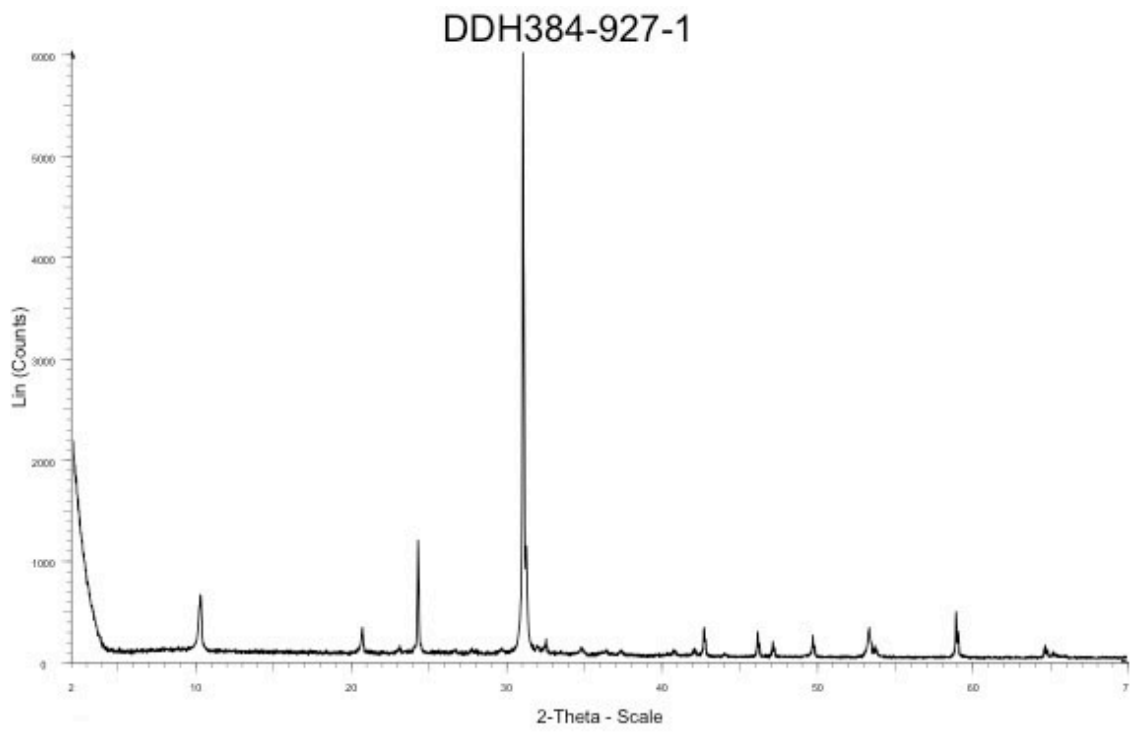
DDH351-867-1



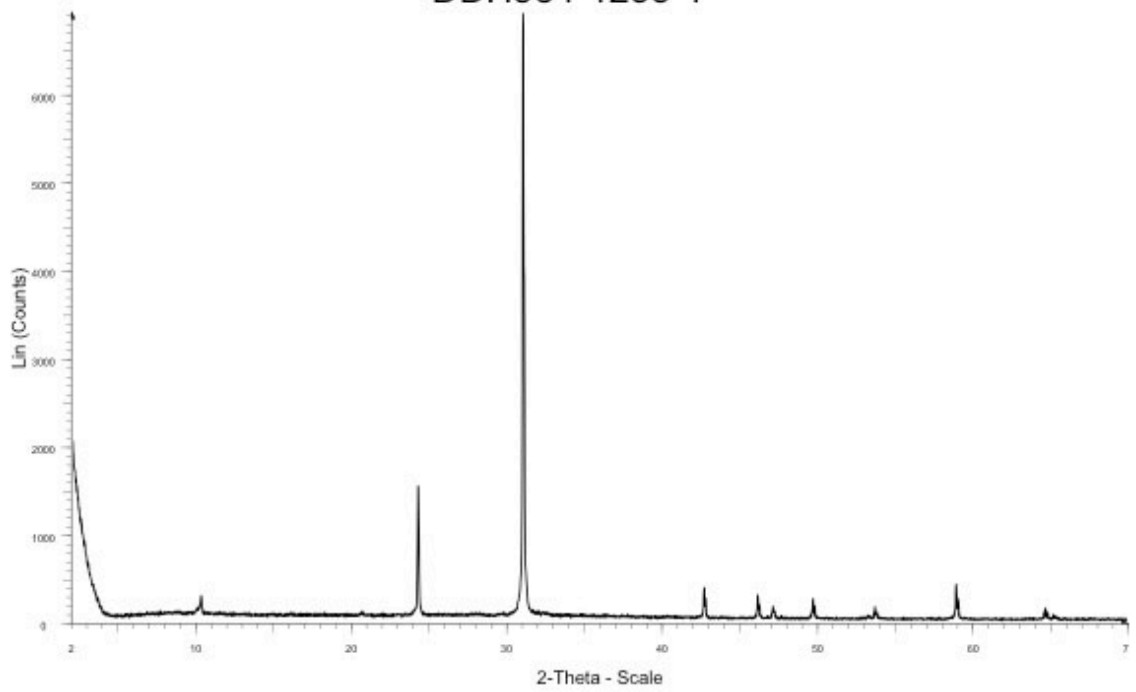
DDH351-867-2



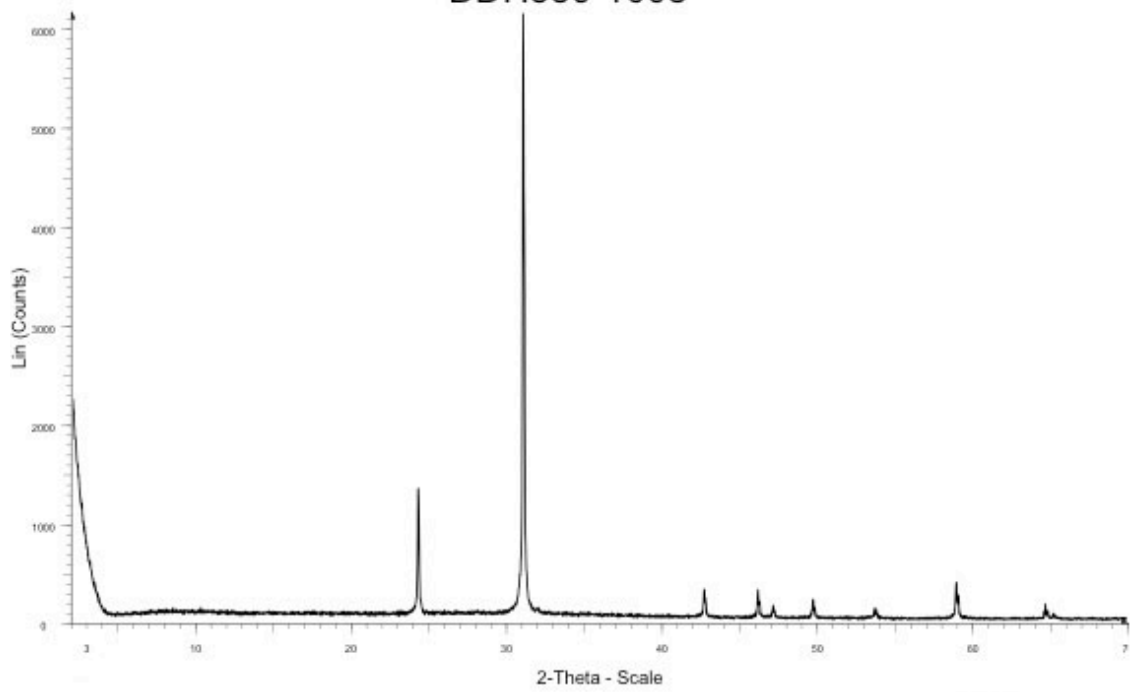


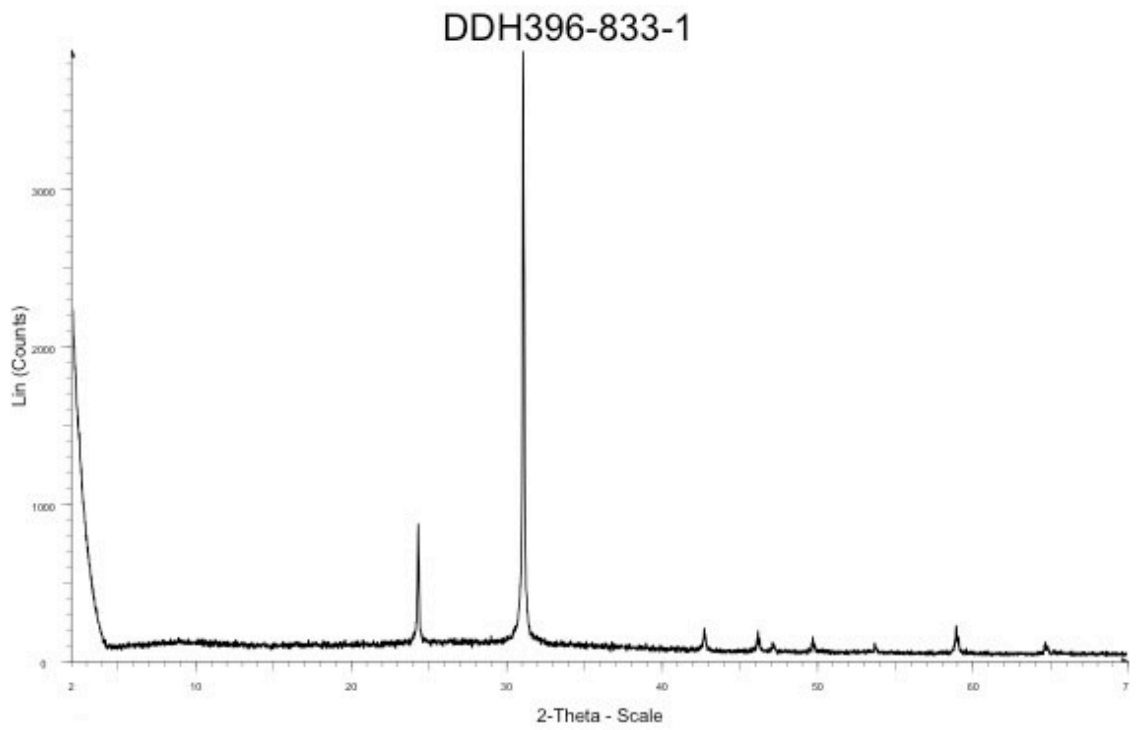
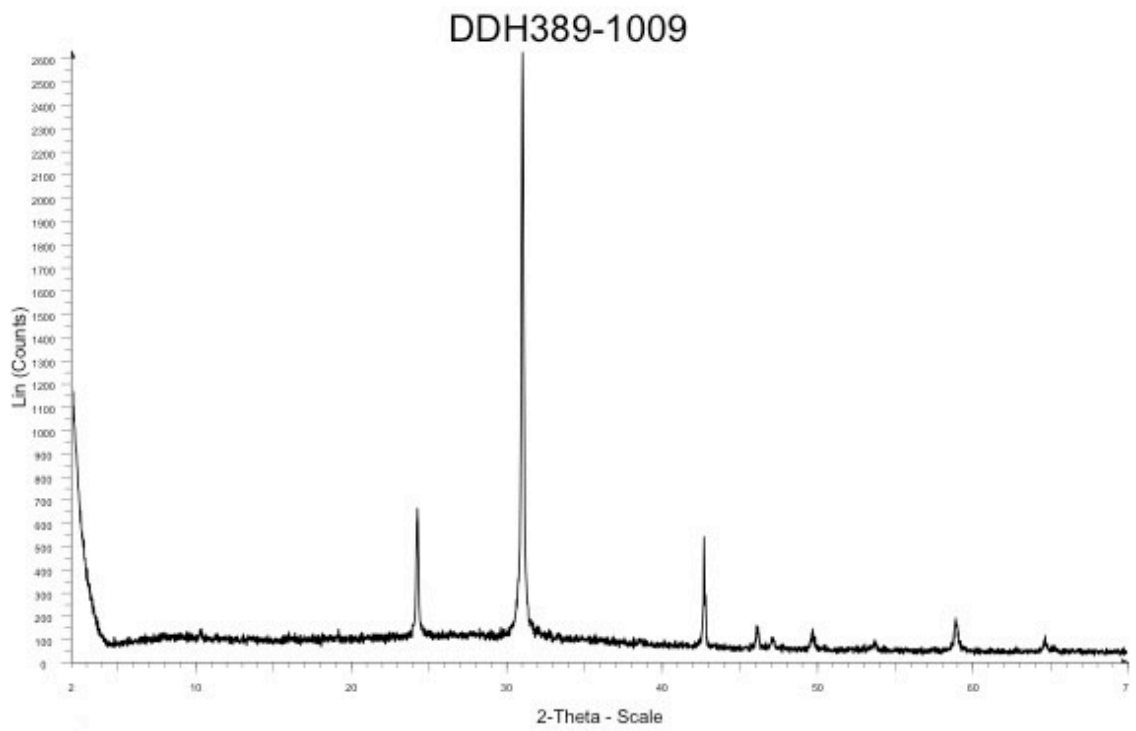


DDH384-1253-1

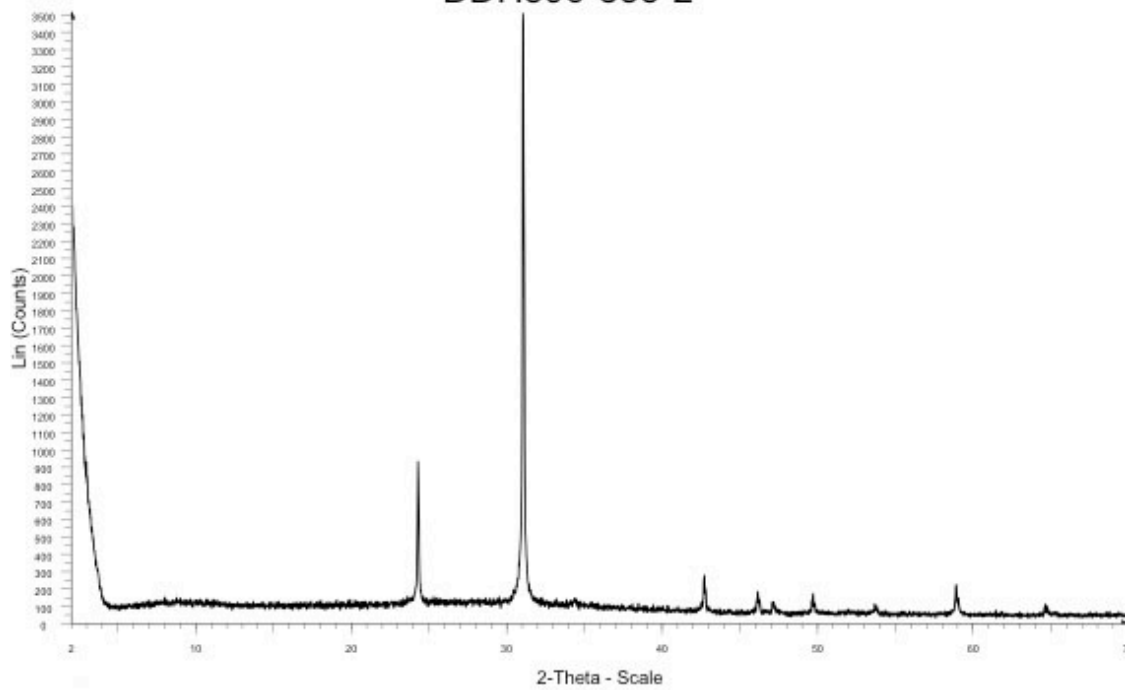


DDH389-1008

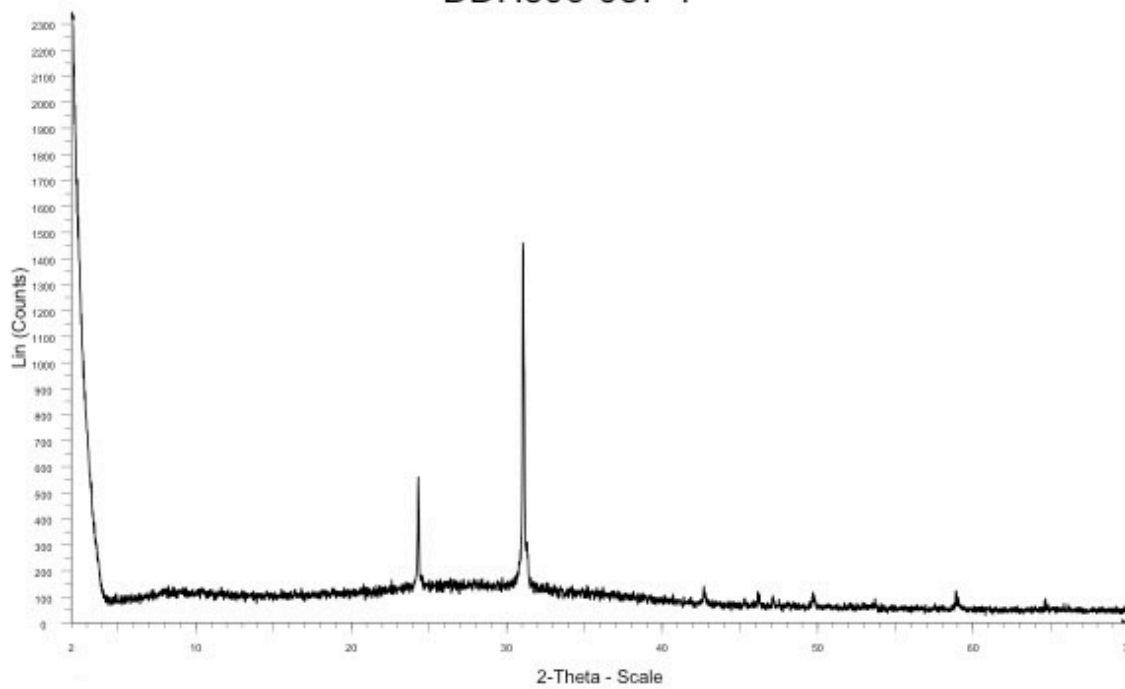




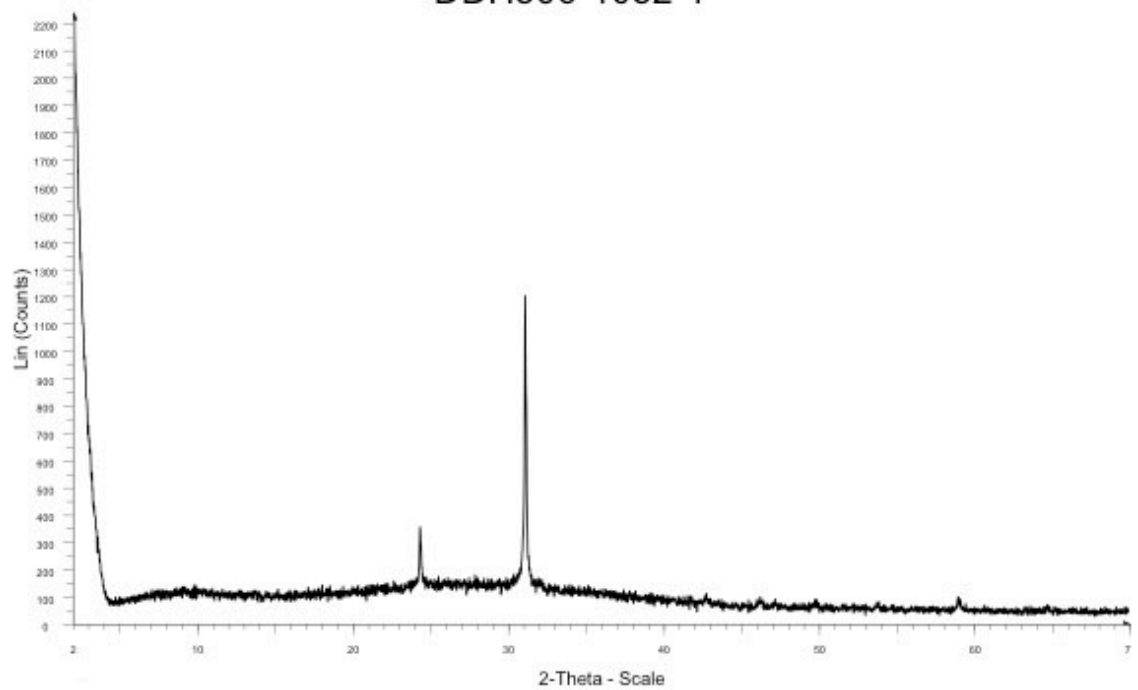
DDH396-833-2



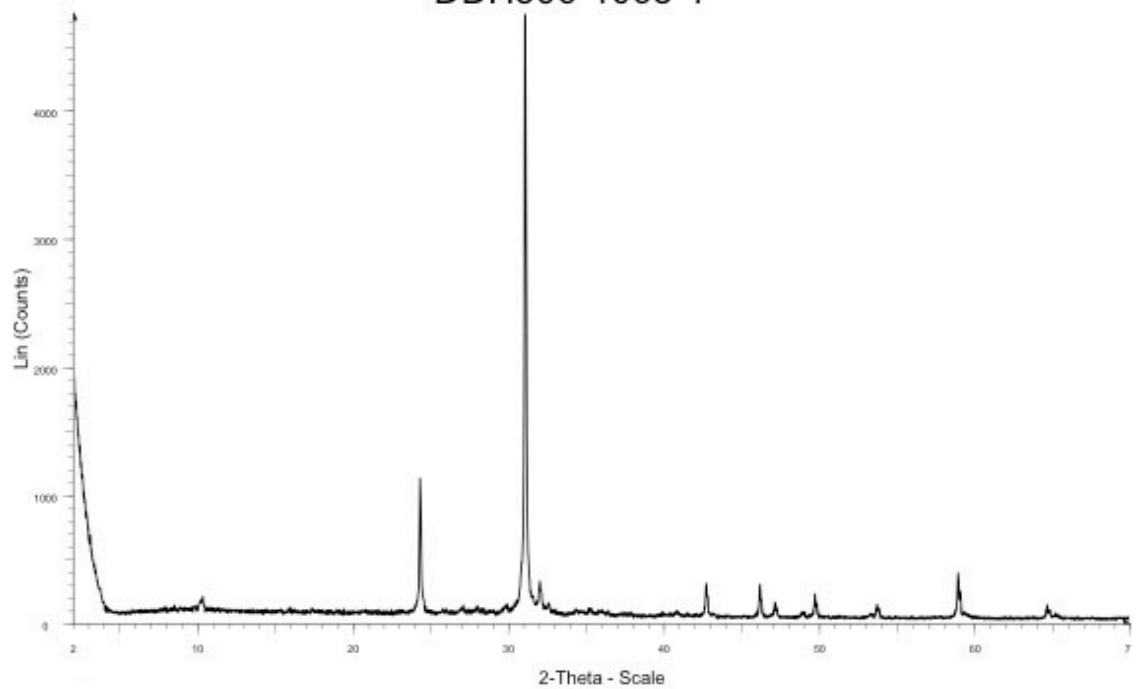
DDH396-937-1

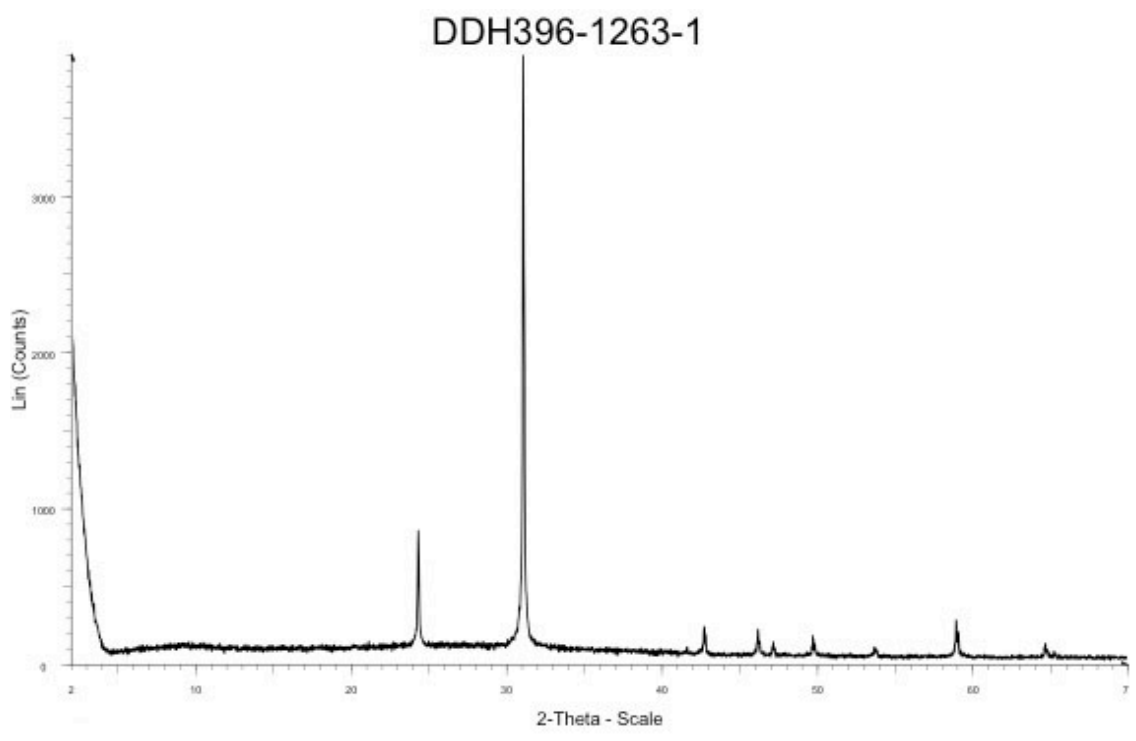
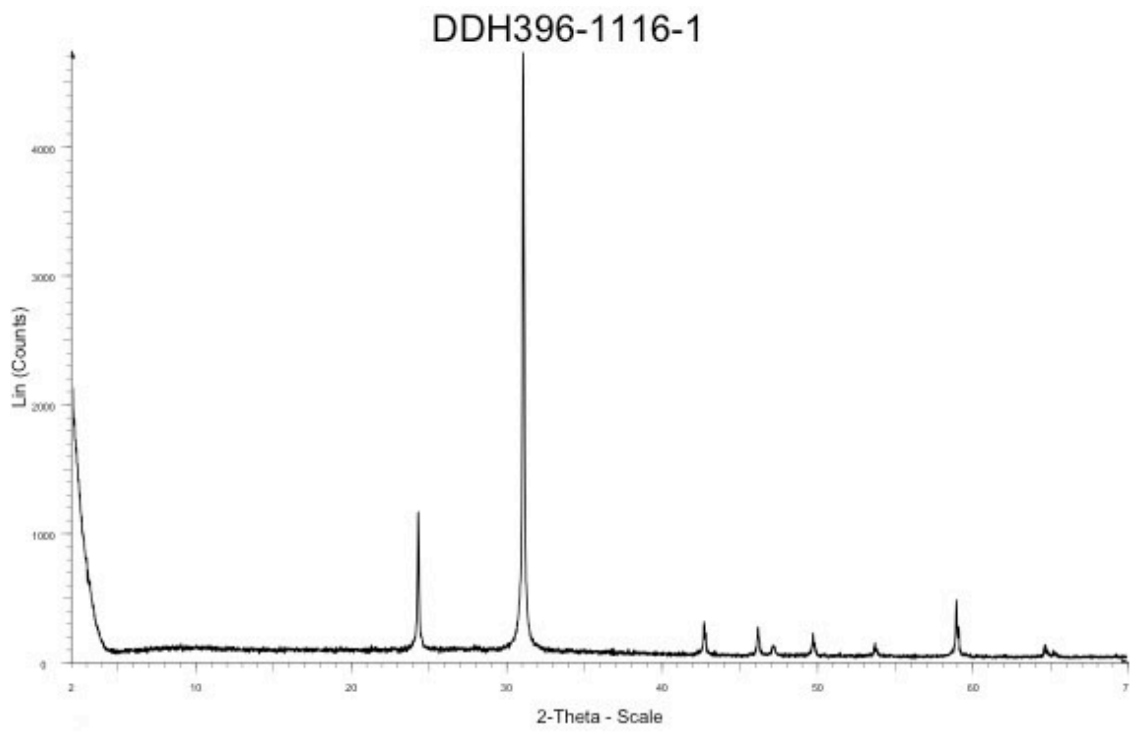


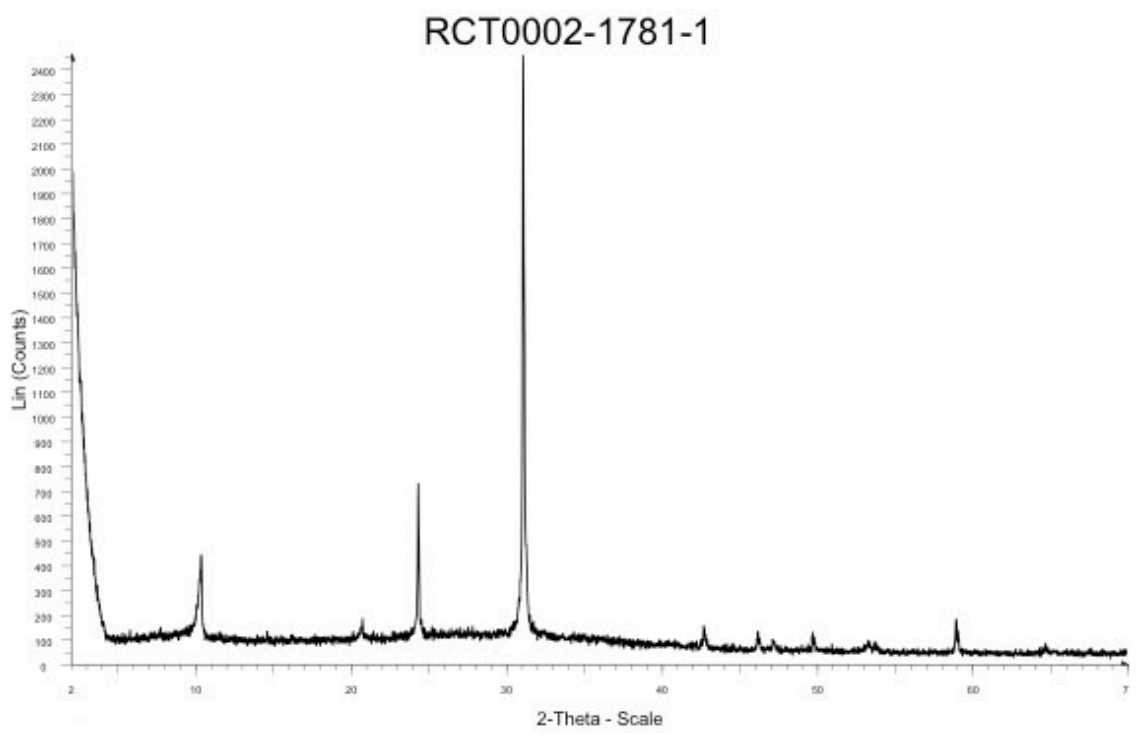
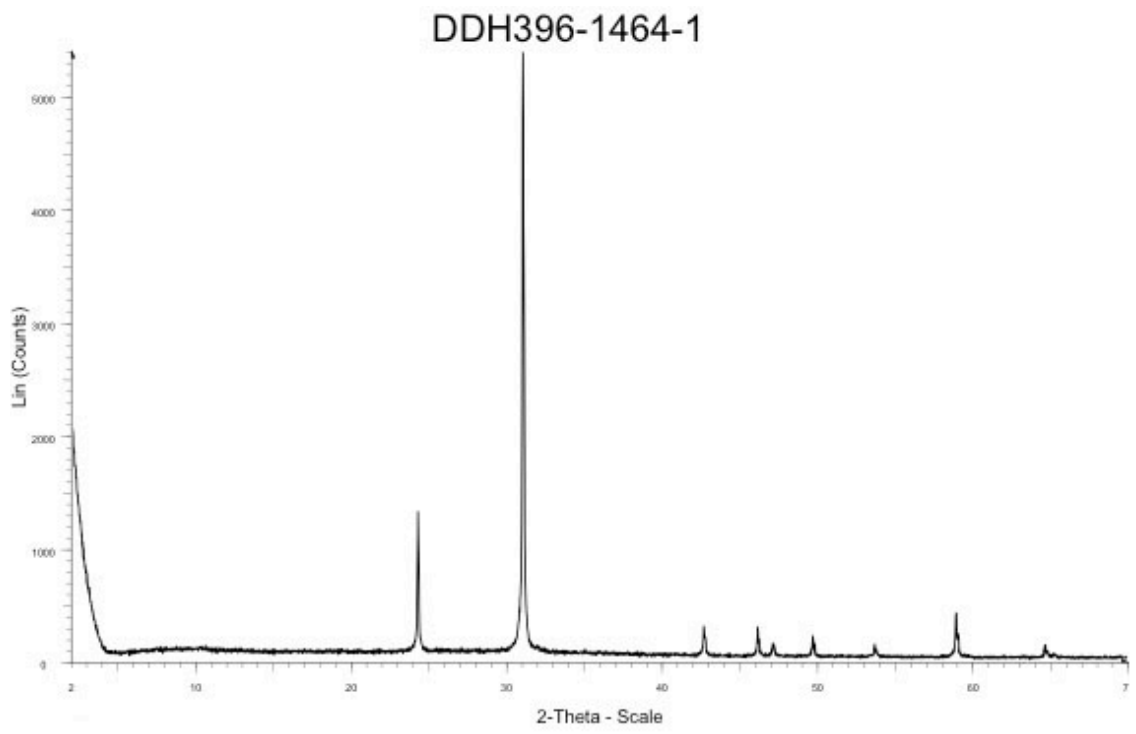
DDH396-1052-1

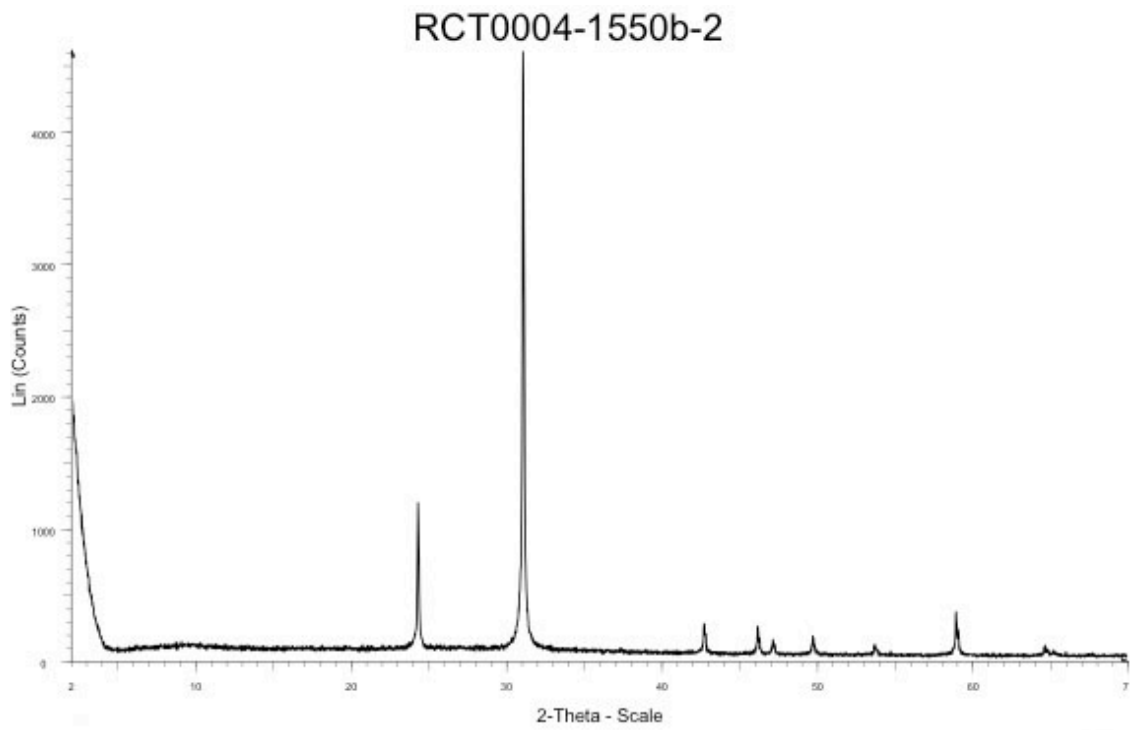
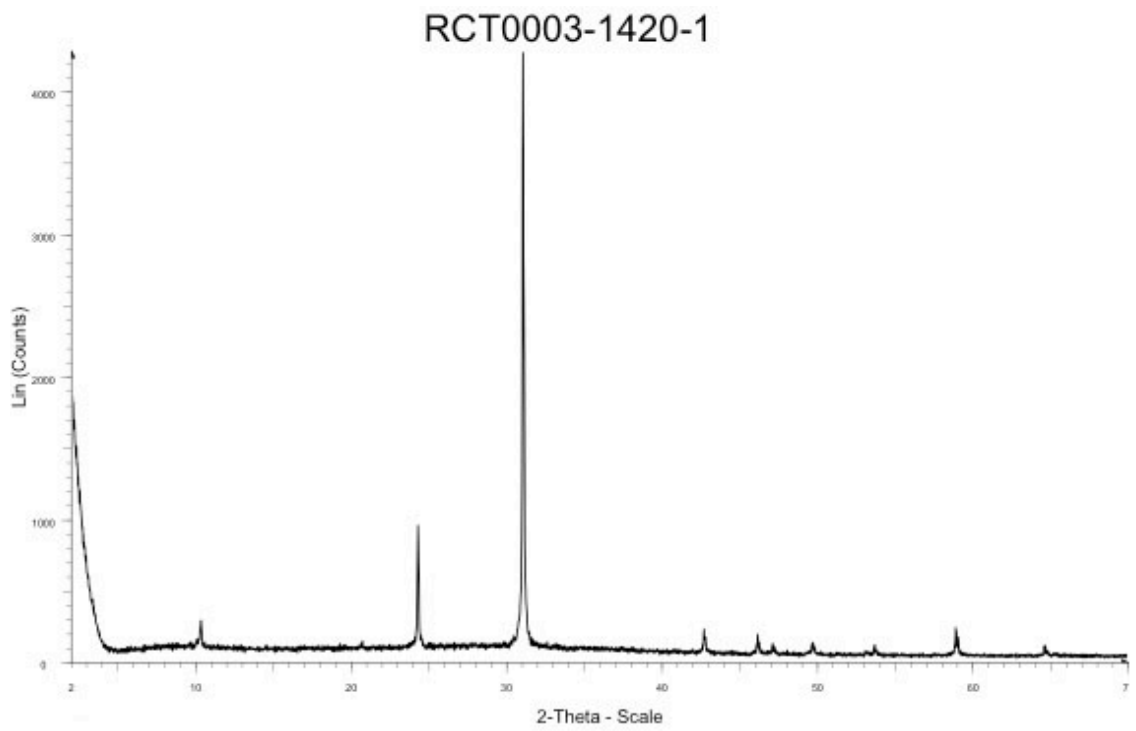


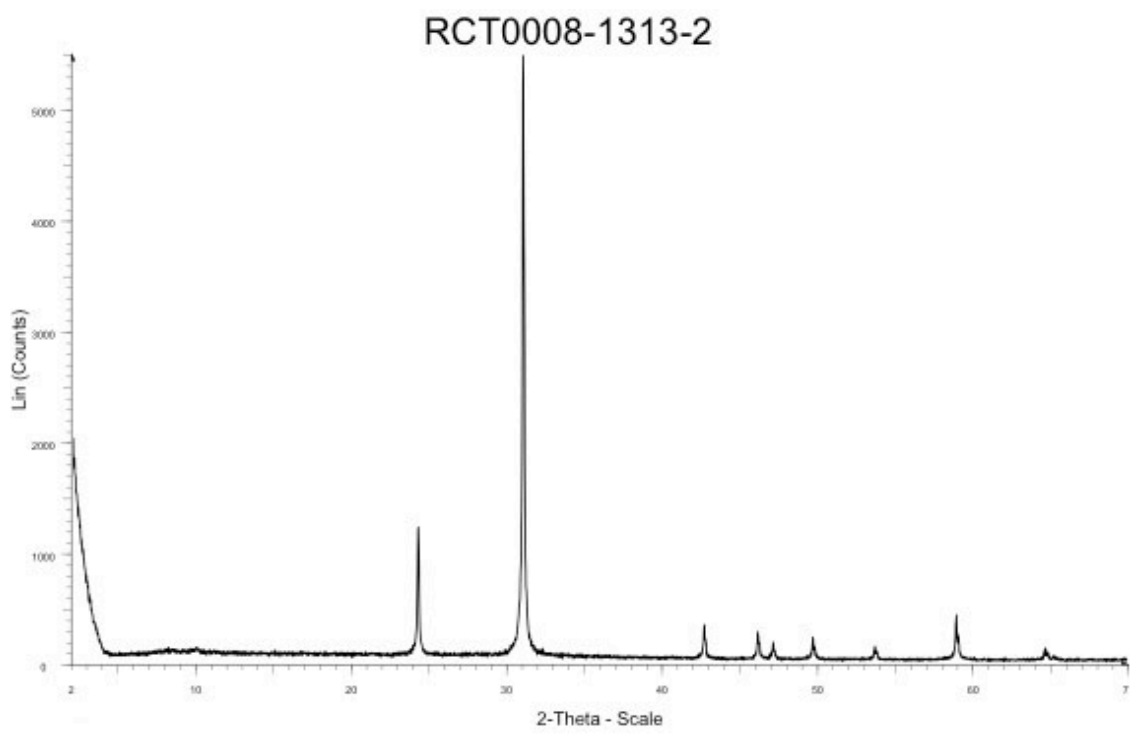
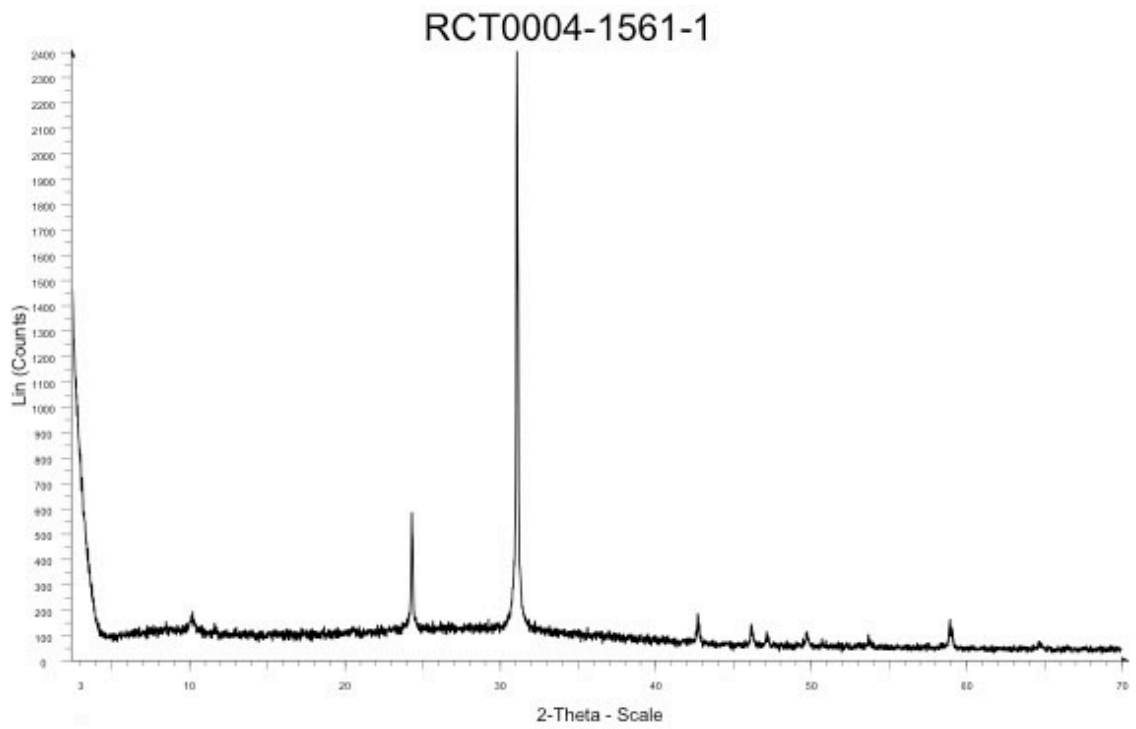
DDH396-1068-1

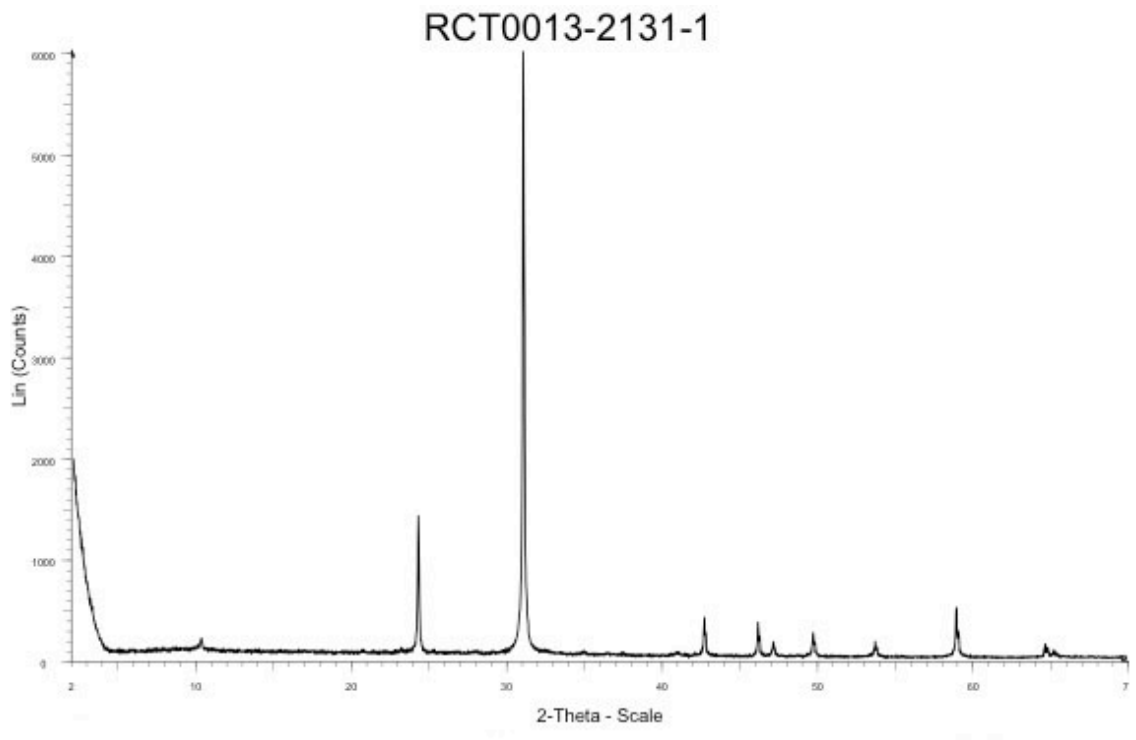
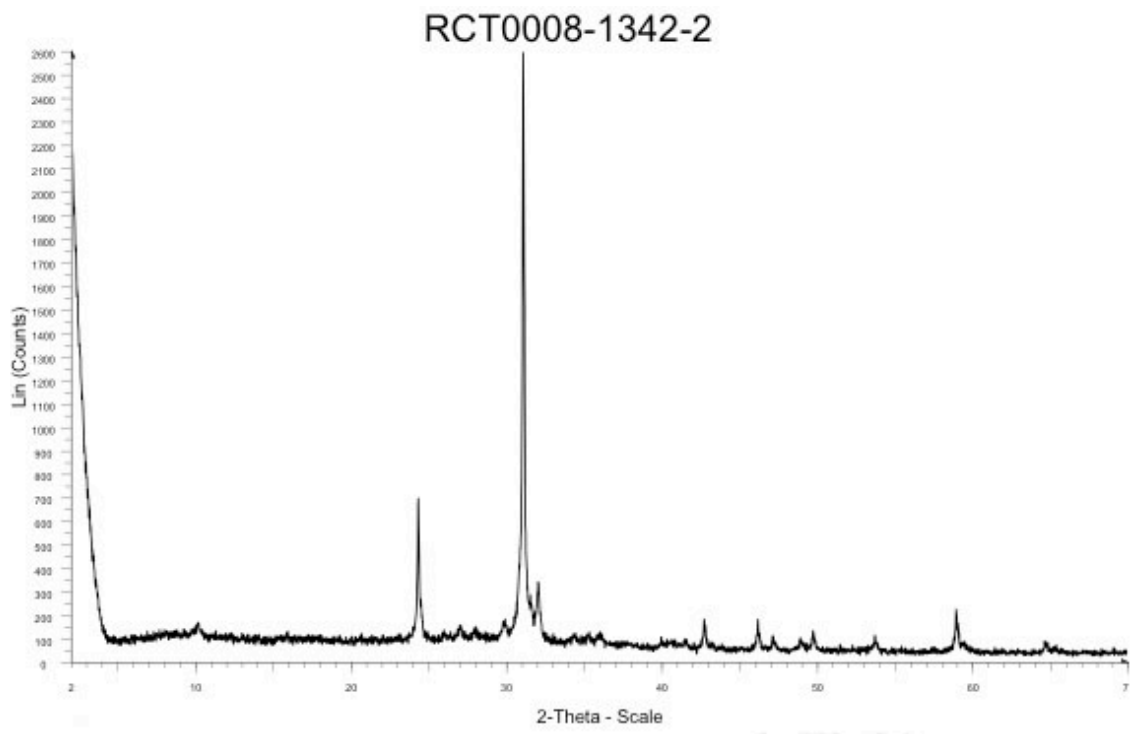


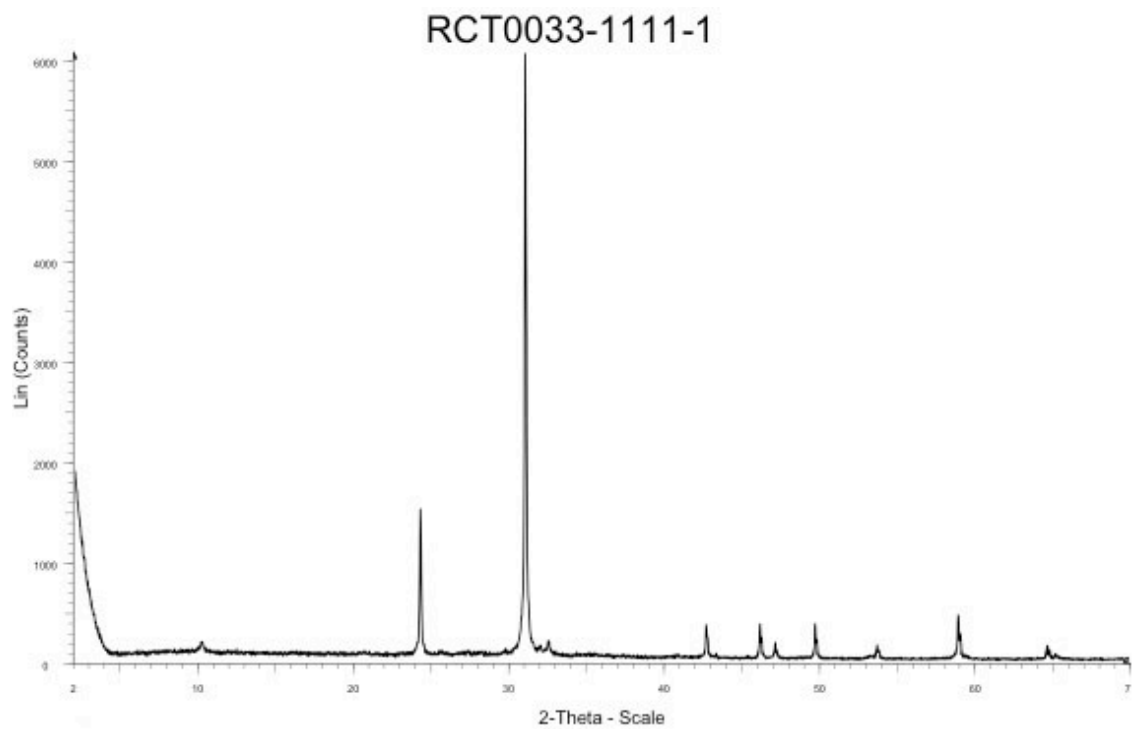
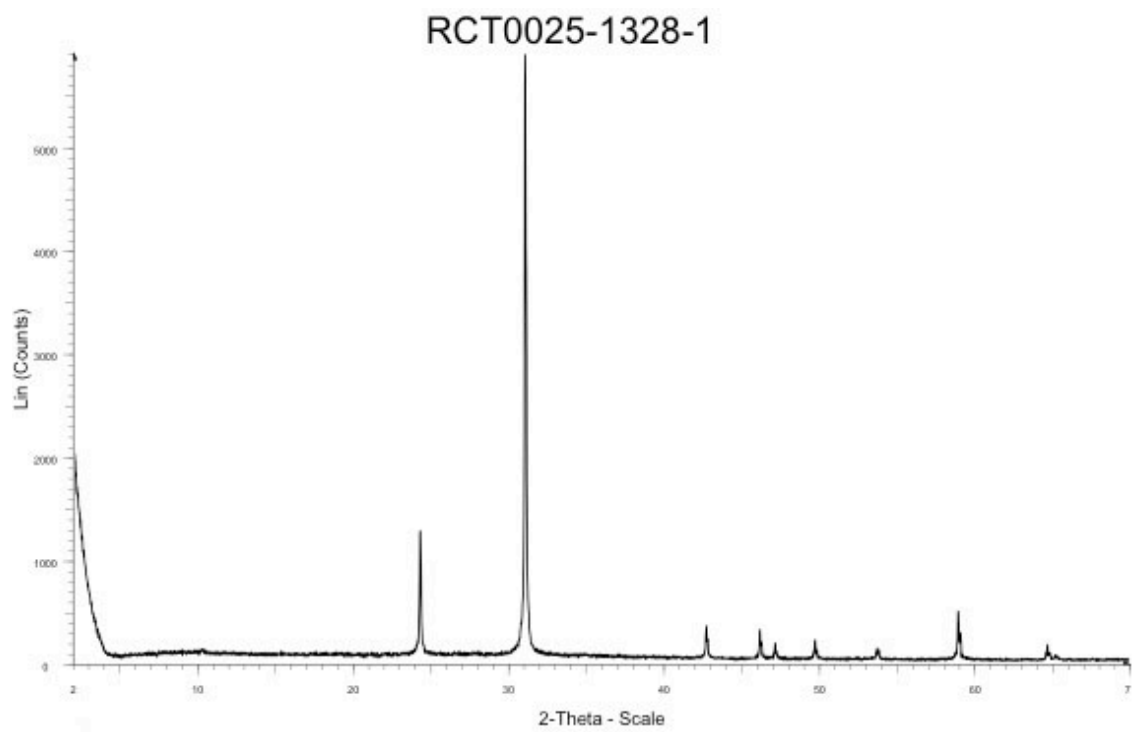


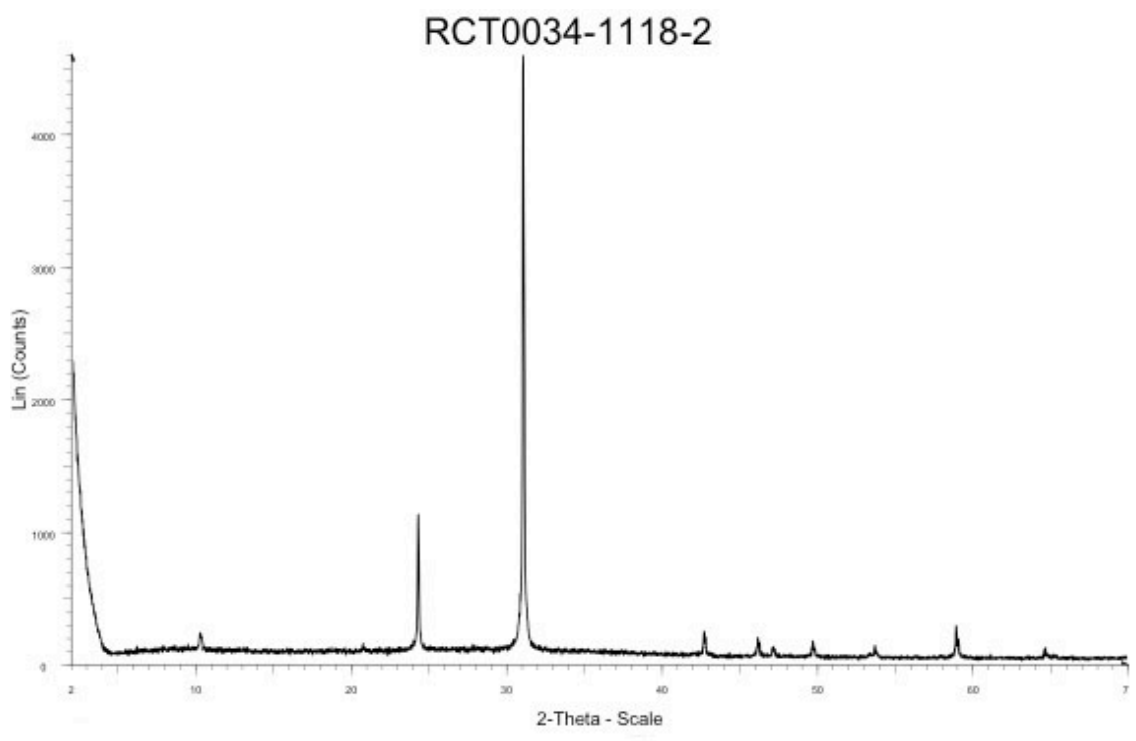
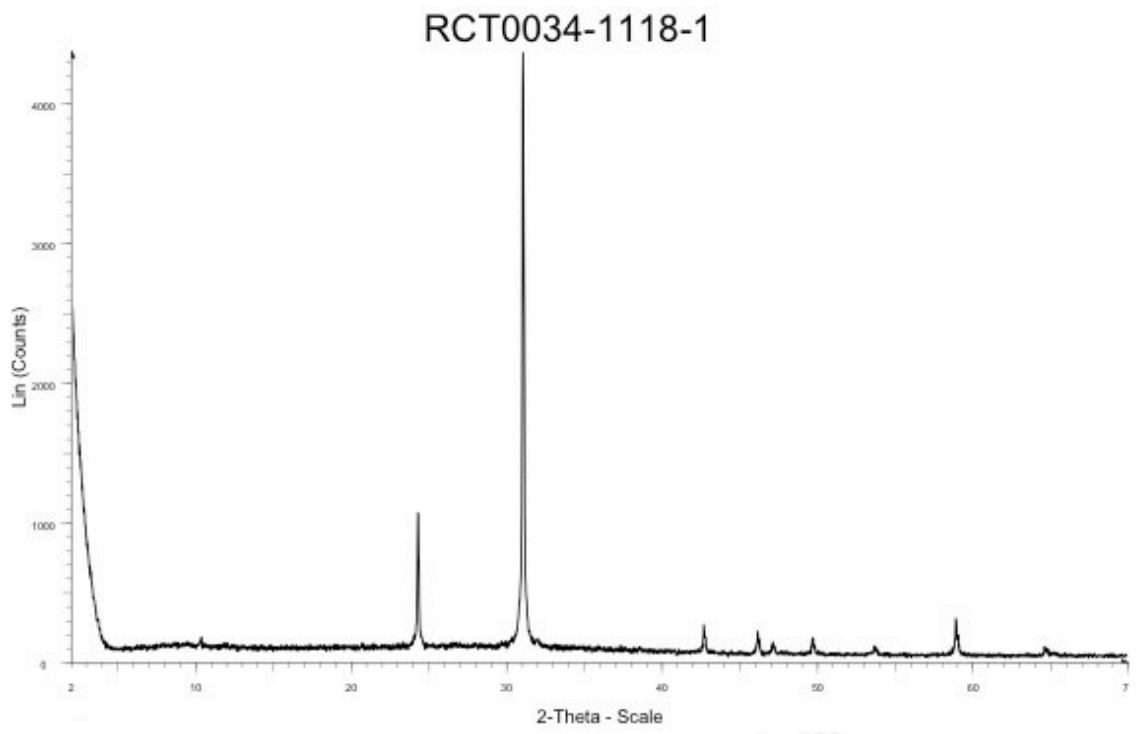




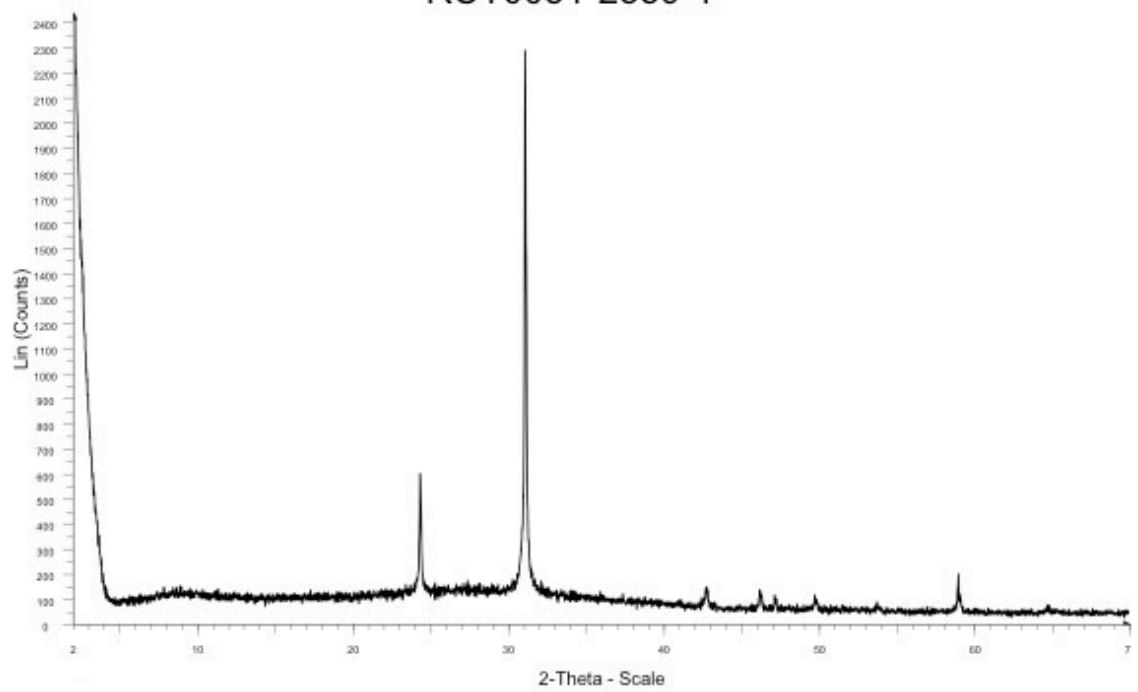




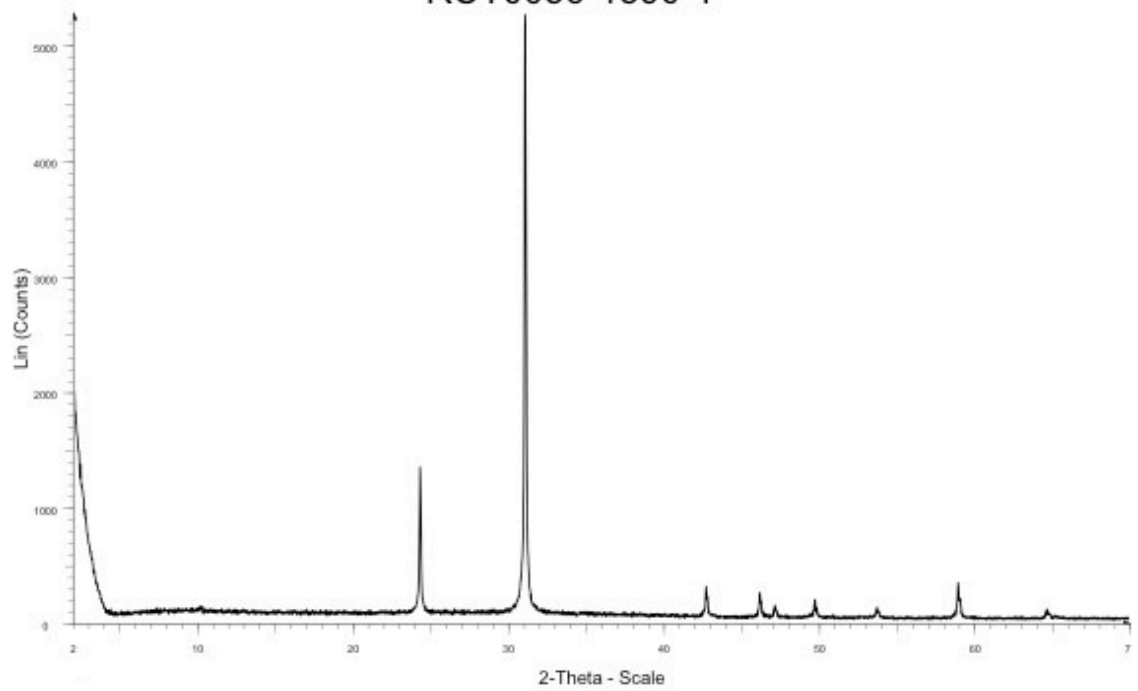


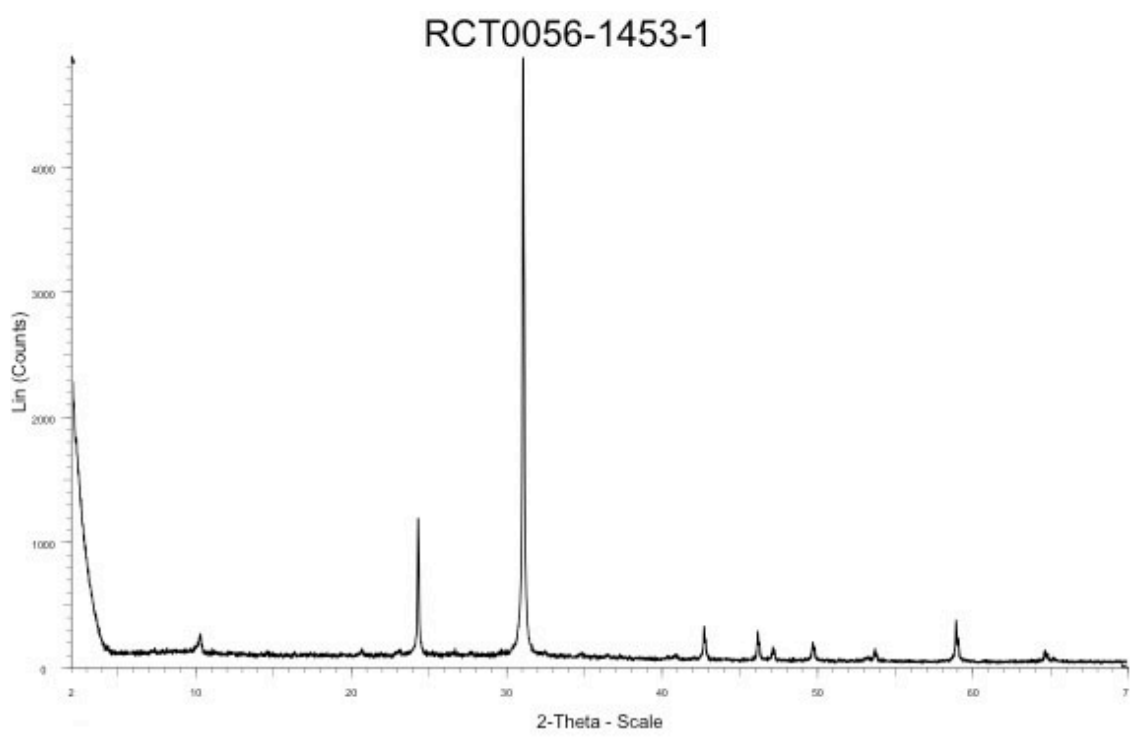
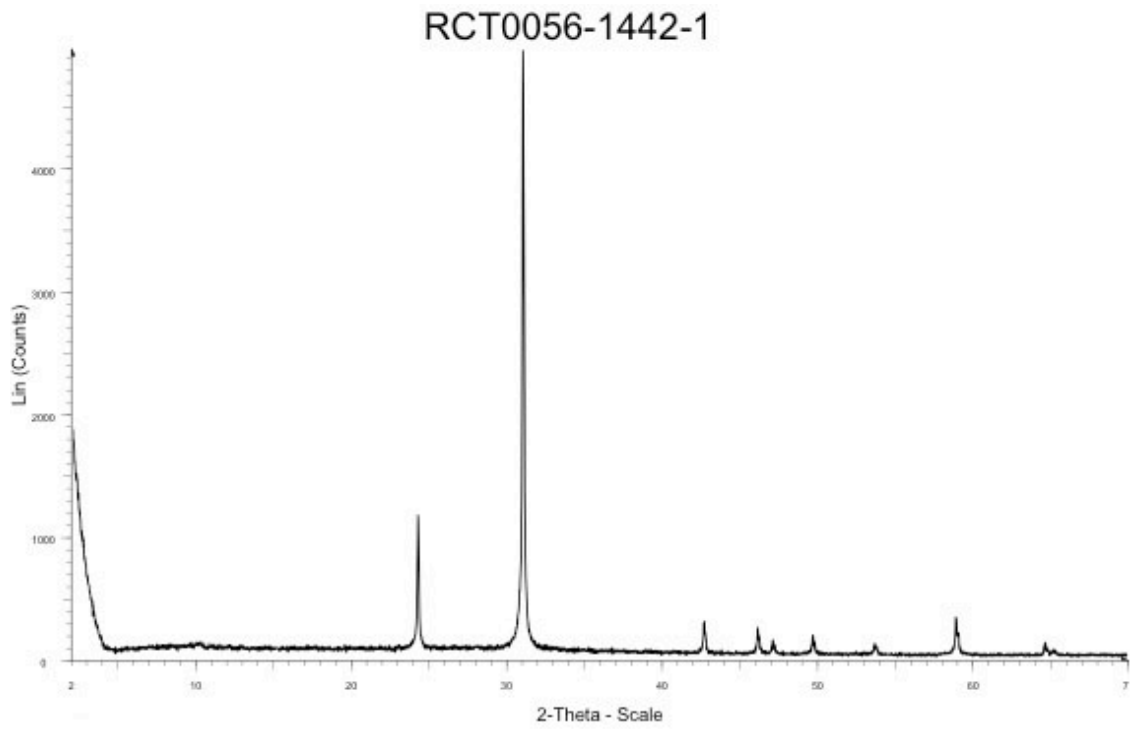


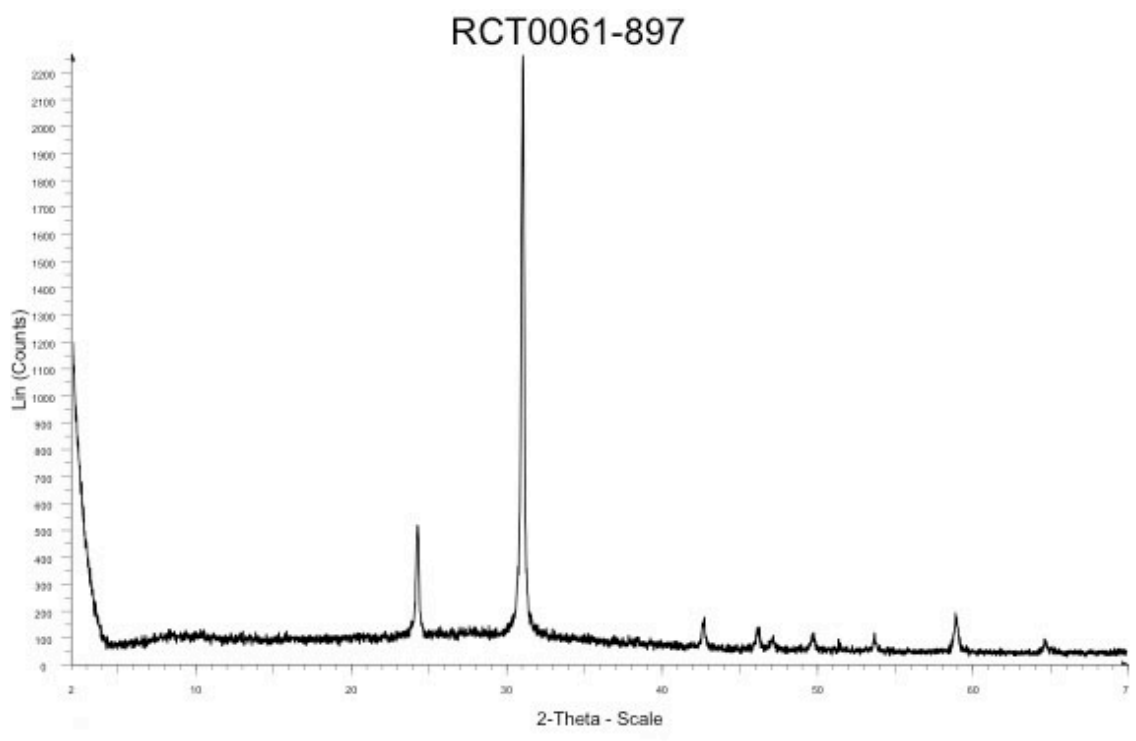
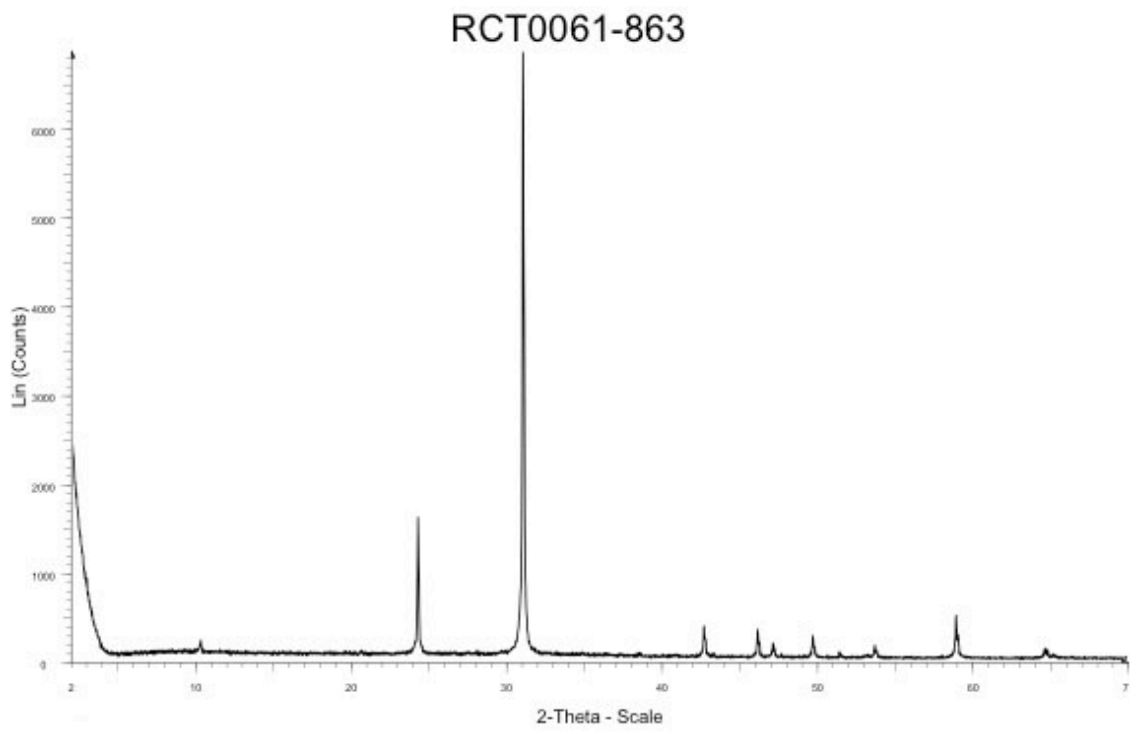
RCT0051-2359-1



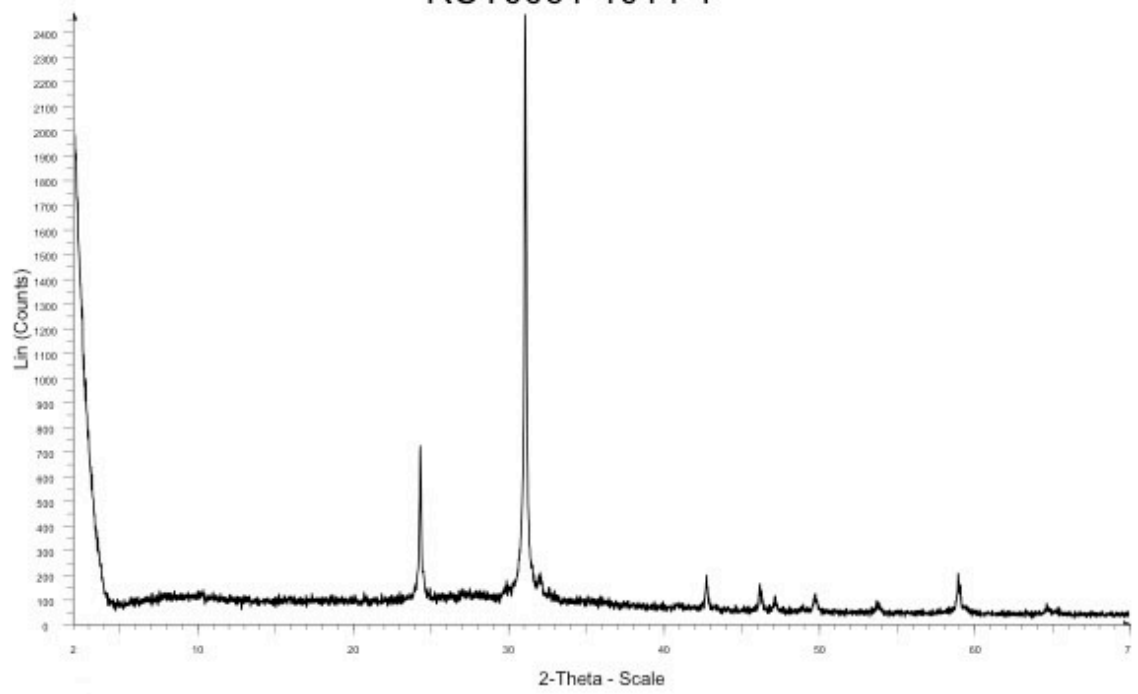
RCT0056-1390-1



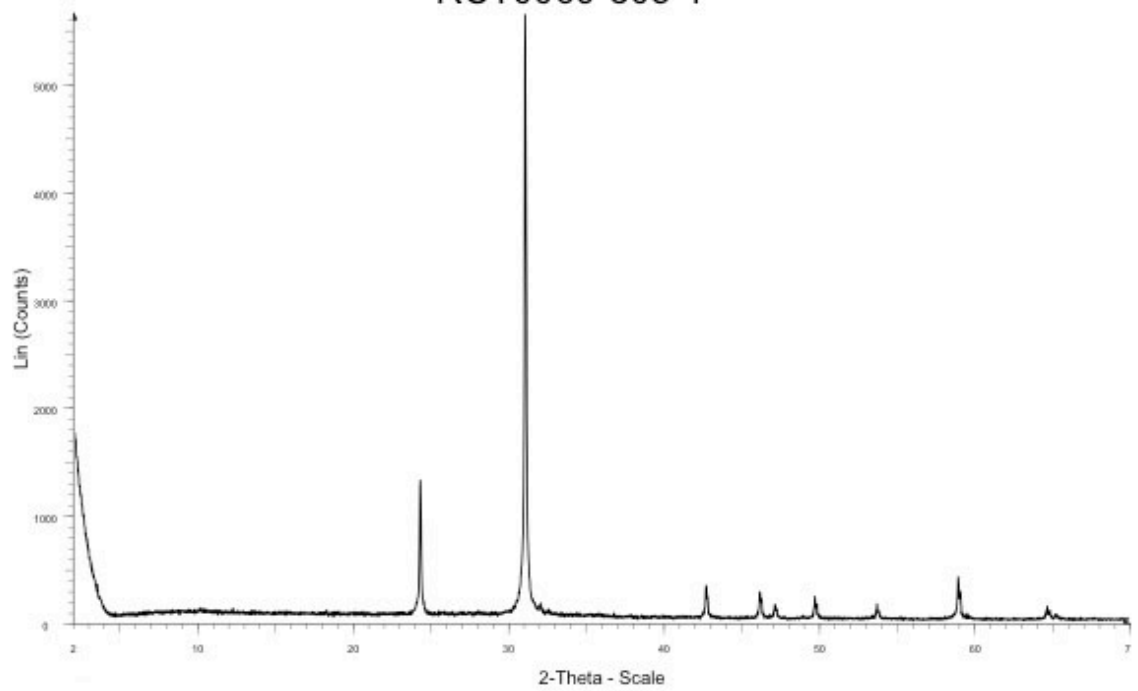




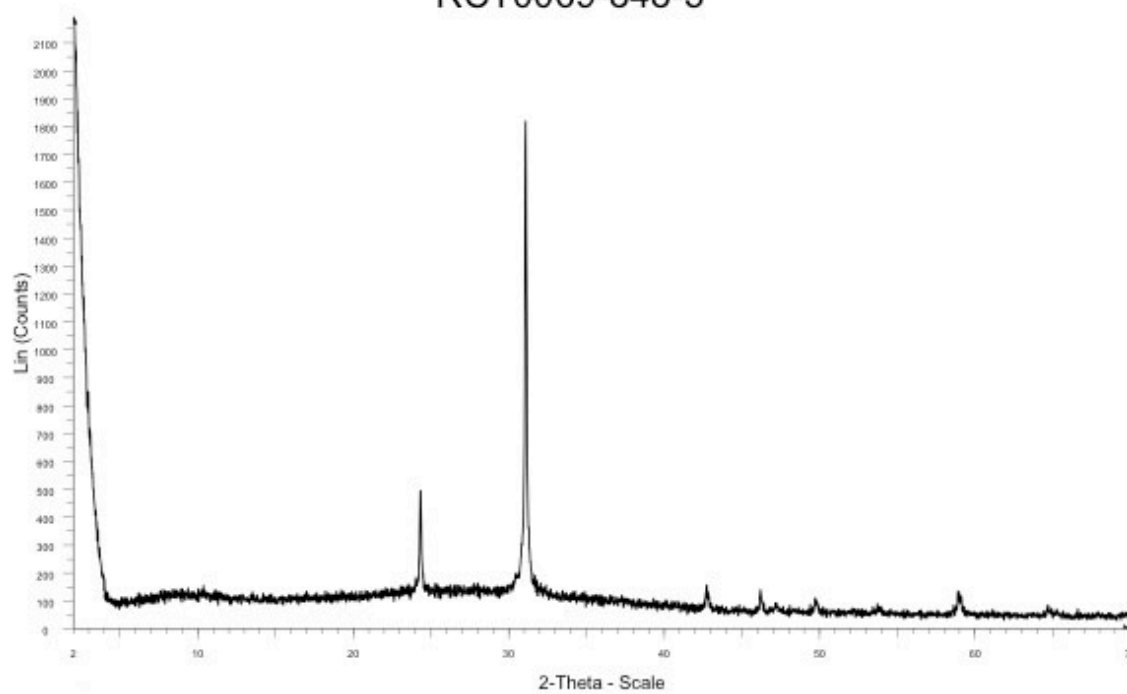
RCT0061-1014-1



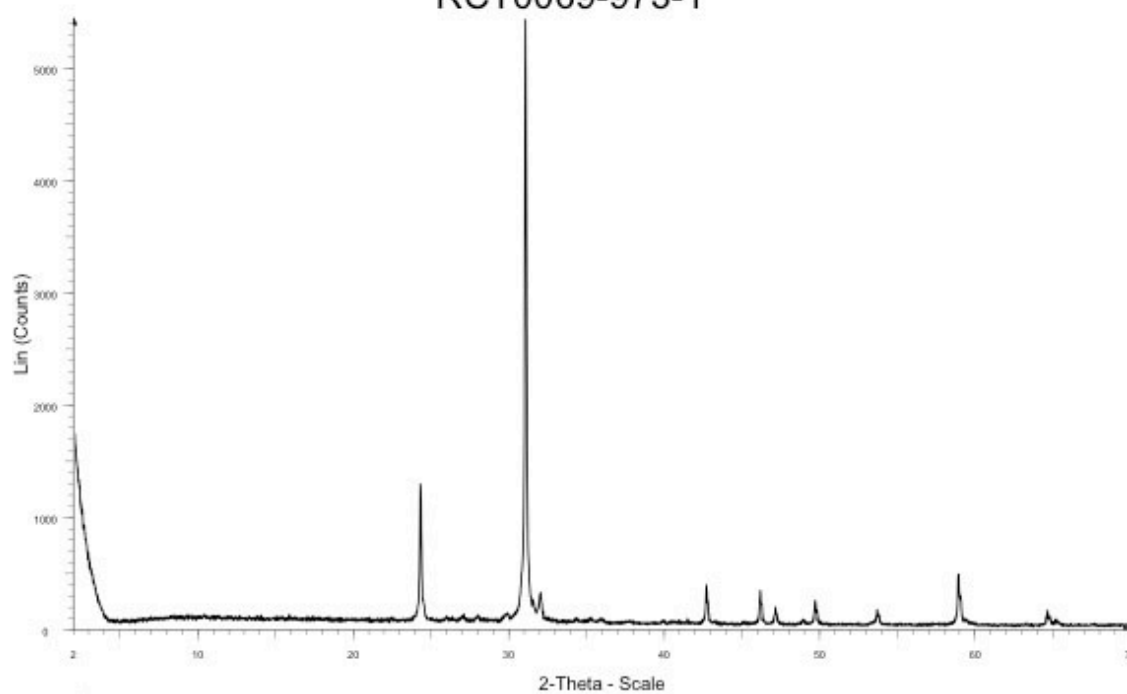
RCT0069-805-1



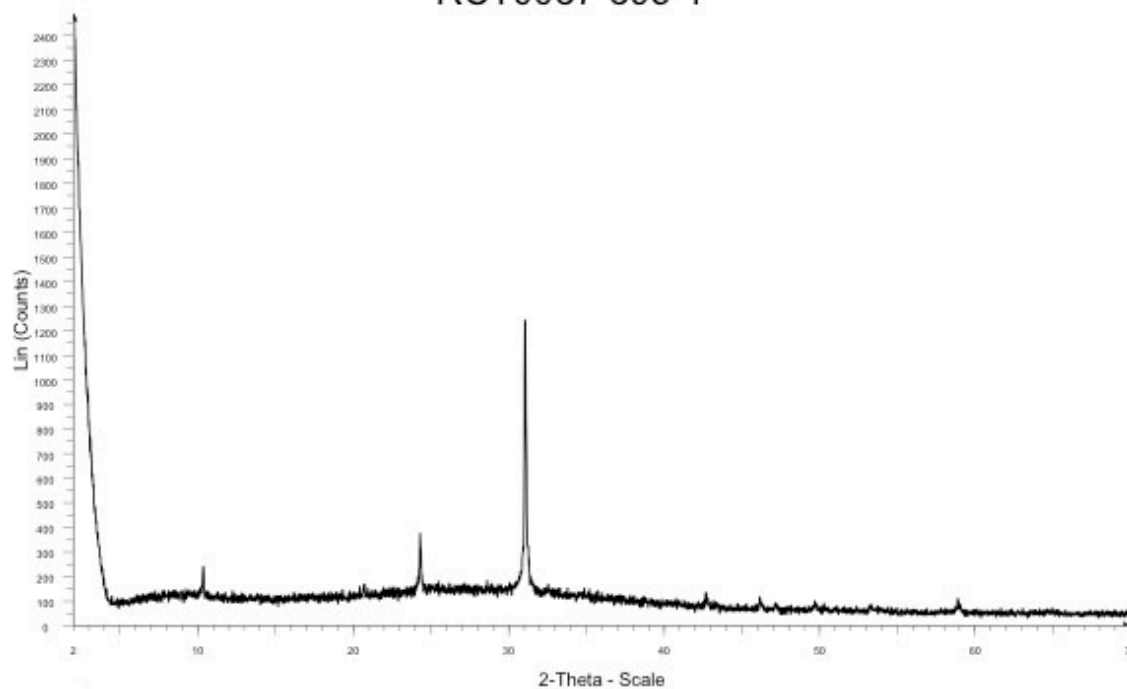
RCT0069-848-3



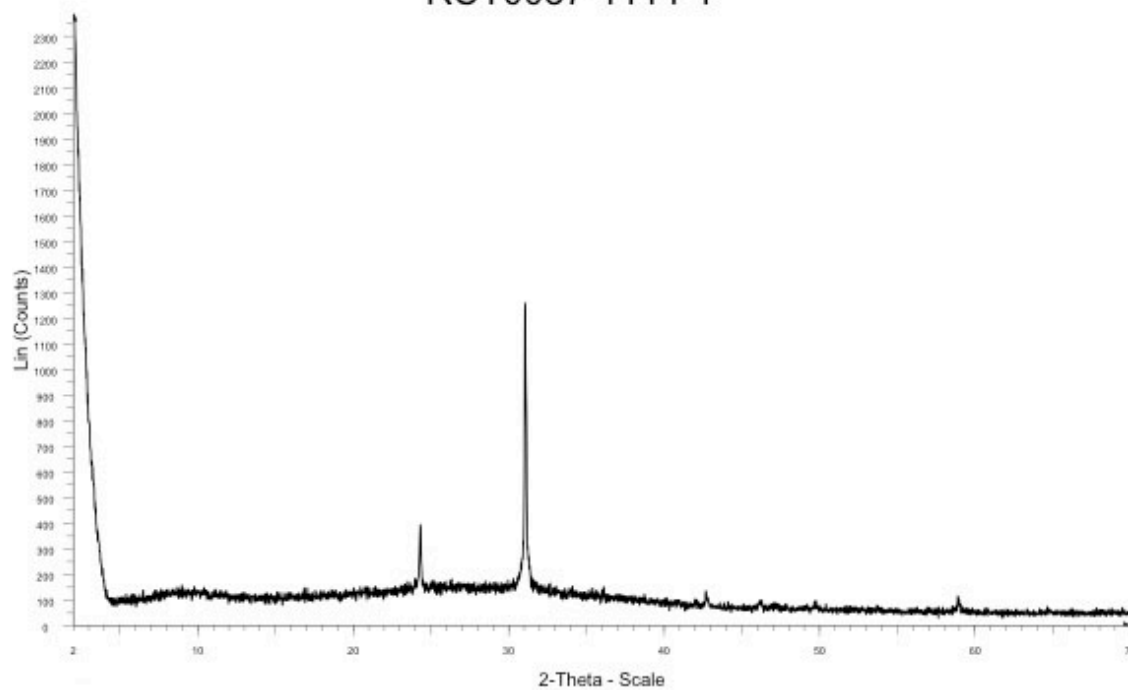
RCT0069-973-1



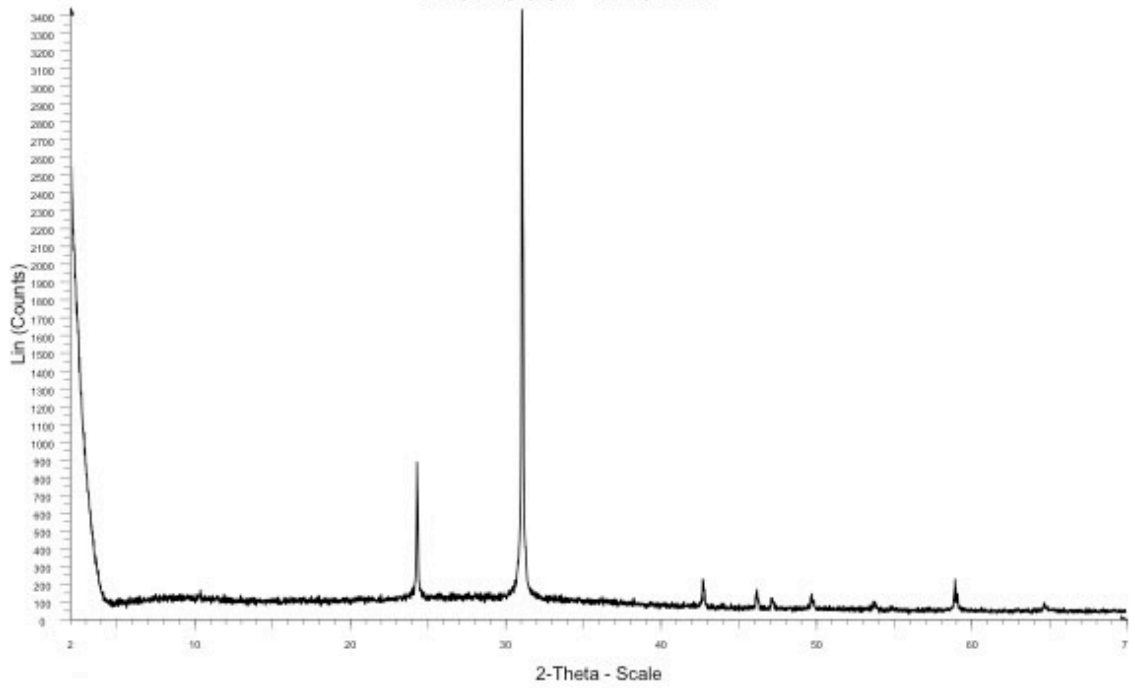
RCT0087-895-1



RCT0087-1114-1



RCT0087-1132-1



RCT0087-1132-2

